University of Alberta

Adaptive and Nonlinear Control of a Voltage Source Converter

by

Rasoul Mohammadi Milasi

A thesis submitted to the Faculty of Graduate Studies and Research
in partial fulfillment of the requirements for the degree of

Doctor of Philosophy

in

Control Systems

Electrical and Computer Engineering

Fall 2012
Edmonton, Alberta

Abstract

Over the past decade improvements in semiconductor technology have led to faster power electronic switches with higher ratings. These devices have been used to improve the performance of various power converter systems. In particular, the Voltage Source Converter (VSC) has been widely used in power systems to facilitate power flow control and improve power quality. The research described in this dissertation mainly relates to two important power quality applications of the VSC: the Static Synchronous Compensator (STATCOM) which performs power factor compensation (PFC), and the Active Power Filter (APF) which attenuates system harmonics. Both applications can be formulated as trajectory tracking problems for a nonlinear dynamic system, and the approaches taken here involve a direct model-based compensation for the nonlinearity in order to establish a formal statement regarding the stability of the closed-loop system. An emphasis of these designs is placed on adaptive control to directly account for uncertainties in the system parameter.

First, the thesis focuses on the STATCOM application of the VSC. We present two different third order models based on different power balances. Using these models we propose a nonlinear flatness-based control which guarantees tracking of constant dc voltages and q-axis current. The particular novelty of the approach lies in the use of steady state relations to improve existing work. Next we present the state-of-the art in nonlinear adaptive control theory and apply an existing approach to PFC while dealing with uncertainty in two system parameters. We show that it is not possible to apply existing theory to an important choice of uncertainty in parameters. Hence, we propose two alternate adaptive designs which directly account for uncertainty in three parameters. The first design is a so-called adaptive PI vector control which

is reminiscent of the classical vector control method. The other approach is the so-called full adaptive control. A Lyapunov function is derived to demonstrate these designs provide asymptotic convergence of the tracking error. Two designs are presented for the APF application: a traditional PI control and an adaptive control. The adaptive control shows improved tracking of power factor, harmonic compensation, and robustness to model error. In parallel to the control theory derived and simulation work, experimental validation was performed on a VSC test stand.

Acknowledgements

I would like to express my gratitude to all those who help me in completion of this thesis. Especially, I would like to acknowledge my supervisors Dr. Alan Lynch and Dr. Yun Wei Li for their invaluable guidance and advices during my Ph.D. program. I also acknowledge Prof. Biao Huang for his kindness in making it possible to experience working with Process System and Control group. My sincere thanks to the Ph.D. examination committee members, Prof. Amir Aghdam and Prof. Andy Knight, for their insightful readings and suggestions for improving the thesis. Additional thanks to my colleagues at Applied Nonlinear Control Lab (ANCL) for their cooperation and encouragement. I also want to thank Albert Terheide for lending some of the experimental equipment. I would like to thank fellow graduate students in Advanced Control System Lab (ACSL) for their kind friendship. Last but not least, thanks to my family for their support and love.

Contents

List of Tables

List of Figures

Chapter 1

Introduction

Voltage source converters (VSCs) have a number of important applications in the area of power conversion. For example they can be used as active power filters which compensate the power factor of the supply or reject the harmonic content injected by a load. Both objectives have important consequences on the efficiency of power delivery. The proposed research investigates the use of model-based adaptive and nonlinear control methods to achieve trajectory tracking for a number of power factor correction and active power filter applications using a VSC.

1.1 Power Converters for Power Quality Improvement

The main objective of a power system is to deliver reliable power to loads with good power quality, e.g. to provide sinusoidal voltage at a fairly constant magnitude throughout the system. Important power quality issues include regulating power factor and current harmonics which result from nonlinear or inductive loads [1, 2]. Power Factor (PF) is defined as the ratio of real to apparent power:

$$\text{PF} = \frac{\text{Real Power}}{\text{Apparent Power}} \leq 1 \tag{1.1}$$

Real power is expressed in Watts and apparent power in Volt-Amperes. If both voltage and current are sinusoidal then apparent power is calculated simply by multiplying the RMS voltage and current amplitudes while real power is the apparent power times $\cos\theta$ where θ is the phase angle between voltage and

current sinusoids. For example, inductive loads make current lag voltage and this lagging PF or reactive power flow leads to lower load voltage and inefficient transmission [1, 3]. Nonlinear loads such as rectifiers in televisions, ovens, and commercial lighting can lead to significant unbalance currents, reactive currents and harmonic currents in the power system. These nonlinear currents will cause more heating, false tripping and resonance. The level of distortion in a waveform is related to the amplitudes of harmonic components in the waveform compared with its fundamental component; it is measured by Total Harmonic Distortion (THD) [1]. For non-sinusoidal waveforms, THD is the ratio of the sum of the RMS value of the harmonics to the RMS value of the fundamental [3]. For a current waveform we have

$$\mathrm{THD}_I = \frac{\sqrt{\sum_{k=2}^{\infty} I_k^2}}{I_1} \tag{1.2}$$

where $I_k, k \geq 2$ are the current harmonic amplitudes and I_1 is the amplitude of the fundamental. That is, the current waveform has the expansion

$$i(t) = I_{dc} + \sum_{k=1}^{\infty} I_k \sin(\omega k t + \phi_k)$$

where I_{dc} is the dc value of the current. We should remark that PF formula in the case that the voltages and currents are non-sinusoidal is

$$\mathrm{PF} = \frac{P_{avg}}{V_{1rms} I_{1rms}} \frac{1}{\sqrt{1 + \mathrm{THD}_V^2}\sqrt{1 + \mathrm{THD}_I^2}} \tag{1.3}$$

where P_{avg} is the average power in which each harmonic makes a contribution, THD_I and THD_V are current and voltage THDs [4]. Traditional methods for PFC and harmonic compensation use passive circuits. For example, capacitor banks are usually used for PFC and passive LC filters are used to reduce harmonic currents. However, passive circuits have the disadvantage of large size, extra losses, and can create system resonance [1, 5, 6]. On the other hand, an alternative for PFC and harmonic compensation uses power converters which are actively controlled to produce the required reactive power and harmonic currents. Generally when a power converter is used for PFC it is called Static Synchronous Compensator (STATCOM), and when it is used for

harmonics compensation it is called Active Power Filter (APF) [2, 7, 8]. In some literature, an APF can provide both PFC and harmonics reduction [5]. Fig. 1.1 shows a typical configuration of a STATCOM or APF which is shunt connected across the utility and load. A digital control generates appropriate PWM gating signals for the VSC so that it injects the required current to the line and compensates reactive power or harmonic currents. A STATCOM or APF can be a two-wire single-phase, three-wire three-phase, or four-wire three-phase configuration. The four wire VSC is used for compensating imbalanced loads. Furthermore, an APF can be shunt connected as in the example or series connected between the source and load [7, 8]. In this work, a three-wire three phase shunt connected VSC system is considered.

In addition to PFC and harmonic compensation, the Fig. 1.1 VSC topology can also be used as an ac-dc rectifier to feed a dc load (e.g. battery charger) or used as the front end of a motor drive system. The front end converter is connected to an ac source on its ac side and on its dc side to another converter which feed the ac motor. The control of these rectifiers shares a common control objectives with the STATCOM. That is, ac side PFC and dc side voltage control. Hence, due to the similarity of control objectives, this thesis also treats the rectifier application of a VSC. We remark for rectifier applications, unlike STATCOMs, significant real power can flow through the converter to the load on the dc side.

1.2 Literature Review

The versatility of VSCs has led their popularity in diverse applications such as transmission systems, motor drives, uninterrupted power supplies and renewable energy systems [9, 10, 11]. This has led to a significant amount of research in modeling and control of VSCs. In this section we review this existing work.

1.2.1 Voltage Source Converter (VSC) Control

VSCs have replaced or complemented passive filter solutions for a number of power quality problems [2, 7, 8]. As mentioned above, two important appli-

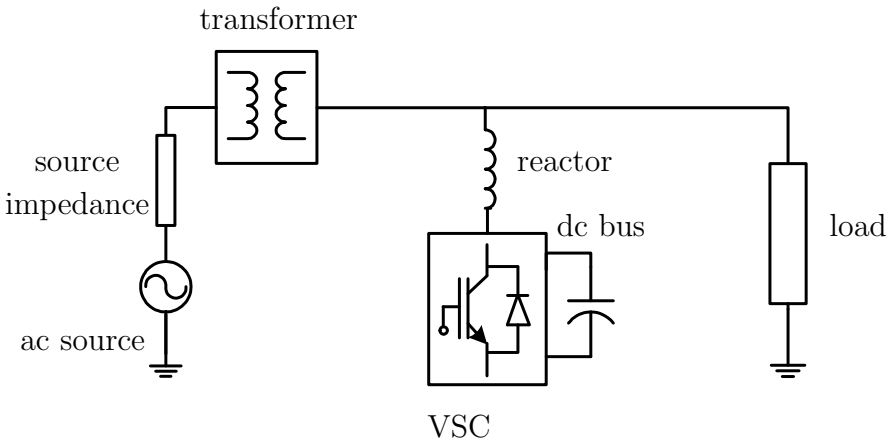

Figure 1.1: A shunt connected VSC system for STATCOM or APF applications

cations involving power flow and power quality improvement are PFC and harmonic elimination which are output tracking problems. The tracking outputs are reactive or q-axis current and dc voltage. In harmonic elimination, a d-axis current reference is required. A number of approaches have been taken to solve these tracking problems. A few approaches use some form of decoupled Proportional Integral (PI) control for currents and dc voltage dynamics [12, 13]. The benefits of traditional PI control and its alternatives are discussed in [14]. Many researchers have proposed alternatives to PI control, using flatness or passivity-based techniques, which can offer improved performance [15, 16, 17]. Some researchers exploit the time scale separation between the voltage and current dynamics in order to achieve a simpler decoupled design [13]. In order to facilitate controller tuning, improve transient and steady-state performance, other approaches directly compensate for system nonlinearity [15, 18, 19, 20, 21, 22]. Work in [19] shows that input-output state feedback linearization using dc voltage and q-axis current as tracking outputs leads to a non-minimum phase system. Taking the d- and q-axis currents as outputs the system is minimum phase and a PI control cascaded with the d-axis current control yields a robust tracking of constant dc voltage. In [23, 24] a control method is proposed for a third order VSC model. Work [23] considers a rectification application and applies Lyapunov stability results

to derive the control. The work assumes a constant dc load current so the controller is independent of circuit parameters. A nonlinear sliding mode control provides robustness to parameter uncertainty and dc load disturbances in [25]. Another approach exploits the differential flatness of the system and takes VSC energy and q-axis current as linearizing outputs [21]; this method has been experimentally validated in [22]. In [26] a Model Predictive Control scheme using a fast gradient method is proposed. Here, the optimization is fast enough to be performed in real time. Adaptive nonlinear control has been used to improve robustness to model error. In [27] a backstepping controller was developed for uncertainty in the resistance at the dc side. Lyapunov function-based adaptive control for a second order system model is considered in [28, 29]. Model Reference Adaptive Control (MRAC) was used for PFC in a second order single phase VSC with two unknown parameters [30]. In order to apply the MRAC, the second order nonlinear model is linearized around an equilibrium point.

Although the abovementioned methods can provide improved performance relative to classical PI methods, they can suffer from their complexity and difficulty of tuning. Ideally, a control design could provide a compromise between the simplicity of classical PI vector control and yet provide a robust performance guarantee to system uncertainty. This approach has been taken by a number of researchers by modifying vector control in order to rigourously improve its robust performance. For example, a methodology to design PI controllers for a large class of switched converters is in [31]. The main result is that if an affine nonlinear system is passified via a constant feedback control then it can be stabilized by a PI controller. Even the knowledge of the constant stabilizing feedback is not necessary for designing the PI controller. The technique is applied to a VSC feeding a dc load modeled as ideal current source. The method is extended for a larger class of converters with unknown dc loads in [32]. In work [33] the authors propose a multi-variable PI controller which improves decoupling of the d- and q-axis current dynamics.

1.2.2 VSC Modeling

The early work in [34] discussed control methods for current, power and voltage of a three phase VSC. The authors also provide some discussion regarding the VSC dynamic model. A four state model of VSC in the three phase coordinate was derived in [35, 36]. This model was time varying, nonlinear and included switching functions. The same authors improved their previous work in [37] with three modeling techniques including the Fourier series model to avoid switching functions. The use of the rotating frame transformation in VSC modeling was introduced, and a linearized model was derived.

The simplified time-average mathematical model of a VSC was first presented in [12] where the concept of VSC vector control was introduced. The proposed model was derived using phasors, Kirchhoff's laws and dc and ac side power balances. The third order average model made it possible to obtain transfer functions and derive vector control (PI) for the VSC.

Using the fourth order switched model of a three phase VSC which was presented in [35, 37], a third order mathematical switched model for a VSC in stationary and synchronous reference frames was developed in [38]. Complex vector notation was used in order to present the synchronous reference frame model. The VSC model based on real and reactive components of power was presented in [39]. The advantage of this model was that, unlike previous models, it does not rely on any particular reference frames and does not require Phase Lock Loop (PLL) angle.

1.3 Research Contribution

In this section a brief overview of the contributions made in this dissertation is presented.

1.3.1 Modeling

The VSC third order nonlinear system model which first appeared in [12] is considered in this thesis. This model has been used in several works to control the VSC, e.g. [16, 40]. Due to the dc voltage dynamics, the model is a bilinear

with a usual definition of input. With the definition of the new variables, a new VSC third order nonlinear dynamic model is presented in this thesis. This model considers system nonlinearity as a disturbance term Δ in the dc voltage dynamics. It is challenging to design an adaptive controller for the nonlinear VSC model with uncertainty in all circuit parameters. Therefore, a linear model whose dc voltage dynamics assumes no resistive losses on the ac side is also derived in this work. These losses are indirectly compensated using an effective dc side resistance. The relation between effective resistance and actual one is derived as a function of dc and ac side instantaneous real powers.

1.3.2 Power Factor Correction (PFC)

In this thesis different control techniques are developed to improve the VSC system robustness and tracking performance for PFC. In particular, the flatness-based control is reviewed and extended. In comparison with [16, 22], improved tracking accuracy in the presence of a dc load is also obtained through the newly generated references based on the steady state expressions for the system state.

Although vector control introduced in [12] has been widely used, its robustness to system uncertainty is of concern. To address this concern an adaptive PI vector control is proposed in this thesis. In particular, using a Lyapunov function method we modify the classic vector control in [12] to guarantee robust asymptotic tracking of the currents. Using a variable gradient method, a proof of asymptotic stability of the dc voltage tracking dynamics is given. The nonlinear average model of the VSC is used to investigate the controller performance in simulation. These simulations show that the inductance estimate converges to its real value and the controller achieves exact trajectory tracking in presence of a system parameter uncertainty. On the other hand, a classic vector controller's performance is sensitive to the inductance parameter variation. Experimental results obtained from a VSC test stand confirm the asymptotic stability of the tracking error. Remark that the term adaptive vector control has been used in different applications in the literature [41, 42, 43],

but they are mostly based on fuzzy, neural network, etc., and are different from adaptive PI vector control method proposed in this thesis.

If the ac side and dc side resistances are assumed unknown, the VSC nonlinear dynamics is a linearly parameterized dynamics which satisfied the linearization and parametric-pure-feedback conditions in [44, 45]. Therefore, an adaptive control for this uncertainty can be systematically designed with existing theory. In this thesis, a systematic adaptive control design procedure for a VSC with three unknown parameters is presented. It is shown that the parametric-pure-feedback condition for the nonlinear VSC model with all three unknown parameters is not satisfied, even for a linear approximate VSC model. An approximate linear model of the VSC is used to facilitate the adaptive design in this case. The convergence of the trajectory tracking error for the approximate model is proven. Nonlinear average and switched models of the VSC are employed to investigate controller performance in simulation. In particular, the simulations show that the steady-state dc side resistance estimate converges to a value which is consistent with the model error. This allows for a simpler design based on an approximate VSC model but yet achieves asymptotic trajectory tracking for the actual nonlinear model. The performance of the adaptive control is compared with a traditional vector control in simulation and experiment. The results confirm the asymptotic stability of the tracking error and the relative ease in controlling the transient closed loop performance.

1.3.3 Harmonic Compensation

A VSC can also be used as an Active Power Filter (APF) which compensates imbalance, harmonics, and reactive load current components. A PI based APF is presented in [13, 46]. The authors proposed the control for harmonic and reactive current compensation and dc voltage regulation. The closed loop control has two loops: an inner current loop and an outer dc voltage loop. Since the dc voltage in the capacitor is related to the amount of real current entering the VSC, it is indirectly controlled by d-axis current. A bias reference current for d-axis current is derived to ensure the VSC has good PFC. The

bias reference current is added to the harmonic reference current of the d-axis current loop to generate the reference current for the d-axis current dynamics. In this thesis, an adaptive current control method is proposed for the inner loop which improves system performance and robustness in the presence of the model error. In addition, with the definition of new variable $x_3 = \frac{C}{3v_d}v_{dc}^2$, a simpler expression for the dc voltage outer loop control is derived. Simulation results investigate the controllers' performance and show the benefits of the proposed adaptive method relative to the design in [13, 46].

1.4 Thesis Overview and Organization

This thesis consists of nine chapters

- Chapter 2: The operation of a VSC when sinusoidal pulse width modulation (SPWM) is used is reviewed. In particular, the relation between SPWM parameters and the VSC average output voltage is investigated. The chapter concludes with the mathematical models of the VSC in different coordinate systems. These models will be used in the next chapters for control design.

- Chapter 3: Classical vector control is introduced and simulation results are provided for the nonlinear and switched VSC models. A flatness-based control for the VSC is presented. With the assumption that the reference signals are constant, the steady state analysis of the VSC is provided. This steady state analysis is used to modify the d-axis current reference. Simulation of a time-varying q-axis current reference shows that for operating conditions where i_d is small, practical tracking of i_q and v_{dc} is possible. The flatness-based control depends on system parameters which are not known exactly. This motivates the investigation of adaptive controls which are presented in the next chapters.

- Chapter 4: First a literature review on relevant adaptive control methods is provided. The existing theory on adaptive control for nonlinear systems with linearly parameterized uncertainty is presented. The VSC

with two and three unknown parameters is used as an example to illustrate the established theory. It is shown that this theory is not applicable to the case of three unknown parameters.

- Chapter 5: An adaptive PI vector controller PFC is proposed. The method relies on a third order nonlinear model of the VSC which includes uncertainty in three system parameters i.e. the resistance and inductance of filter inductor and dc side resistance. The proposed method ensures asymptotic tracking of the q-axis current using an inner loop which contains two PI controllers with adaptive decoupling terms. An outer loop PI controller's output defines the reference for the d-axis current control. The asymptotic stability of the closed-loop is proven using Lyapunov's method. The performance of the proposed method is validated in simulation.

- Chapter 6: This chapter presents two adaptive designs which account for uncertainty in three circuit parameters. First an adaptive control consisting of two loops is considered: an adaptive current loop and PI dc voltage loop. Next, the so-called *full* adaptive control is presented. This design is termed *full* since there is no two loop structure in the design. The choice of adaptive controller gains is discussed using the linearized closed-loop dynamics. Finally, simulation validation demonstrates the full adaptive method's performance.

- Chapter 7: PI and an adaptive control techniques for the current control loop are presented. The dc voltage regulation with two different PI control methods is explained. The simulation results explore the controllers' performance and demonstrate the benefits of the adaptive control.

- Chapter 8: The experimental setup is described and experimental results are provided to check the performance of the vector control, adaptive PI vector control, and full adaptive control.

- Chapter 9: A summary of the research and some suggestions for future works are presented in this chapter.

Chapter 2

VSC Operation and Modeling

Understanding the mathematical model of a VSC is important for deriving its control or analysing its behaviour. This chapter presents the basic VSC setup and its method of operation when sinusoidal pulse width modulation (SPWM) is used. A number of time average models are presented in different coordinate frames.

2.1 Basic Method of Operation

The VSC system studied in this chapter is shown in Fig. 2.1. It contains six IGBTs, each having an anti-parallel diode to provide a path for current to flow when it is off. Each leg of the converter has two IGBTs operating in a complementary fashion, i.e., when the upper IGBT is on the lower IGBT switch is off. Since in practice simultaneous conduction of both switches in each VSC leg short-circuits the dc-link, a dead time between switching of the transistors for each leg is included. The VSC is connected to a point of common coupling (PCC) to a three-phase source and inductive load through filter inductors. This shunt configuration is shown in Fig. 2.6. The filter inductors reduce current harmonics from the VSC. The impedance of the each filter inductor, which also models IGBT conduction losses, is assumed balanced and equal to $R+j\omega L$, where ω is the ac source frequency. The point of common coupling (PCC) voltages are denoted v_a, v_b, v_c, the currents flowing into the converter are i_a, i_b, i_c, and the VSC terminal voltages are e_a, e_b, e_c. The VSC gating signals $g_1, \ldots, g_6$ are binary valued and generated by a Sinusoidal Pulse

Width Modulation (SPWM) scheme.

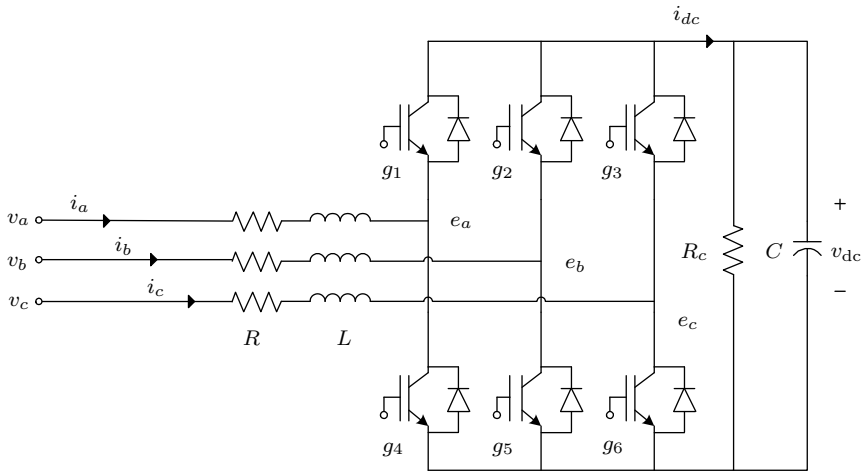

Figure 2.1: Circuit diagram of a VSC

2.1.1 Sinusoidal Pulse Width Modulation

The objective of Pulse Width Modulation (PWM) is to manipulate the low frequency components of the converter output voltage via high-frequency switching. There are several techniques used to drive the VSC gates e.g. sinusoidal PWM (SPWM), space vector PWM (SVPWM), selected harmonic PWM and delta modulation [47]. Three-phase SPWM signals are generated based on comparing a triangle carrier waveform with three-phase modulation signals. The modulation signals are phase shifted by $2\pi/3$ rad. and by δ relative to the ac source. Depending on whether a modulation signal is larger or smaller than the carrier waveform, different values of the instantaneous voltages appear at the VSC terminal voltages. Since the carrier waveform frequency is chosen significantly higher than the modulation signal frequency, the average output signal over a period of carrier waveform is proportional to the amplitude of the modulation signal during that period. The typical frequency of the carrier waveform for a VSC in PFC and APF applications is in the range $2--15$ kHz. The modulation frequency is in the range $50--60$ Hz. The VSC terminal voltages contain the desired fundamental frequency component as well as high frequency components near the carrier frequency.

Consider three-phase supply

$$\begin{aligned} v_a &= V_m \sin(\omega t) \\ v_b &= V_m \sin\left(\omega t - \frac{2\pi}{3}\right) \\ v_c &= V_m \sin\left(\omega t + \frac{2\pi}{3}\right) \end{aligned} \tag{2.1}$$

A three phase six pulse VSC has six switches to be controlled. Since the inputs of two switches in the same leg are complements of each other, and the inputs for switches in the third leg depends on the other two legs, there are effectively only two independent control signals to the VSC. We consider the following three-phase modulation signals

$$\begin{aligned} v_{ma} &= A_m \sin(\omega t + \delta) \\ v_{mb} &= A_m \sin\left(\omega t - \frac{2\pi}{3} + \delta\right) \\ v_{mc} &= A_m \sin\left(\omega t + \frac{2\pi}{3} + \delta\right) \end{aligned} \tag{2.2}$$

where δ is a phase shift relative to the ac source. If the amplitude of the triangle carrier is A_c, the ratio $m_a = A_m/A_c$ is known as amplitude modulation index. We can influence the amplitude and phases of the fundamental component of the VSC output voltages by varying m_a and δ. This control process works well for $0 \leq m_a \leq 1$. For $m_a > 1$ there are periods of the carrier waveform where it does not intersect the modulation signals. This case is known as over-modulation which is in general undesirable since it generates harmonic currents that degrade the VSC current control performance. Over-modulation increases the input to output transfer ratio at the expense of low order harmonics in the input currents and output voltages. Also, a drive with high-performance over-modulation range operating capability is less sensitive to dc voltage sag in the converter which can often happen with diode rectifier front ends [48, 49]. Typical modulation and over-modulation waveforms are shown in Fig. 2.2.

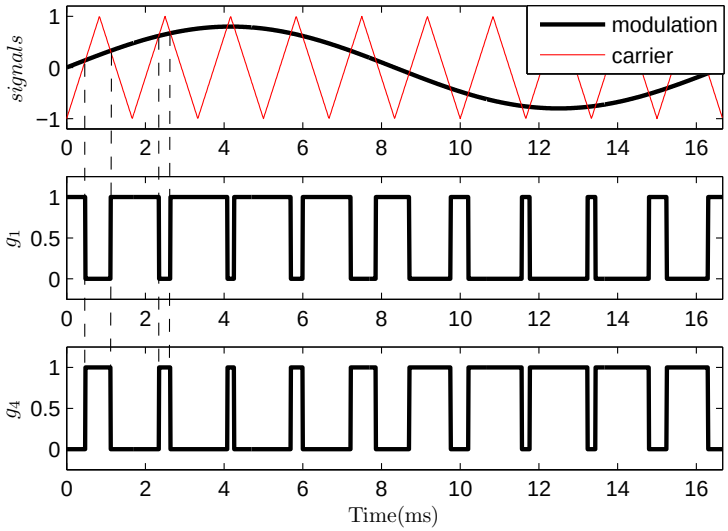

(a) Typical Modulation

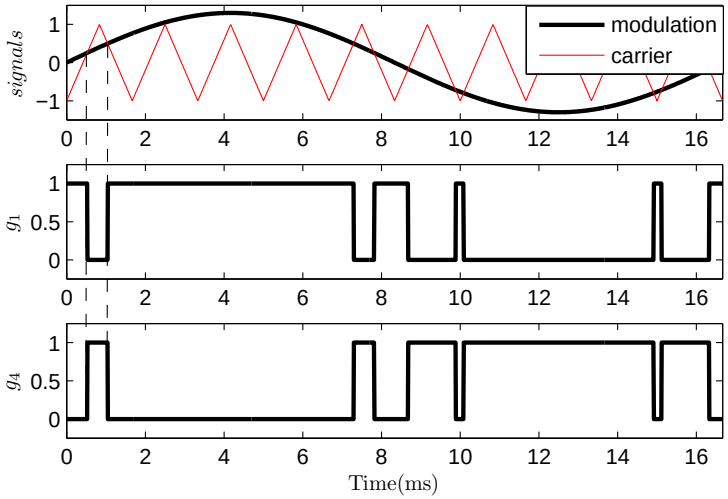

(b) Over-Modulation

Figure 2.2: The SPWM for each phase is generated by comparing the three-phase modulation signals with a carrier waveform. When the modulation signal is greater than the carrier waveform the SPWM output is high. When the modulation signal is lower than the carrier signal the SPWM output is low

2.1.2 Sinusoidal Pulse Width Modulation (SPWM) Spectra

The frequency spectra of a SPWM with $n = f_c/f_m = 15$ and $m_a = 0.8$ is shown in Fig. 2.3 in which f_c and f_m stand for the carrier and modulation signal frequencies respectively. Evidently the dominant harmonics for the SPWM waveform other than the fundamental component is of order n and $n \pm 2$. Since in a typical operation of the VSC n is large, the inductor filter on the ac side should be designed to reduce these high order harmonic components in the VSC output currents. Therefore, the inductance value is chosen based on output current ripple and fundamental current flow.

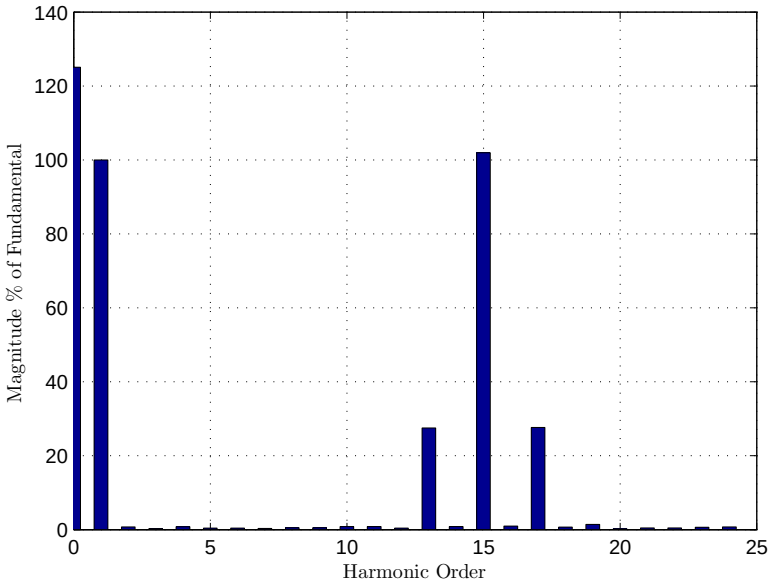

Figure 2.3: SPWM harmonic spectra for $n = 15$ and $m_a = 0.8$

2.1.3 VSC ac Terminals Voltage Average Values

In this section, the fundamental frequency components of the VSC output voltages are obtained and their relationship with the modulation index m_a and phase shift δ is investigated. There are eight possible switching configurations for (g_1, g_2, g_3) and hence (g_4, g_5, g_6). Using circuit analysis the corresponding VSC output voltages for each switching configuration is obtained. For example

for $(g_1, g_2, g_3) = (1, 1, 0)$, using Kirchhoff's voltage law in Fig. 2.6

$$e_a = e_b, \quad e_b - e_c = v_{dc} \tag{2.3}$$

If we assume balanced line filter impedance and a balanced source then

$$e_a + e_b + e_c = 0 \tag{2.4}$$

results $e_a = v_{dc}/3$, $e_b = v_{dc}/3$ and $e_c = -2v_{dc}/3$. All possible configuration results are shown in Table 2.1.

$\{g_1\ g_2\ g_3\}$	$\{g_4\ g_5\ g_6\}$	e_a	e_b	e_c
$\{1\ 1\ 1\}$	$\{0\ 0\ 0\}$	0	0	0
$\{1\ 1\ 0\}$	$\{0\ 0\ 1\}$	$v_{dc}/3$	$v_{dc}/3$	$-2v_{dc}/3$
$\{1\ 0\ 1\}$	$\{0\ 1\ 0\}$	$v_{dc}/3$	$-2v_{dc}/3$	$v_{dc}/3$
$\{1\ 0\ 0\}$	$\{0\ 1\ 1\}$	$2v_{dc}/3$	$-v_{dc}/3$	$-v_{dc}/3$
$\{0\ 1\ 1\}$	$\{1\ 0\ 0\}$	$-2v_{dc}/3$	$v_{dc}/3$	$v_{dc}/3$
$\{0\ 1\ 0\}$	$\{1\ 0\ 1\}$	$-v_{dc}/3$	$2v_{dc}/3$	$-v_{dc}/3$
$\{0\ 0\ 1\}$	$\{1\ 1\ 0\}$	$-v_{dc}/3$	$-v_{dc}/3$	$2v_{dc}/3$
$\{0\ 0\ 0\}$	$\{1\ 1\ 1\}$	0	0	0

Table 2.1: The VSC output voltages for the different PWM switch configurations. The terminal voltages take on the discrete values $\pm 2v_{dc}/3, \pm v_{dc}/3, 0$.

The magnitude and frequency of the triangle carrier wave is fixed. Hence, the state of switches is controlled by m_a and δ. The control sampling frequency f_s is equal to f_c or $2f_c$. This means the three-phase modulation signals are constant during half period of the carrier waveform. In each period of the carrier, there are six possible switch configurations for v_{ma}, v_{mb} and v_{mc} based on their magnitudes. These six possibilities are shown in Fig. 2.4. We consider only the region where $v_{ma} \geq v_{mb} \geq v_{mc}$. The results can be easily extended to other regions.

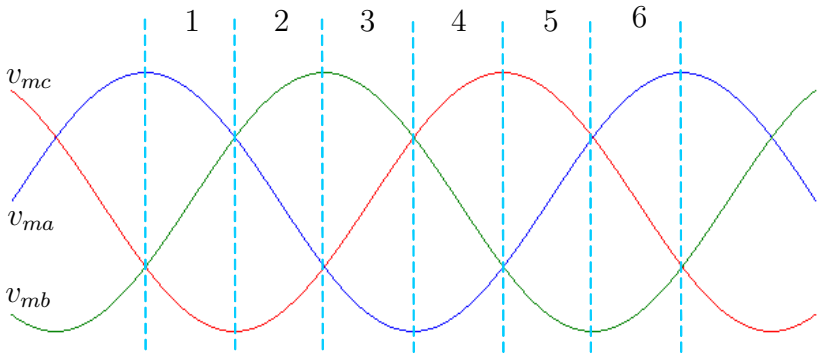

Figure 2.4: Three phase modulation signals in one period with 6 regions based on their relative magnitudes

The pulses of e_a for a half period of carrier wave in region 1 is shown in Fig. 2.5. Four switchings occur on this period. If, for simplicity, we assume the carrier wave A_c magnitude is 1, the average value for e_a is

$$\begin{aligned} e_a &= \frac{1 - v_{ma}}{2} \cdot 0 + \frac{v_{ma} - v_{mb}}{2} \cdot \frac{2v_{dc}}{3} + \frac{v_{mb} - v_{mc}}{2} \cdot \frac{v_{dc}}{3} + \frac{v_{mc} + 1}{2} \cdot 0 \\ &= \frac{v_{dc}}{6}(2v_{ma} - v_{mb} - v_{mc}) \end{aligned} \tag{2.5}$$

With similar analysis, e_b and e_c for region 1 are obtained as

$$\begin{aligned} e_b &= \frac{v_{dc}}{6}(-v_{ma} + 2v_{mb} - v_{mc}) \\ e_c &= \frac{v_{dc}}{6}(-v_{ma} - v_{mb} + 2v_{mc}) \end{aligned} \tag{2.6}$$

It can be shown that the expressions for e_a, e_b and e_c for other regions are the same as (2.5) and (2.6). The detailed of the derivation of these expressions for other regions is in [16]. With the assumption of $A_c = 1$, substituting the

modulation signals (2.2) into (2.5) and (2.6) gives

$$\begin{aligned} e_a &= \frac{1}{2} v_{dc} m_a \sin(\omega t + \delta) \\ e_b &= \frac{1}{2} v_{dc} m_a \sin\left(\omega t + \delta - \frac{2\pi}{3}\right) \\ e_c &= \frac{1}{2} v_{dc} m_a \sin\left(\omega t + \delta + \frac{2\pi}{3}\right) \end{aligned} \tag{2.7}$$

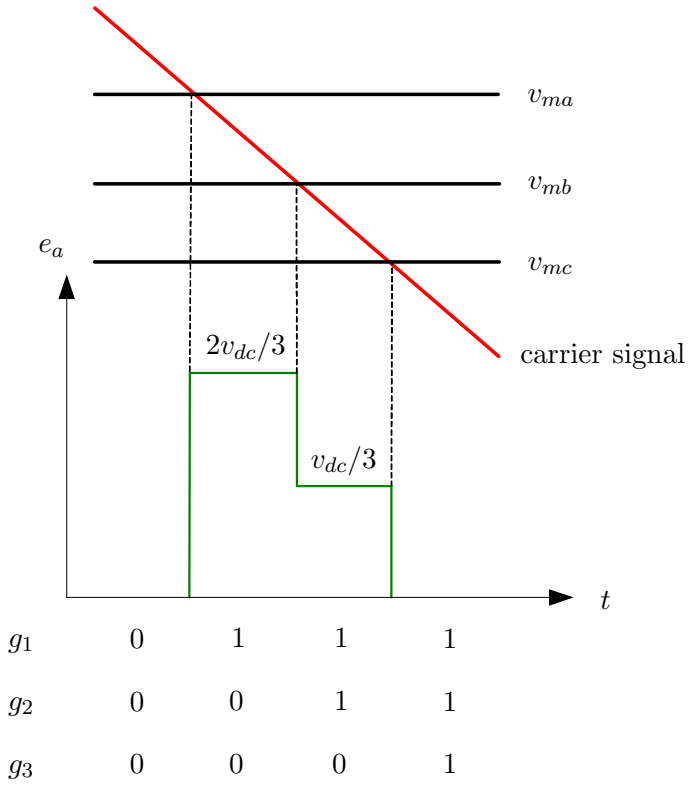

Figure 2.5: The e_a value for a half switching period when the VSC operates in region 1 i.e., $v_{ma} \geq v_{mb} \geq v_{mc}$. There are four switching configurations three IGBT state values during this half carrier period

2.2 Reference Frame Theory and Transformation

The introduction of reference frame theory was a significant breakthrough in the analysis of the three-phase systems. Reference frames transform the

system's variables from the abc coordinate to a new coordinate which simplifies the system's dynamics.

Consider a balanced three phase sinusoidal vector $f_{abc} = (f_a, f_b, f_c)^T$ with

$$\begin{aligned} f_a &= F\sin(\omega t + \phi) \\ f_b &= F\sin\left(\omega t + \phi - \frac{2\pi}{3}\right) \\ f_c &= F\sin\left(\omega t + \phi + \frac{2\pi}{3}\right) \end{aligned} \tag{2.8}$$

where F, ω and ϕ are the amplitude, angular velocity and constant phase of the f_{abc}. We consider the constant matrix

$$S = \frac{2}{3}\begin{bmatrix} 1 & -\frac{1}{2} & -\frac{1}{2} \\ 0 & \frac{\sqrt{3}}{2} & -\frac{\sqrt{3}}{2} \\ \frac{1}{2} & \frac{1}{2} & \frac{1}{2} \end{bmatrix}$$

The linear transformation $f_{\alpha\beta 0} = S \cdot f_{abc}$ is called the stationary reference frame transformation (SRT) or Clark Transformation. Substitution of (2.8) into $f_{\alpha\beta 0} = S \cdot f_{abc}$, $f_{\alpha\beta 0}$ gives

$$f_{\alpha\beta 0} = F\begin{bmatrix} \sin(\omega t + \phi) \\ -\cos(\omega t + \phi) \\ 0 \end{bmatrix} \tag{2.9}$$

That is, the components of $f_{\alpha\beta 0}$ in phasor form are $F_\alpha = F\angle\phi$, $F_\beta = F\angle(\phi - \pi/2)$ and $F_0 = 0$.

Next we define $R(\omega t)$ which is a rotation about the third axis

$$R(\omega t) = \begin{bmatrix} \sin(\omega t + \phi_0) & -\cos(\omega t + \phi_0) & 0 \\ \cos(\omega t + \phi_0) & \sin(\omega t + \phi_0) & 0 \\ 0 & 0 & 1 \end{bmatrix}$$

The matrix $R(\omega t)$ transforms the vector $f_{\alpha\beta 0}$ to a constant f_{dqo} given by

$$f_{dqo} = R(\omega t) \cdot S \cdot f_{abc} = F\begin{bmatrix} \cos(\phi - \phi_0) \\ \sin(\phi - \phi_0) \\ 0 \end{bmatrix}$$

We remark that when $\phi = \phi_0$ the d-axis component of f_{dqo} is the amplitude of the variable in the abc frame and the q-axis component is zero. Therefore, in a

balanced three-phase system the dqo transformation of the three phase time-varying quantities results in constants and this leads to a simplified system analysis. The transformation which maps the phasors from abc to dqo is given by

$$K(t) = R(\omega t)\cdot S = \frac{2}{3}\begin{bmatrix} \sin(\omega t+\phi_o) & \sin(\omega t+\phi_o-\frac{2\pi}{3}) & \sin(\omega t+\phi_o+\frac{2\pi}{3}) \\ \cos(\omega t+\phi_o) & \cos(\omega t+\phi_o-\frac{2\pi}{3}) & \cos(\omega t+\phi_o+\frac{2\pi}{3}) \\ \frac{1}{2} & \frac{1}{2} & \frac{1}{2} \end{bmatrix} \tag{2.10}$$

This linear transformation is called the Park Transformation or synchronous rotating reference frame transformation (RFT) matrix [50].

2.3 VSC Modeling

2.3.1 Nonlinear Model

Fig. 2.6 shows a typical application of a VSC where the ac source currents are i_{sa}, i_{sb}, i_{sc}.

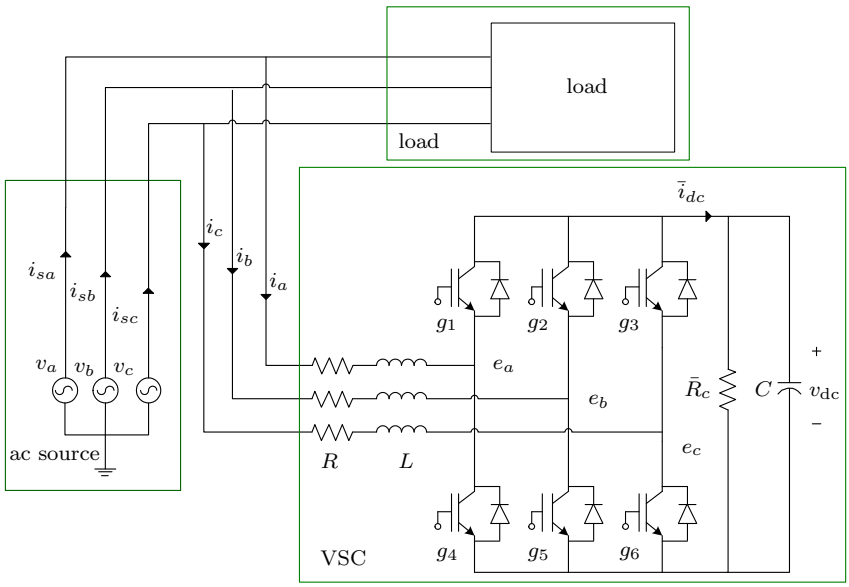

Figure 2.6: A typical shunt configuration of a VSC in a three-phase power system

The VSC current dynamics can be written as

$$\begin{aligned} L\frac{di_a}{dt} + Ri_a &= v_a - e_a \\ L\frac{di_b}{dt} + Ri_b &= v_b - e_b \\ L\frac{di_c}{dt} + Ri_c &= v_c - e_c \end{aligned} \tag{2.11}$$

As in [39], the power balance between the dc and ac sides of the VSC is

$$p - P_Z = v_{dc}\bar{i}_{dc} \tag{2.12}$$

where p is the instantaneous power into the VSC at the PCC, P_Z is the instantaneous power dissipated in the impedance $R + j\omega L$, and $\bar{i}_{dc}$ is the dc side current which related to dc voltage v_{dc} by

$$\bar{i}_{dc} - \frac{v_{dc}}{\bar{R}_c} = C\frac{dv_{dc}}{dt} \tag{2.13}$$

where the capacitor resistance and switching losses are lumped into $\bar{R}_c$ [51]. From (2.12) and (2.13) we have

$$\frac{dv_{dc}}{dt} = \frac{p - P_Z}{Cv_{dc}} - \frac{v_{dc}}{C\bar{R}_c} \tag{2.14}$$

The expressions for p and P_Z are

$$\begin{aligned} p &= v_a i_a + v_b i_b + v_c i_c \\ P_Z &= \underbrace{R(i_a^2 + i_b^2 + i_c^2)}_{P_R} + \underbrace{L\left(i_a\frac{di_a}{dt} + i_b\frac{di_b}{dt} + i_c\frac{di_c}{dt}\right)}_{P_L} \end{aligned}$$

where P_R and P_L are resistance and inductor powers, respectively.

The synchronously rotating reference frame transformation discussed in Section 2.2 is used to express the system equations in dqo frame which is more convenient for control design. From (2.10) with $\phi_0 = 0$ we perform the transformations $(i_d, i_q, i_o)^T = K \cdot (i_a, i_b, i_c)^T$ and $(v_d, v_q, v_o)^T = K \cdot (v_a, v_b, v_c)^T$.

If we substitute (2.7) into (2.11) and apply the synchronous reference frame transformation (2.10) then we have

$$\begin{aligned} \frac{di_d}{dt} &= -\frac{R}{L}i_d + \omega i_q + \frac{v_d}{L} - \frac{e_d}{L} \\ \frac{di_q}{dt} &= -\frac{R}{L}i_q - \omega i_d + \frac{v_q}{L} - \frac{e_q}{L} \end{aligned} \tag{2.15}$$

where v_d and v_q are d- and q-axis components of the ac source voltage. The VSC terminal voltages are denoted by e_d and e_q and given by

$$e_d = \frac{1}{2} v_{dc} m_a \cos\delta, \quad e_q = \frac{1}{2} v_{dc} m_a \sin\delta \tag{2.16}$$

Note that if the ac supply is assumed balanced, the q-axis source voltage v_q is zero.

The differential equation for dc voltage in dqo frame can be obtained by applying the RFT to (2.14)

$$\frac{dv_{dc}}{dt} = \frac{3}{2} \cdot \frac{v_d i_d + v_q i_q}{C v_{dc}} - \frac{v_{dc}}{C\bar{R}_c} - \frac{P_Z}{C v_{dc}} \tag{2.17}$$

where the expression for P_Z in dqo frame is

$$P_Z(x,u) = P_R(x) + P_L(x,u)$$

with

$$P_R = \frac{3}{2} R(i_d^2 + i_q^2), \quad P_L = \frac{3}{2} L \left(i_d \frac{di_d}{dt} + i_q \frac{di_q}{dt} \right)$$

From (2.15) and (2.17) we have

$$\begin{aligned} \frac{di_d}{dt} &= -\frac{R}{L} i_d + \omega i_q + \frac{v_d}{L} - \frac{e_d}{L} \\ \frac{di_q}{dt} &= -\frac{R}{L} i_q - \omega i_d + \frac{v_q}{L} - \frac{e_q}{L} \\ \frac{dv_{dc}}{dt} &= \frac{3}{2} \cdot \frac{v_d i_d + v_q i_q}{C v_{dc}} - \frac{v_{dc}}{C\bar{R}_c} - \frac{P_Z}{C v_{dc}} \end{aligned} \tag{2.18}$$

Since the fundamental component of the VSC terminal voltage has an amplitude of $v_{dc} m_a/2$, the dc voltage must be controlled so that $v_{dc} > 2v_d$ to ensure proper VSC operation and bidirectional power flow. In other words the maximum amplitude of VSC terminal voltages must be more than the amplitude of the PCC voltage.

We rewrite the power balance between the dc and ac sides of the converter as

$$i_a e_a + i_b e_b + i_c e_c = v_{dc} \bar{i}_{dc} \tag{2.19}$$

Therefore, from the equations (2.19) and (2.13) we have

$$\frac{dv_{dc}}{dt} = \frac{i_a e_a + i_b e_b + i_c e_c}{C v_{dc}} - \frac{v_{dc}}{C\bar{R}_c} \tag{2.20}$$

The differential equation for dc voltage in the dq frame can be obtained by applying the RFT to (2.20)

$$\frac{dv_{dc}}{dt} = \frac{3}{2} \cdot \frac{e_d i_d + e_q i_q}{C v_{dc}} - \frac{v_{dc}}{C \bar{R}_c} \tag{2.21}$$

From (2.15) and (2.21) we have

$$\begin{aligned} \frac{di_d}{dt} &= -\frac{R}{L} i_d + \omega i_q + \frac{v_d}{L} - \frac{e_d}{L} \\ \frac{di_q}{dt} &= -\frac{R}{L} i_q - \omega i_d + \frac{v_q}{L} - \frac{e_q}{L} \\ \frac{dv_{dc}}{dt} &= \frac{3}{2} \cdot \frac{e_d i_d + e_q i_q}{C v_{dc}} - \frac{v_{dc}}{C \bar{R}_c} \end{aligned} \tag{2.22}$$

2.3.2 Linear Model

We define the input $u = (u_1, u_2)^T$ as

$$u_1 = v_d - e_d, \quad u_2 = v_q - e_q$$

and the state as $x = (x_1, x_2, x_3)^T = (i_d, i_q, \frac{C}{3v_d} v_{dc}^2)^T$. With the new choices of the state and input dynamics (2.18) can be written

$$\dot{x} = \bar{A}x + Bu + \Delta(x, u) \tag{2.23}$$

with

$$\bar{A} = \begin{bmatrix} -R/L & \omega & 0 \\ -\omega & -R/L & 0 \\ 1 & v_q/v_d & -2/(C\bar{R}_c) \end{bmatrix}, B = \begin{bmatrix} 1/L & 0 \\ 0 & 1/L \\ 0 & 0 \end{bmatrix},$$

$$\Delta(x, u) = \begin{bmatrix} 0 & 0 & -\frac{2P_Z(x,u)}{3v_d} \end{bmatrix}^T$$

P_Z can be expressed as a function of u

$$P_Z(x, u) = P_R(x) + P_L(x, u) = \frac{3}{2}(u_1 i_d + u_2 i_q)$$

Since the VSC system is assumed balanced, it can be shown that P_L is negligible and P_R is almost constant. The effect of ac side resistor losses P_R can be included in the effective dc side resistance denoted R_c. Then, (2.12) and (2.14) can be replaced with

$$p = v_{dc} i_{dc} \tag{2.24}$$

and

$$\frac{dv_{dc}}{dt} = \frac{p}{Cv_{dc}} - \frac{v_{dc}}{CR_c} \tag{2.25}$$

We remove the overbar from R_c and i_{dc} in (2.24) to emphasize they can be different from $\bar{R}_c$ and $\bar{i}_{dc}$ as they relate to a different VSC model.

After transforming (2.25) into dq frame, the VSC dynamics is

$$\dot{x} = Ax + Bu \tag{2.26}$$

where

$$A = \begin{bmatrix} -R/L & \omega & 0 \\ -\omega & -R/L & 0 \\ 1 & v_q/v_q & -2/(CR_c) \end{bmatrix}$$

Comparison of (2.25) with (2.22) gives

$$\frac{v_{dc}}{CR_c} - \frac{v_{dc}}{C\bar{R}_c} = \frac{P_Z}{Cv_{dc}}$$

Since we assume that P_L is negligible, $P_Z = P_R = \frac{3}{2}R(i_d^2 + i_q^2)$. Therefore, We can express the relation between R_c and $\bar{R}_c$ using

$$v_{dc}^2 \left(\frac{1}{R_c} - \frac{1}{\bar{R}_c} \right) = \frac{3}{2} R(i_d^2 + i_q^2) \tag{2.27}$$

Solving (2.27) for R_c gives

$$\begin{aligned} R_c &= \left(1 + \frac{3R(i_d^2 + i_q^2)}{2v_{dc}^2} \bar{R}_c \right)^{-1} \bar{R}_c \\ &= \frac{\bar{R}_c}{1 + P_R/P_{DC}} \end{aligned} \tag{2.28}$$

where $P_{DC} = v_{dc}^2/\bar{R}_c$ is the power losses of the dc side resistance $\bar{R}_c$.

2.4 Summary

In this chapter, the VSC basic operation is reviewed. A third order nonlinear mathematical model for a VSC in presented. Finally, a linear model is proposed in which ac side resistor losses are included in the effective dc side resistance. In the next chapters, the nonlinear model is used to design the flatness-based control. It will be shown that the nonlinear model can not be used for designing an adaptive control with three unknown VSC parameters. On the other hand, the linear model can be used.

Chapter 3

Power Factor Correction with Known Parameters

This chapter describes two control methods used for PFC. Both designs assume all system parameters are known. The chapter is organized as follows: in section 3.1, the classical vector control method is reviewed. The simulation results for this control applied to the nonlinear and switched models of the VSC are given in section 3.2. A flatness-based control is presented in section 3.3. Assuming reference signals for q-axis current and dc voltage are constant, the steady state analysis of the VSC is discussed in section 3.5. In the last section, we use this steady state relation to define the d-axis current reference of the flatness-based control.

3.1 Classical Vector Control of a VSC

From (2.21), the nonlinear model of the VSC in dq frame is

$$\begin{aligned}
\frac{di_d}{dt} &= -\frac{R}{L}i_d + \omega i_q + \frac{v_d}{L} - \frac{e_d}{L} \\
\frac{di_q}{dt} &= -\frac{R}{L}i_q - \omega i_d + \frac{v_q}{L} - \frac{e_q}{L} \\
\frac{dv_{dc}}{dt} &= \frac{3}{2}\cdot\frac{e_d i_d + e_q i_q}{C v_{dc}} - \frac{v_{dc}}{C R_c}
\end{aligned} \tag{3.1}$$

where R_c is used instead of $\bar{R}_c$ for simplicity. Defining e_d and e_q as

$$\begin{aligned}
e_d &= v_d + L(\omega i_q - p_1) \\
e_q &= v_q + L(-\omega i_d - p_2)
\end{aligned} \tag{3.2}$$

where p_1 and p_2 are the outputs from the PI compensators of i_d and i_q, respectively. Substituting (3.2) into the current dynamics in (3.1) gives the decoupled equations

$$\begin{aligned} \frac{di_d}{dt} &= -\frac{R}{L}i_d + p_1 \\ \frac{di_q}{dt} &= -\frac{R}{L}i_q + p_2 \end{aligned} \tag{3.3}$$

Hence, we can easily independently control i_d and i_q. We consider the PI feedback

$$\begin{aligned} p_1 &= k_{p_d}(i_d^* - i_d) + k_{i_d}\int_0^t (i_d^* - i_d)d\tau \\ p_2 &= k_{p_q}(i_q^* - i_q) + k_{i_q}\int_0^t (i_q^* - i_q)d\tau \end{aligned} \tag{3.4}$$

where $(\cdot)^*$ denotes a desired reference value. In frequency domain we have

$$\begin{aligned} P_1(s) &= \left(k_{p_d} + \frac{k_{i_d}}{s}\right)(I_d^* - I_d) \\ P_2(s) &= \left(k_{p_q} + \frac{k_{i_q}}{s}\right)(I_q^* - I_q) \end{aligned} \tag{3.5}$$

From (3.3) and (3.4), the closed-loop transfer functions of current dynamics are

$$\frac{I_d}{I_d^*} = \frac{k_{p_d}s + k_{i_d}}{s^2 + (R/L + k_{p_d})s + k_{i_d}} \tag{3.6}$$

and

$$\frac{I_q}{I_q^*} = \frac{k_{p_q}s + k_{i_q}}{s^2 + (R/L + k_{p_q})s + k_{i_q}} \tag{3.7}$$

The choice of parameters for the vector control gains are straightforward. Since (3.6) and (3.7) are second order linear transfer functions, their outputs can not track time varying references. Therefore, if i_d^* and i_q^* are considered to be constant, then the above two equations represent second order systems with undamped natural frequencies $\omega_{nd} = \sqrt{k_{i_d}}$ and $\omega_{nq} = \sqrt{k_{i_q}}$, damping ratios $\zeta_d = (R/L + k_{p_d})/(2\sqrt{k_{i_d}})$ and $\zeta_q = (R/L + k_{p_q})/(2\sqrt{k_{i_q}})$, respectively.

In some works, filters are also used to cancel the closed-loop zeros [13]. For PFC the basic requirement is that i_q tracks the load reactive current i_q^*. At the same time the controller should force v_{dc} to track a constant reference v_{dc}^*. In designing the controller for the dc voltage dynamics, it is assumed that the dc voltage varies on a slower time scale than the d-axis current. That is,

when designing the control for dc voltage we assume i_d tracks its reference i_d^* perfectly. Since dc voltage of the capacitor is related to the amount of real current entering the VSC, dc voltage is indirectly controlled by d-axis current i_d. The output of the PI compensator for dc voltage is

$$I_d^*(s) = \left(k_{p_v} + \frac{k_{i_v}}{s}\right)(v_{dc}^* - V_{dc}) \tag{3.8}$$

The block diagram of the vector control is given in Fig. 3.1. The PI gains in

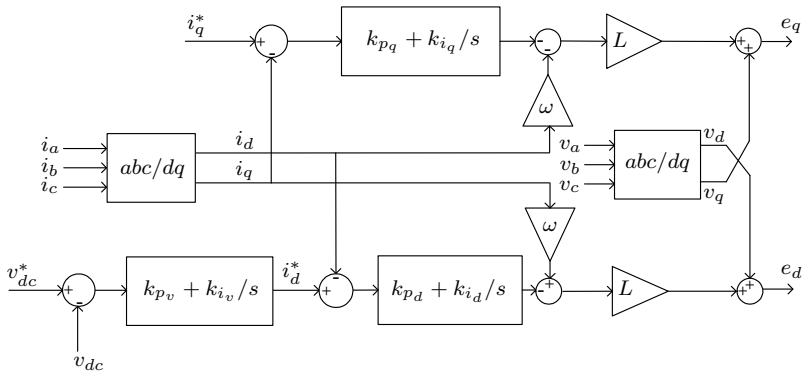

Figure 3.1: Block diagram of traditional vector control

the dc voltage loop are taken sufficiently lower in magnitude than those in the current loops. The PI gains for the dc voltage loop can also be obtained from the transfer function of the dc voltage dynamics [13].

3.2 Simulation Results

A number of simulations of the vector control are performed in MATLAB/Simulink. The control is applied to the third order nonlinear model (3.1) and a nonlinear switched model of the VSC based on (3.1) and Simulink's SimPowerSystems Library. The q-axis current reference varies between -3 A and 3 A, and the dc voltage reference changes between 170 V and 200 V. The references change levels at different times. We remark that the ac load is not included unless otherwise mentioned.

3.2.1 Nonlinear Average Model

As shown in Figs. 3.2–3.4, the vector control achieves good tracking performance with control inputs within their bounds. The transient performance of the tracking error has a fast rise and settling time and zero steady-state error is achieved. The system parameters and controller gains are provided in Tables 3.1 and 3.2, respectively. We have chosen the controller parameters to ensure that the current dynamics is 10 times faster than dc voltage dynamics.

Parameters	Value
L	2 mH
C	1100 μF
R	0.21 Ω
R_c	1.45 kΩ
ω	120π rad/s
T	100 μs
v_d	60 V
v_q	0 V

Table 3.1: Nominal parameters used in simulation

Gains	Value
(k_{dp}, k_{di})	(2 V/A, 100 V/(A.s))
(k_{qp}, k_{qi})	(4000 V/A, 30000 V/(A.s))
(k_{vp}, k_{vi})	(1 A/V, 5 A/(V.s))

Table 3.2: Vector controller gains used in simulation

3.2.2 Switched Model

To further verify the VSC vector control performance, simulation results of the control applied to the switched model of the VSC are provided. Since the q-axis and dc voltage references are constant in these simulations, the VSC states converge to constant steady state values. From Figs. 3.5–3.7, the q-axis current and dc voltage track their references with good transient and steady state performances. The control inputs also vary in their unsaturated ranges. Since the q-axis current dynamics is decoupled from d-axis current dynamics,

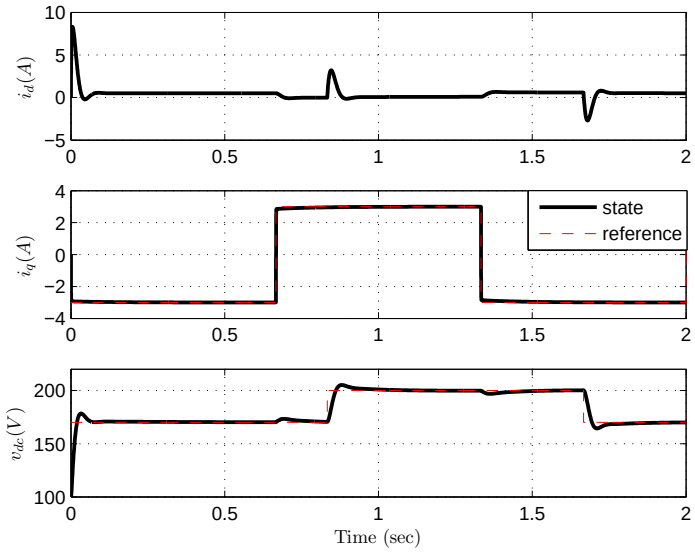

Figure 3.2: Simulation results of VSC vector control using nonlinear model: VSC state and desired reference trajectories

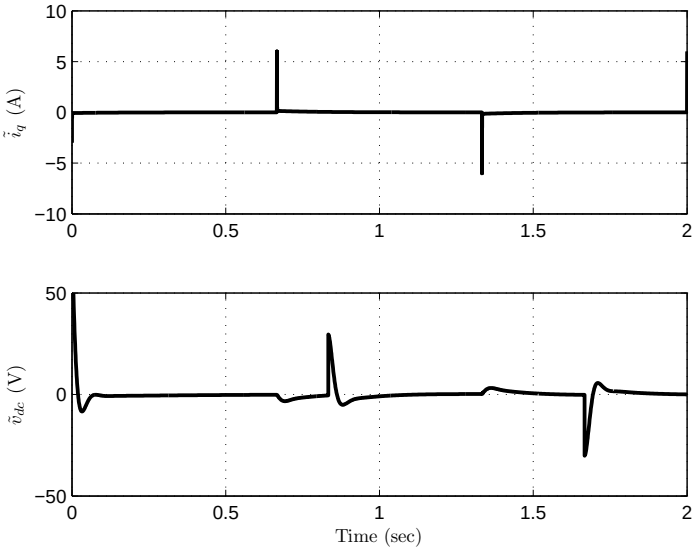

Figure 3.3: Simulation results of VSC vector control using nonlinear model: trajectory of tracking error

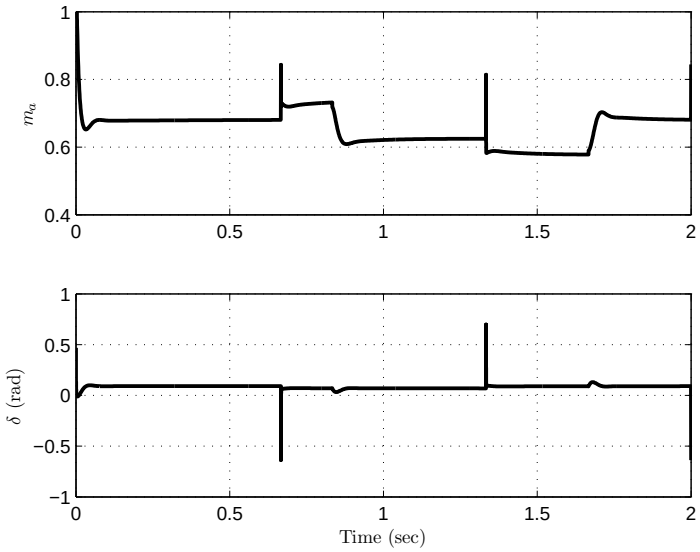

Figure 3.4: Simulation results of VSC vector control using nonlinear model: control inputs m_a and δ

any change in the dc voltage reference trajectory will not affect the q-axis current trajectory. We remark that the filtered results are provided to show the VSC outputs without high frequency components and to verify that the VSC q-axis current and dc voltage converge to their references. The utilized filters are first order low pass with cut-off frequency of $\omega_c = 1500$ rad/s.

3.2.3 Switched Model and Imbalanced Source

The performance of the vector control for an imbalanced ac source is considered. We introduce a phase shift of $\pi/8$ in phase-a of the source. Graphs of the VSC state, tracking error and control input are given in Figs. 3.8–3.10. The results demonstrate the control's ability to reject the effect of the source imbalance. A close-up view of the control signals is shown in Fig. 3.11. The control inputs also contain sinusoidal components with frequency twice the ac source frequency; this effectively compensates for the sinusoidal v_{dqo}. Note that the v_o component in the dqo frame is non-zero and also v_d and v_q have sinusoidal components with frequency twice that of the source's fundamental.

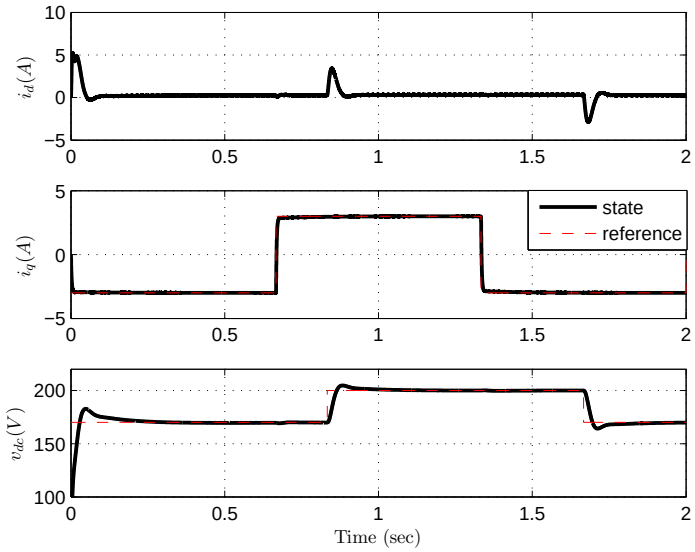

Figure 3.5: Simulation of the vector control with switched model: VSC state and desired reference trajectories

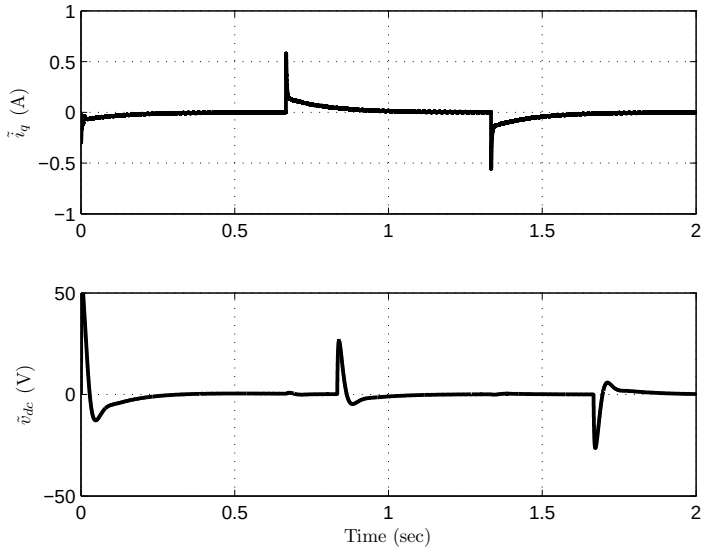

Figure 3.6: Simulation of the vector control with switched model: trajectory tracking error

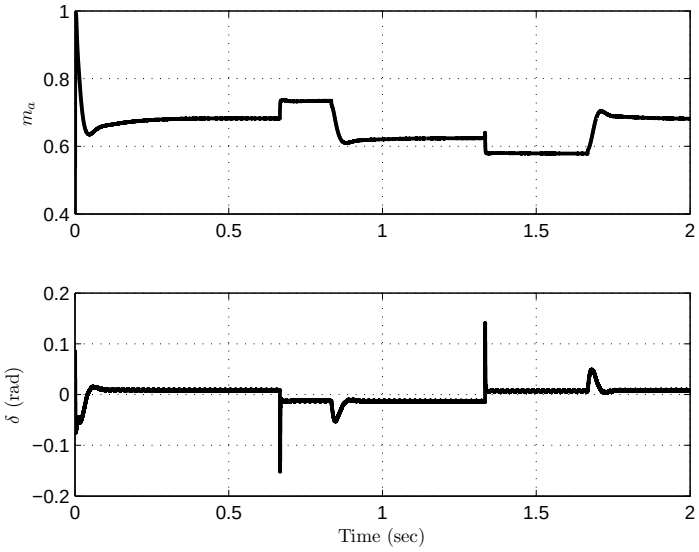

Figure 3.7: Simulation results of the vector control with switched model: control inputs m_a and δ

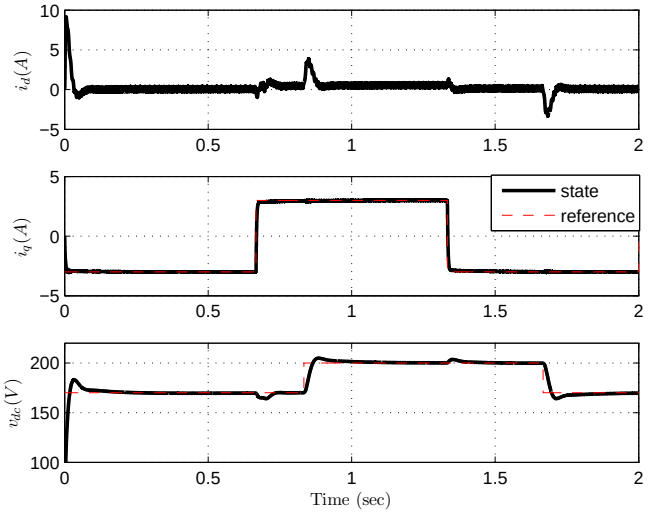

Figure 3.8: Simulation results of the VSC vector control VSC switched model and imbalanced ac source: VSC state and desired reference

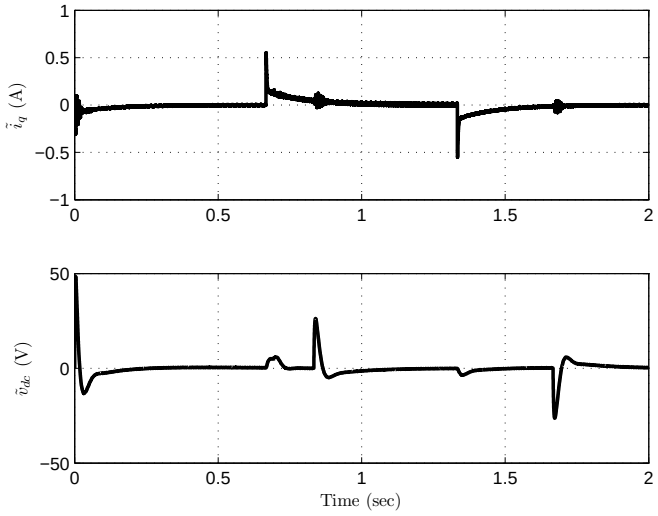

Figure 3.9: Simulation results of the VSC vector control with switched model and imbalanced ac source: trajectory tracking error

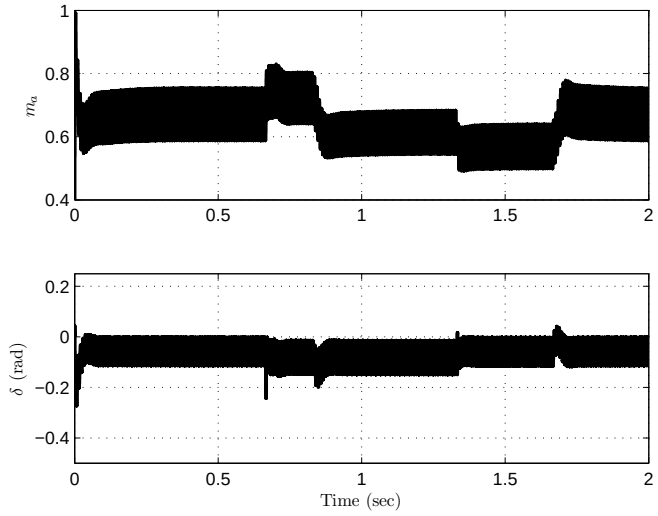

Figure 3.10: Simulation results of the VSC vector control with switched model and imbalanced ac source: control inputs m_a and δ

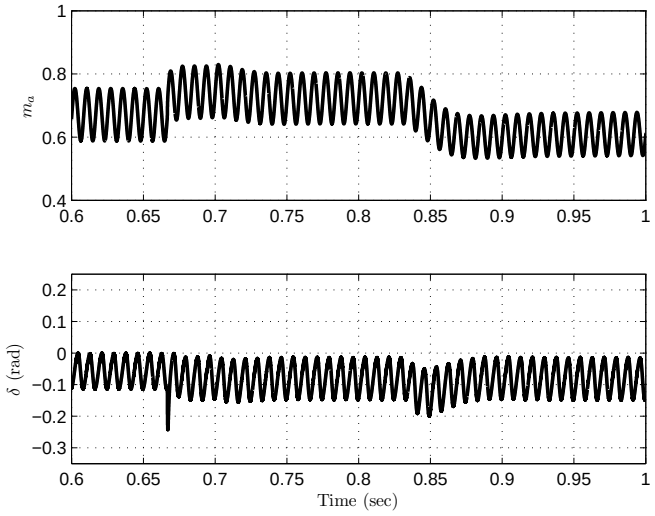

Figure 3.11: Simulation results of the VSC vector control with switched model and imbalanced ac source

3.3 Flatness-based Control of a VSC

Flat or feedback linearizable systems are a special class of nonlinear systems whose structure allows for simple solutions to output tracking and motion planning [52, 53]. A necessary condition for feedback linearization and flatness is that an n-state m-input nonlinear system

$$\dot{x} = f(x) + \sum_{i=1}^{m} g_i(x)u_i, \quad x \in \mathbb{R}^n, \tag{3.9}$$

is controllable. Adopting the standard differential geometric notation in [54, 55] we define controllability using *controllability indices* $\{k_1, \ldots, k_m\}$ which are defined as

$$k_i = \text{card}\{m_j \geq i : j \geq 0\}, \quad 1 \leq i \leq m,$$

where

$$\begin{aligned} m_0 &= \text{rank } \mathcal{G}_0 \\ m_1 &= \text{rank } \mathcal{G}_1 - \text{rank } \mathcal{G}_0 \\ &= \vdots \\ m_{n-1} &= \text{rank}\, \mathcal{G}_{n-1} - \text{rank}\, \mathcal{G}_{n-2} \end{aligned}$$

with

$$\mathcal{G}_i = \text{span}\{ad_f^i g_j, 1 \leq j \leq m\}, \quad 0 \leq i \leq n-1.$$

The system is controllable about some point if controllability indices can be defined locally and $\Sigma_{i=1}^{m} k_i = n$.

A control system $\dot{x} = f(x,u)$ is flat if there exists a "differentially invertible" map $y = h(x,\bar{u})$ where $\bar{u} = \left(u, \dot{u}, \cdots, u^{(r)}\right)$ [56]. This means

- components of h are differentially independent i.e. full rank $\left(h, \dot{h}, \cdots, h^{(k)}\right)$
- on the other hand $x = \mathcal{A}(\bar{y})$ and $u = \mathcal{B}(\bar{y})$ for some $\mathcal{A}$ and $\mathcal{B}$

If we choose the VSC state $x = (x_1, x_2, x_3)^T = (i_d, i_q, v_{dc})^T$ and input as $u = (u_1, u_2)^T = (m_a \cos\delta, m_a \sin\delta)^T$, the system's dynamics (3.1) is

$$\dot{x} = f(x) + g_1(x)u_1 + g_2(x)u_2, \tag{3.10}$$

with

$$f(x) = \begin{bmatrix} -\frac{R}{L}x_1 + \omega x_2 + \frac{v_d}{L} \\ -\omega x_1 - \frac{R}{L}x_2 + \frac{v_q}{L} \\ -\frac{x_3}{CR_c} \end{bmatrix}, \quad g_1(x) = \begin{bmatrix} -\frac{x_3}{2L} \\ 0 \\ \frac{3x_1}{4C} \end{bmatrix}, \quad g_2(x) = \begin{bmatrix} 0 \\ -\frac{x_3}{2L} \\ \frac{3x_2}{4C} \end{bmatrix}.$$

For this model the controllability indices are $\{2, 1\}$. It was proven that any $(m+1)$-dimensional system with m-inputs is flat iff it is controllable [56]. Therefore, the VSC model (3.10) is flat. Using the Multi-Input Feedback Linearization theorem in [54], the VSC is in fact feedback linearizable with *static* (as opposed to dynamic) state feedback.

One choice of flat output is

$$\begin{aligned} y_1 &= \phi_1(x) = E_L + E_C = \frac{3}{4}L(x_1^2 + x_2^2) + \frac{1}{2}Cx_3^2 \\ y_2 &= \phi_2(x) = x_2 \end{aligned} \tag{3.11}$$

We remark that y_1 has a physical interpretation: it is the energy E_L and E_C stored in L and C, respectively. The corresponding linearizing state coordinate transformation is

$$\begin{aligned} z_1 &= y_1 = \phi_1(x) = \frac{3}{4}L(x_1^2 + x_2^2) + \frac{1}{2}Cx_3^2 \\ z_2 &= L_f\phi_1(x) = p - P_R - P_{R_c} = \frac{3}{2}(v_d x_1 + v_q x_2) - \frac{3}{2}R(x_1^2 + x_2^2) - \frac{x_3^2}{R_c} \\ z_3 &= y_2 = \phi_2(x) = x_2 \end{aligned} \tag{3.12}$$

where $P_{R_c} = v_{dc}^2/R_c$. The coordinate z_2 is a measure of instantaneous power absorbed in L and C which is equal the VSC input power p minus the power absorbed in the resistances R, R_c. From (3.12) we can express the state as a function of the flat output and its derivatives:

$$x = \mathcal{A}(y_1, \dot{y}_1, y_2)$$

where $\mathcal{A}$ is a smooth function on some domain.
Using (3.11) we can compute $\mathcal{A}$ as

$$\begin{aligned} x_1 &= \frac{-3CR_c v_d + \psi(y, \dot{y})}{6\sigma} \\ x_2 &= y_2 \\ x_3 &= \frac{\sqrt{R_c\zeta(y, \dot{y}) - LR_c(8Ry_1 + 4L\dot{y}_1 - 6Lv_q y_2 - v_d\psi(y, \dot{y}))}}{2\sigma} \end{aligned} \tag{3.13}$$

where

$$\psi(y, \dot{y}) = \sqrt{9C^2R_c^2v_d^2 + 12\sigma(4y_1 - 3Ly_2^2 + CR_c(2\dot{y}_1 - 3y_2(v_q - Ry_2)))}$$

with $\sigma = L - CR_cR$ and $\zeta(y, \dot{y}) = CR_c(8R^2y_1 + L(4R\dot{y}_1 - 3v_d^2 - 6Rv_q y_2))$. Note that it is assumed that v_d and v_q are constant. To express the inputs as a function of the flat output i.e. $u = \mathcal{B}(y_1, \dot{y}_1, \ddot{y}_1, y_2, \dot{y}_2)$ where $\mathcal{B}$ is a smooth function, we introduce the decoupling matrix

$$\begin{aligned} F(x) &= \begin{bmatrix} L_{g_1}L_f\phi_1 & L_{g_2}L_f\phi_1 \\ L_{g_1}\phi_2 & L_{g_2}L_f\phi_1 \end{bmatrix} \\ &= \begin{bmatrix} \frac{3x_3(2CR_cRx_1 - CR_cv_d - 2Lx_1)}{4LCR_c} & \frac{3x_3(2CR_cRx_2 - CR_cv_q - 2Lx_2)}{4LCR_c} \\ 0 & -\frac{x_3}{2L} \end{bmatrix} \end{aligned}$$

so that

$$u = F^{-1}(x) \begin{bmatrix} \ddot{y}_1 - L_f^2\phi_1(x, t) \\ \dot{y}_2 - L_f\phi_2(x) \end{bmatrix} \tag{3.14}$$

$$= \frac{-2L}{x_3} \begin{bmatrix} \frac{2CR_c}{3(CR_cv_d + 2x_1\sigma)} & \frac{-L(2x_2\sigma + CR_cv_q)}{2x_1\sigma + CR_cv_d} \\ 0 & 1 \end{bmatrix} \begin{bmatrix} \ddot{y}_1 - \frac{3(v_{dq} - v_q(\omega Lx_1 + 3Rx_2) + v_d(\omega Lx_2 - 3Rx_1) + 2R^2x_{12})}{2L} - \frac{2x_3^2}{CR_c^2} \\ \dot{y}_2 + \omega x_1 + \frac{R}{L}x_2 - \frac{v_q}{L} \end{bmatrix} \tag{3.15}$$

where $v_{dq} = v_d^2 + v_q^2, x_{12} = x_1^2 + x_2^2$, and expressions for x in terms of y and $\dot{y}$ from (3.13) can be substituted.

The closed-loop control is defined using the tracking errors

$$\begin{aligned} e_1(t) &= \int_0^t (y_1(\tau) - y_1^*(\tau))d\tau \\ e_2(t) &= y_1(t) - y_1^*(t) \\ e_3(t) &= \frac{dy_1}{dt}(t) - \frac{dy_1^*}{dt}(t) \\ e_4(t) &= \int_0^t (y_2(\tau) - y_2^*(\tau))d\tau \\ e_5(t) &= y_2(t) - y_2^*(t) \end{aligned} \tag{3.16}$$

where y_1^*, y_2^* denote the desired flat output trajectories. The control inputs are obtained as

$$u = F^{-1}(x) \begin{bmatrix} -k_1 e_1 - k_2 e_2 - k_3 e_3 + \ddot{y}_1^* - L_f^2 \phi_1(x,t) \\ k_4 e_4 - k_5 e_5 + \dot{y}_2^* - L_f \phi_2(x) \end{bmatrix} \tag{3.17}$$

which gives linear time invariant tracking error dynamics:

$$\begin{bmatrix} \dot{e}_1 \\ \dot{e}_2 \\ \dot{e}_3 \\ \dot{e}_4 \\ \dot{e}_5 \end{bmatrix} = \begin{bmatrix} 0 & 1 & 0 & 0 & 0 \\ 0 & 0 & 1 & 0 & 0 \\ -k_1 & -k_2 & -k_3 & 0 & 0 \\ 0 & 0 & 0 & 0 & 1 \\ 0 & 0 & 0 & -k_4 & -k_5 \end{bmatrix} \begin{bmatrix} e_1 \\ e_2 \\ e_3 \\ e_4 \\ e_5 \end{bmatrix}. \tag{3.18}$$

With proper choice of k_i (i.e., $k_i > 0, k_2 \cdot k_3 > k_1$), the above tracking error dynamics is exponentially stable. The integrators in (3.16) are included to reject unmodelled disturbances. They are not required to achieve output tracking if we assume the model is perfect [22]. We remark that the control u_2 is quite simple and could be obtained directly by linearizing the q-axis current dynamics. In fact, u_2 is independent of x_3 and y_1^*.

3.4 Simulation Results of Flatness-Based Control

3.4.1 References with Step Change

Simulation of the flatness-based control is performed in Simulink/Matlab. The nonlinear model is used to investigate the controller performance. The VSC

parameters and control gains are provided in Table 3.1 and Table 3.3 respectively. The q-axis current changes between -3 A and 3 A and the dc voltage reference changes between 170 V and 200 V. Fig. 3.12 verifies the controller good tracking performance. The control inputs modulation index m_a and phase shift are depicted in Fig. 3.13. It is clear from the figures that the control inputs stay in unsaturated ranges in steady state.

Gains	k_1	k_2	k_3	k_4	k_5
Value	$3 \cdot 10^6$	$6.5 \cdot 10^4$	450	$1.5 \cdot 10^4$	250

Table 3.3: Flatness controller gains used in simulation

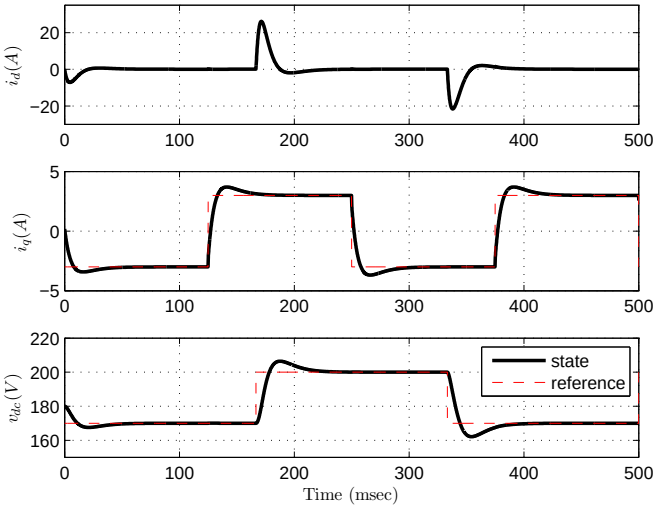

Figure 3.12: Simulation results of flatness-based control using VSC nonlinear model: VSC state and desired reference trajectories

3.4.2 Time-varying q-axis Reference

The simulation results of the flatness-based control of VSC with sinusoidal q-axis reference trajectory while dc voltage reference trajectory has a step change is investigated in this subsection. The q-axis current is a sinusoidal signal $3 + \sin(200\pi t)$ and the dc voltage reference changes between 170 V and 200 V. The reference trajectory for i_d was taken to zero in the calculation of y_1^*. In practise the reference value for i_d is some small nonzero value. Fig. 3.14 verifies the

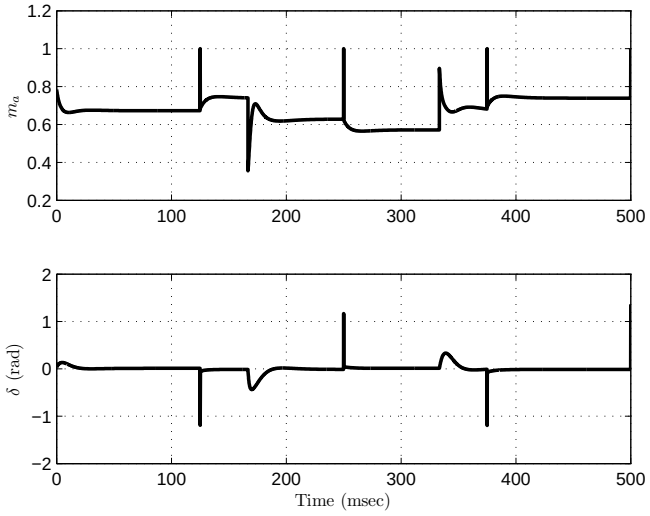

Figure 3.13: Simulation results of flatness-based control using VSC nonlinear model: control inputs m_a and δ

controller good tracking performance. The control inputs modulation index m_a and phase shift are depicted in Fig. 3.15. It is clear that the control signals are varying in their bounds.

3.5 Steady State Solution of the System

The basic requirement for PFC is that i_q tracks the load reactive current i_q^* and also the controller should regulate v_{dc} to a constant reference v_{dc}^*. In order to apply the flatness-based control, we require a trajectory for y_1^* which corresponds to the desired i_q^* and v_{dc}^*. This amounts to computing the corresponding i_d^* for a given i_q^* and v_{dc}^*. For the case where i_q^* and v_{dc}^* are constant we can use the VSC model's equilibrium set obtained by setting the left hand side of (3.10) to zero:

$$\begin{aligned} -\frac{R}{L}i_d + \omega i_q + \frac{v_d}{L} - \frac{e_d}{L} &= 0 \\ -\frac{R}{L}i_q - \omega i_d + \frac{v_q}{L} - \frac{e_q}{L} &= 0 \\ \frac{3}{2}\cdot\frac{e_d i_d + e_q i_q}{C v_{dc}} - \frac{v_{dc}}{C R_c} &= 0 \end{aligned} \tag{3.19}$$

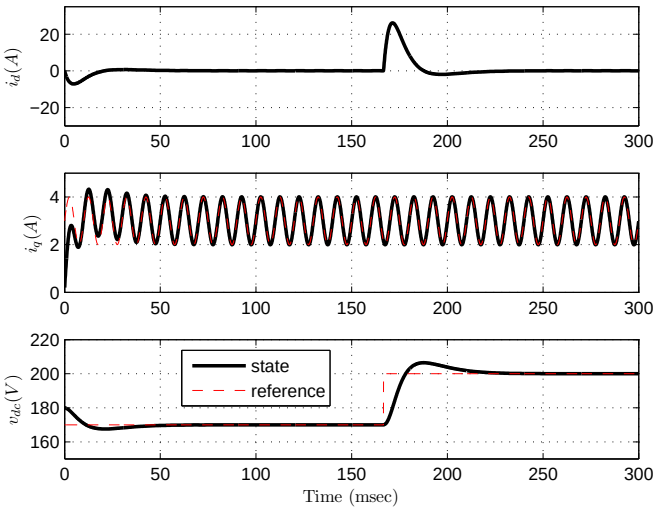

Figure 3.14: Simulation results of flatness-based control with time varying reference trajectories using VSC nonlinear model: VSC state and desired reference trajectories

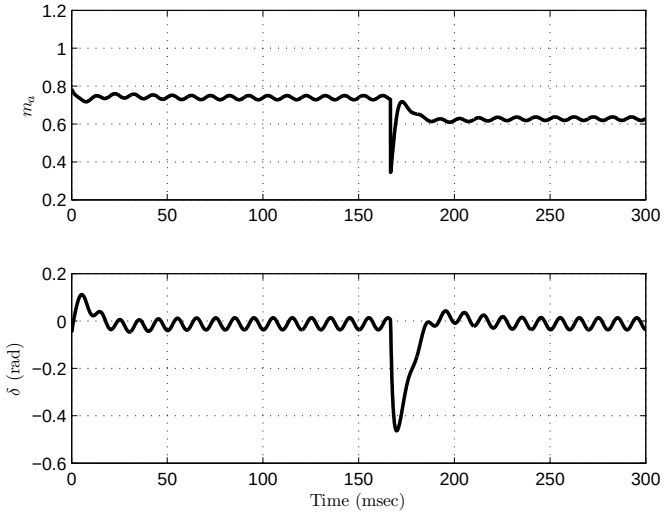

Figure 3.15: Simulation results of flatness-based control with time varying reference trajectories using VSC nonlinear model: control inputs m_a and δ

Denoting I_d, I_q, and V_{dc} as steady state solutions of (3.19), we obtain a quadratic equation for I_d:

$$I_d^2 - \frac{v_d}{R} I_d + (\frac{2V_{dc}^2}{3R_c R} + I_q^2) = 0, \tag{3.20}$$

where we assumed $v_q = 0$ which is the case for a balanced ac source. Equation (3.20) has two distinct roots

$$I_d = \frac{v_d}{2R} \pm \sqrt{\frac{v_d^2}{4R^2} - (I_q^2 + \frac{2}{3}\frac{V_{dc}^2}{R_c R})} \tag{3.21}$$

It should be pointed out that there is no real solution for I_d, if

$$R_c < \frac{8V_{dc}^2 R}{3(v_d^2 - 4R^2 I_q^2)} \tag{3.22}$$

In other words, load current $I_{R_c} = V_{dc}/R_c$ can not be in the following region:

$$I_{R_c} > \frac{3(v_d^2 - 4R^2 I_q^2)}{8V_{dc}R} \tag{3.23}$$

The above inequalities determine the upper limit of dc load current and lower limit on R_c. In other words, the flatness-based control cannot be applied where the decoupling matrix F is singular. These points of uncontrollability can be also obtained by setting the determinant of F to zero. The determinant's roots define two perpendicular planes: one is $v_{dc} = 0$ and the other $i_d = \frac{v_d}{2R}$. In fact the obtained i_d value also minimizes the left hand side of (3.20).

3.6 Application of Steady State Relations

Beside harmonic elimination and PFC, a VSC can also be used as a rectifier to feed dc loads or as part of a motor drive system. Although the rectifier application serves a different need, the VSC systems model remains the same as in PFC. For rectifier applications the parameter R_c models the dc load and the value of R_c can be much lower. This implies the size of i_d will be considerably larger due to real power flow through the converter into the load.

It has been shown that the flatness-based control can achieve satisfactory performance for i_q and v_{dc} tracking if the steady-state value of i_d is sufficiently

small [22]. However, assuming small steady-state i_d will result in steady state tracking errors for rectifier applications. This is illustrated in simulation in Fig. 3.16(a) where $R_c = 18\ \Omega$. The flatness-based control in [22], which assumes the steady-state $i_d = 0$, results in steady state tracking error for v_{dc}. This is to be expected from the steady state relations which predict a non-negligible steady-state i_d.

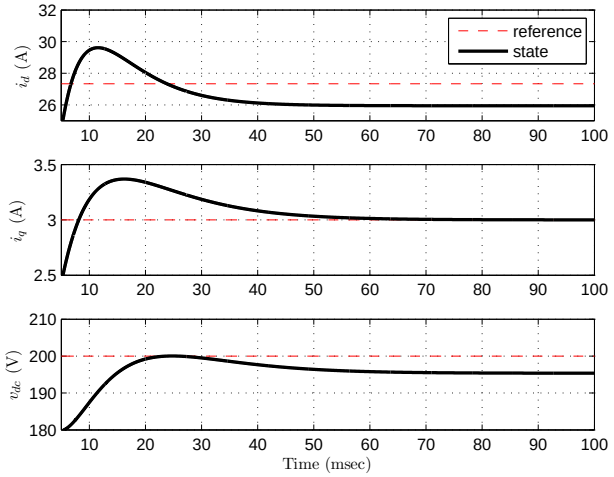

(a) assuming $i_d = 0$

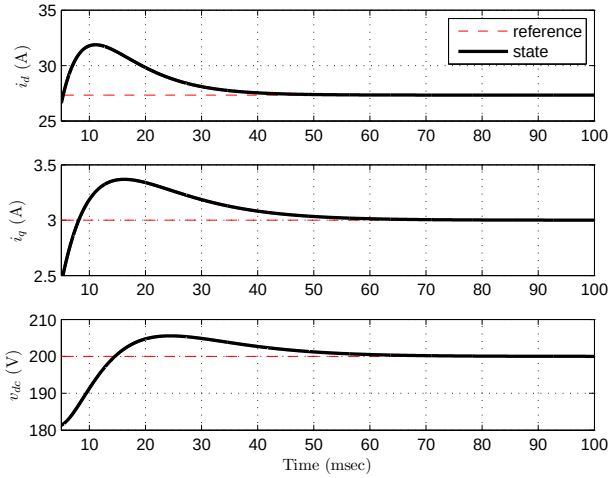

(b) using steady state relationship

Figure 3.16: Simulation results of the flatness-based control for small R_c

To improve the tracking performance, the steady state relations developed in the previous section can be employed to adjust the reference value y_1^*. The simulation results in Fig. 3.16(b) clearly shows the perfect tracking with zero steady state error. We remark that for these parameters , $\min R_c$ and $\max I_{R_c}$ are 6.22 Ω and 32.13 A, respectively.

3.7 Summary

This chapter considers PFC when all VSC parameters are known. First, the classical vector control is introduced. The simulation results for this controller are presented which verify its good performance. Next, the flatness-based control for a VSC is reviewed. To improve its tracking performance, steady state relations are employed to adjust the reference trajectories. This improvement is especially important when the VSC is used to supply power on dc link e.g. in rectifier applications as a battery charger or the front end of a motor drive system. Both classic vector control and the flatness-based control depend on system parameters which are not known exactly. This motivates the investigation of adaptive control for the VSC in the rest of the thesis.

Chapter 4

Adaptive Control

An adaptive control can be thought of as a feedback law which attempts to reshape the controller by observing its performance. This type of control is usually proposed to compensate for some kind of system uncertainty such as unknown parameters or disturbances. In this chapter, we review a brief history of adaptive control and describe its different types such as direct and indirect adaptive control techniques. Since there is no need to estimate the system parameters in the direct adaptive control method which means lower mathematical computations, this control method is used for the VSC with uncertain parameters. Next the adaptive control for nonlinear systems with linearly parameterized uncertainty is investigated. Finally, the systematic adaptive design procedure is applied to the VSC with two unknown parameters.

4.1 Adaptive Control: A Review

Adaptive control was developed in part in the early 1950s as an extension to the gain scheduling design for aircraft control which accounted for unknown parameters in its dynamics. Adaptive control provided good performance for a wide range of aircraft speeds and altitudes [57]. Due to the shortage of control techniques and theory at that time, research on adaptive control diminished in the late 1950s and 1960s. This period witnessed the development of non-adaptive control theory e.g. state space, stability, and optimal control theories [58, 59, 60, 61, 62]. In the 1970s and 1980s several breakthroughs were made in proofs for stability of adaptive systems [63, 64]. Significant achievement

on adaptive control for nonlinear systems were obtained in the late 1980s and early 1990s [44, 45, 65, 66, 67, 68]. Since the emergence of adaptive control theory, there have been many experimental implementations of adaptive control in industry and academic labs [69, 70]. We present a simple example to demonstrate the basic mechanism of adaptive control. Consider a first order system

$$\dot{y} = y + \frac{u}{a} \tag{4.1}$$

where known constant $a > 0$. We want to design a controller to regulate y to y_r. If a simple state feedback control

$$u = -a(k\tilde{y} + y - \dot{y}_r) \tag{4.2}$$

where $\tilde{y} = y - y_r$, the closed-loop system dynamics is

$$\dot{\tilde{y}}(t) = -k\tilde{y}(t) \tag{4.3}$$

Hence for any $k > 0$, the closed-loop dynamics is asymptotically stable. But if a is unknown, control feedback (4.2) may not regulate output y to the origin. We defined an estimate of a denoted $\hat{a}$ and want to obtain the control and adaptation law such that the closed-loop system is stable for any parameter values and any initial conditions $y(0)$.

If the control law is defined as

$$u = -\hat{a}(\underbrace{k\tilde{y} + y - \dot{y}_r}_{\gamma(y,\tilde{y})}) \tag{4.4}$$

the closed loop system dynamics is

$$\dot{\tilde{y}}(t) = -k\tilde{y}(t) + \gamma(y, \tilde{y})\tilde{\theta} \tag{4.5}$$

in which $\tilde{\theta} = \frac{a-\hat{a}}{a} = \frac{\tilde{a}}{a}$. We consider the following Lyapunov function candidate

$$V = \frac{1}{2}p\tilde{y}^2 + \frac{1}{2}\frac{\tilde{\theta}^2}{\eta}$$

where constant gains $p, \eta > 0$. The time derivative of V along the system dynamics (4.5) is

$$\dot{V} = p\tilde{y}\dot{\tilde{y}} + \frac{1}{\eta}\tilde{\theta}\dot{\tilde{\theta}} = p\tilde{y}(-k\tilde{y}(t) + \gamma\tilde{\theta}) + \frac{1}{\eta}\tilde{\theta}\dot{\tilde{\theta}}$$

To have $\dot{V} \leq 0$ we choose

$$\dot{\hat{\theta}} = -\dot{\tilde{\theta}} = \eta\gamma p\tilde{y} \tag{4.6}$$

as an update law for $\hat{\theta}$. This leads to

$$\dot{V} = -kp\tilde{y}^2 \leq 0$$

The closed loop dynamics is

$$\begin{bmatrix} \dot{\tilde{y}} \\ \dot{\tilde{a}} \end{bmatrix} = \begin{bmatrix} -k & \gamma \\ \eta\gamma p & 0 \end{bmatrix} \begin{bmatrix} \tilde{y} \\ \tilde{\theta} \end{bmatrix} \tag{4.7}$$

Defining $S = \{(\tilde{y}, \tilde{\theta})^T \in \mathbb{R}^2 : \dot{V} = 0\}$ and since

$\dot{V} = 0 \Rightarrow \tilde{y} = 0 \Rightarrow$ with assumption $\gamma(y_r, 0) = y_r - \dot{y}_r \neq 0 \Rightarrow \tilde{\theta} = 0$
This implies the only point in S is the origin $(\tilde{y}, \tilde{\theta}) = 0$ which is an invariant solution. Thus by LaSalle's Theorem [71] the origin is asymptotically stable.

4.2 Types of Adaptive Control

Adaptive control methods are generally divided into three basic categories which are briefly outlined here.

4.2.1 Indirect Adaptive Control

In an indirect adaptive control the plant parameters are adaptively estimated first, then the control gains calculated from some algebraic design equations using the estimates of unknown plant parameters [69, 72]. The scheme is called indirect due to the two stages of the approach:

1. plant parameter estimation

2. controller gains calculation based on the estimated plant model

The technique uses the estimated plant parameters as if they are the true ones in order to calculate the controller gain.

4.2.2 Direct Adaptive Control

In direct adaptive control, the control parameters are directly updated from an adaptive law [69]. The difference between the plant output and a reference model output is used for deriving the adaptation mechanism in order to directly adjust the controller parameters and force the output tracking error to zero. In direct control there is no explicit identification of the plant but the control parameters are tuned so that the error between the plant output and that of a reference model converges to zero asymptotically [73]. An adaptive PI control is a simple example of direct adaptive control [14, 74].

4.2.3 Gain-Scheduling Adaptive Control

Gain-scheduling can be thought of as a simple form of adaptive control where controller parameters are determined from a stored look-up table whose values depend on a measurement of the operating condition. The method assumes a direct relationship between measured variables which determine the operating condition and the plant's model parameters. Examples of gain scheduling in the 1970s include [75, 76]. Later on gain-scheduling appeared in the context of feedback linearization. An example of gain-scheduling was discussed in a chapter of [77]. The theoretical basis of gain scheduling for nonlinear systems is in [78, 79]. A survey of the results for nonlinear systems design is in [80].

4.3 Adaptive Control of Nonlinear System

Let us consider the following continuous time nonlinear affine system

$$\begin{aligned} \dot{x} &= f(x) + \sum_{j=1}^{m} g_j(x) u_j \\ y &= h(x) \end{aligned} \tag{4.8}$$

where $x \in \mathbb{R}^n$ is the state vector, $y \in \mathbb{R}^q$ is the output vector and $u_j \in \mathbb{R},\ j = 1, 2, ..., m$ are the inputs. In most practical applications, some or all plant model parameters are not exactly known and therefore model (4.8) should be modified accordingly. Let us assume system (4.8) is single input and has a

linearly parameterized uncertainty. In this case, a suitable model is

$$\begin{aligned} \dot{x} &= f_0(x) + \sum_{i=1}^{p} \theta_i f_i(x) + [g_0(x) + \sum_{i=1}^{p} \theta_i g_i(x)]u \\ y &= h(x) \end{aligned} \tag{4.9}$$

where $\theta = [\theta_1, ..., \theta_p]^T$ is the vector of unknown constant parameters and $f_i,\ g_i,\ 0 \leq i \leq p$ are smooth vector fields in a neighborhood of the origin $x = 0$ with $f_i(0) = 0,\ 0 \leq i \leq p$ and $g_0(0) \neq 0$.

4.3.1 Pure-Feedback Form

It was shown in [44, 45] that a systematic design procedure can be applied to design an adaptive control for the nonlinear system (4.9) if the feedback linearization of nominal system and parametric-pure-feedback condition are satisfied. It was proven that with these conditions and using a parameter independent diffeomorphism $z = \phi(x)$, the system (4.9) can be transformed to the parametric-pure-feedback form:

$$\begin{aligned} \dot{z}_1 &= z_2 + \theta^T \gamma_1(z_1, z_2) \\ \dot{z}_2 &= z_3 + \theta^T \gamma_2(z_1, z_2, z_3) \\ &\vdots \\ \dot{z}_{n-1} &= z_n + \theta^T \gamma_{n-1}(z_1, ..., z_n) \\ \dot{z}_n &= \gamma_0 + \theta^T \gamma_n(z) + [\beta_0(z) + \theta^T \beta(z)]u \end{aligned} \tag{4.10}$$

with

$$\gamma_0(0) = \gamma_1(0) = ... = \gamma_n(0) = 0$$

The necessary and sufficient conditions for the existence of such a diffeomorphism are given in [44, Prop. 2.1] which is restated here.

Proposition 1 *A diffeomorphism $z = \phi(x)$ with $\phi(0) = 0$, transforming (4.9) into (4.10), exists in a neighborhood of the origin if and only if the following conditions are satisfied around the origin*

- *Feedback linearization of the nominal plant: the distributions*

$$\mathcal{G}_i = \text{span}\{g_0, ad_{f_0} g_0, \ldots, ad_{f_0}^i g_0\}, \quad 0 \leq i \leq n-1.$$

  are involutive and of constant rank $i + 1$.

- *Parametric-pure-feedback condition*

$$g_i \in \mathcal{G}_0,$$
$$[X, f_i] \in \mathcal{G}_{j+1}, \ \forall X \in \mathcal{G}_j, \quad 0 \leq j \leq n-3, 0 \leq i \leq p$$

The feedback linearizable condition is necessary and sufficient for the existence of a diffeomorphism $z = \phi(x)$ with $\phi(0) = 0$ which transforms the nominal system

$$\dot{x} = f_0(x) + g_0(x)u,$$

into

$$\begin{aligned} \dot{z}_i &= z_{i+1}, \quad 1 \leq i \leq n-1 \\ &\vdots \\ \dot{z}_n &= \gamma_0(z) + \beta_0(z)u \end{aligned}$$

with $\gamma_0(0) = 0, \beta_0(0) \neq 0$. It is shown in [44] that the same parameter independent diffeomorphism $z = \phi(x)$ transforms (4.9) into (4.10).

4.3.2 Uncertainty-Constrained Schemes

The uncertainty-constrained scheme was developed by [81, 82, 83]. The condition for this approach is called extended matching condition (EMC) [81, 82] or strong linearizability condition [72]. The EMC is a special case of the parametric-pure-feedback condition where

$$g_i \in \mathcal{G}_0, \quad f_i \in \mathcal{G}_1, \quad 1 \leq i \leq p$$

If the EMC is satisfied, the system can be expressed in z-coordinates as

$$\begin{aligned} \dot{z}_1 &= z_2 \\ \dot{z}_2 &= z_3 \\ &\vdots \\ \dot{z}_{n-1} &= z_n + \theta^T \gamma_{n-1}(z_1, \ldots, z_n) \\ \dot{z}_n &= \gamma_0(z) + \theta^T \gamma_n(z) + [\beta_0(z) + \theta^T \beta(z)]u \end{aligned}$$

4.4 Adaptive Controller Design for Regulation

A systematic approach to design an adaptive control for a system which satisfies Proposition 1 is presented in [44]. The step-by-step procedure is presented with the change of coordinate and the construction of the parameter update law in each step.

Step 0: define $\zeta_1 = z_1$ and denote $k_1, k_2, \ldots, k_n$ constant coefficients to be chosen later.

Step 1: starting with

$$\dot{\zeta}_1 = z_2 + \theta^T \gamma_1(z_1, z_2) \tag{4.11}$$

let $\hat{\theta}_1$ be an estimate of θ. We define a new state ζ_2 as

$$\zeta_2 = k_1\zeta_1 + z_2 + \hat{\theta}_1^T \gamma_1(z_1, z_2) \tag{4.12}$$

With substitution of (4.12) into (4.11), we obtain

$$\begin{aligned}\dot{\zeta}_1 &= -k_1\zeta_1 + \zeta_2 + (\theta - \hat{\theta}_1)^T \gamma_1(z_1, z_2) \\ &= -k_1\zeta_1 + \zeta_2 + (\theta - \hat{\theta}_1)^T \omega_1(\zeta_1, \zeta_2, \hat{\theta}_1)\end{aligned}$$

The update law is chosen as

$$\dot{\hat{\theta}}_1 = x_1 \omega_1(\zeta_1, \zeta_2, \hat{\theta}_1)$$

Step 2: using the definition for ζ_1, ζ_2 and $\dot{\hat{\theta}}_1$, $\dot{\zeta}_2$ can be written as

$$\begin{aligned}\dot{\zeta}_2 &= k_1[-k_1\zeta_1 + \zeta_2 + (\theta - \hat{\theta}_1)^T \omega_1(\zeta_1, \zeta_2, \hat{\theta}_1)] + z_3 + \theta^T \gamma_2(z_1, z_2, z_3) \\ &\quad \zeta_1 \omega(\zeta_1, \zeta_2, \hat{\theta}_1)^T \gamma_1(z_1, z_2) + \hat{\theta}_1^T [\frac{\partial \gamma_1}{\partial z_1}(z_2 + \theta^T \gamma_1) + \frac{\partial \gamma_1}{\partial z_2}(z_3 + \theta^T \gamma_2)] \\ &= (1 + \hat{\theta}_1^T \frac{\partial \gamma_1}{\partial z_2})[z_3 + \theta^T \gamma_2(z_1, z_2, z_3)] + \phi_2(\zeta_1, \zeta_2, \hat{\theta}_1) + \theta^T \psi_2(\zeta_1, \zeta_2, \hat{\theta}_1)\end{aligned} \tag{4.13}$$

Let us define a new estimation of θ called $\dot{\hat{\theta}}_2$ and define the new state ζ_3 as

$$\begin{aligned}\zeta_3 = k_2\zeta_2 &+ (1 + \hat{\theta}_1^T \frac{\partial \gamma_1}{\partial z_2})[z_3 + \hat{\theta}_2^T \gamma_2(z_1, z_2, z_3)] \\ &+ \phi_2(\zeta_1, \zeta_2, \hat{\theta}_1) + \hat{\theta}_2^T \psi_2(\zeta_1, \zeta_2, \hat{\theta}_1)\end{aligned} \tag{4.14}$$

Substitute (4.14) into (4.13) to obtain

$$\begin{aligned}\dot{\zeta}_2 &= -k_2\zeta_2 + \zeta_3 + (\theta - \hat{\theta}_2)^T[\psi_2(\zeta_1, \zeta_2, \hat{\theta}_1) + (1 + \hat{\theta}_1^T \frac{\partial \gamma_1(z_1, z_2)}{\partial z_2})\gamma_2(z_1, z_2, z_3)] \\ &= -k_2\zeta_2 + \zeta_3 + (\theta - \hat{\theta}_2)^T\omega_2(\zeta_1, \zeta_2, \zeta_3, \hat{\theta}_1, \hat{\theta}_2)\end{aligned}$$

The new update law for the new estimate $\hat{\theta}_2$ can be obtained as

$$\dot{\hat{\theta}}_2 = \zeta_2\omega_2(\zeta_1, \zeta_2, \zeta_3, \hat{\theta}_1, \hat{\theta}_2)$$

Step i $(2 \leq i \leq n-1)$: using the defined $\zeta_1, \ldots, \zeta_i$ and $\dot{\hat{\theta}}_1, \ldots, \dot{\hat{\theta}}_{i-1}$, $\dot{\zeta}_i$ can be expressed as

$$\begin{aligned}\dot{\zeta}_i = (1 + \hat{\theta}_1^T \frac{\partial \gamma_1}{\partial z_2}) \ldots (1 + \hat{\theta}_{i-1}^T \frac{\partial \gamma_{i-1}}{\partial z_i})[z_{i+1} + \theta^T\gamma_i(z_1, \ldots, z_{i+1})] \\ + \phi_i(\zeta_1, \ldots, \zeta_i, \hat{\theta}_1, \ldots, \hat{\theta}_{i-1}) + \theta^T\psi_i(\zeta_1, \ldots, \zeta_i, \hat{\theta}_1, \ldots, \hat{\theta}_{i-1})\end{aligned} \tag{4.15}$$

If $\hat{\theta}_i$ is defined as a new estimation of θ, the new state ζ_{i+1} is obtained as

$$\begin{aligned}\zeta_{i+1} = k_i\zeta_i + (1 + \hat{\theta}_1^T \frac{\gamma_1}{z_2}) \ldots (1 + \hat{\theta}_{i-1}^T \frac{\partial \gamma_{i-1}}{\partial z_i})[z_{i+1} + \hat{\theta}_i^T\gamma_i(z_1, \ldots, z_{i+1})] \\ + \phi_i(\zeta_1, \ldots, \zeta_i, \hat{\theta}_1, \ldots, \hat{\theta}_{i-1}) + \hat{\theta}_i^T\psi_i(\zeta_1, \ldots, \zeta_i, \hat{\theta}_1, \ldots, \hat{\theta}_{i-1})\end{aligned} \tag{4.16}$$

Substituting (4.16) into (4.15) gives

$$\begin{aligned}\dot{\zeta}_i &= -k_i\zeta_i + \zeta_{i+1} + (\theta - \hat{\theta}_i)^T[\psi_i + (1 + \hat{\theta}_1^T \frac{\partial \gamma_1}{\partial z_2}) \ldots (1 + \hat{\theta}_{i-1} \frac{\partial \gamma_{i-1}}{\partial z_i})\gamma_i] \\ &= -k_i\zeta_i + \zeta_{i+1} + (\theta - \hat{\theta}_i)^T\omega_i(\zeta_1, \ldots, \zeta_{i+1}, \hat{\theta}_1, \ldots, \hat{\theta}_i)\end{aligned}$$

The update law for $\hat{\theta}_i$ is

$$\dot{\hat{\theta}}_i = \zeta_i\omega_i(\zeta_1, \ldots, \zeta_{i+1}, \hat{\theta}_1, \ldots, \hat{\theta}_i)$$

Step n: Using the definition for $\zeta_1, \ldots, \zeta_n$ and $\dot{\hat{\theta}}_1, \ldots, \dot{\hat{\theta}}_{n-1}$, the $\dot{\zeta}_n$ can be expressed as

$$\begin{aligned}\dot{\zeta}_n = (1 + \hat{\theta}_1^T \frac{\partial \gamma_1}{\partial z_2})..(1 + \hat{\theta}_{n-1} \frac{\partial \gamma_{n-1}}{\partial z_n})[\beta_0(z) + \theta^T\beta(z)]u + \\ \phi_n(\zeta, \hat{\theta}_1, \ldots, \hat{\theta}_{n-1}) + \theta^T\psi_n(z, \hat{\theta}_1, \ldots, \hat{\theta}_{n-1})\end{aligned}$$

let $\hat{\theta}_n$ be a new estimate of θ and define control law u

$$u = \frac{1}{\bar{\beta}(z, \hat{\theta}_1, \ldots, \hat{\theta}_n)}[-k_n\zeta_n - \phi_n - \hat{\theta_n}^T\psi_n] \tag{4.17}$$

where

$$\bar{\beta}(z,\hat{\theta}_1,\ldots,\hat{\theta}_n) = (1+\hat{\theta}_1^T\frac{\partial\gamma_1}{\partial z_2})\ldots(1+\hat{\theta}_{n-1}^T\frac{\partial\gamma_{n-1}}{\partial z_n})[\beta_0+\hat{\theta}_n^T\beta(z)]$$

Therefore, $\dot{\zeta}_n$ is obtained as

$$\begin{aligned}\dot{\zeta}_n &= -k_n\zeta_n + (\theta-\hat{\theta}_n)[\psi_n + (1+\hat{\theta}_1^T\frac{\partial\gamma_1}{\partial z_2})\ldots(1+\hat{\theta}_{n-1}\frac{\partial\gamma_{n-1}}{\partial z_n})\beta(z)u] \\ &= k_n\zeta_n + (\theta-\hat{\theta}_n)^T\omega_n(\zeta,\hat{\theta}_z\ldots\hat{\theta}_n)\end{aligned}$$

where (4.17) is used in the definition of ω_n. Finally, the update law for the $\hat{\theta}_n$ can be written

$$\dot{\hat{\theta}}_n = \zeta_n\omega_n(\zeta,\hat{\theta}_1,\ldots,\hat{\theta}_n)$$

4.5 Adaptive Control of Multi-Input Systems

Consider a multi-input system with linearly parameterized uncertainty:

$$\dot{x} = f_0(x) + \sum_{i=1}^{p}\theta_i f_i(x) + \sum_{j=1}^{m}[g_{0,j}(x) + \sum_{i=1}^{p}\theta_i g_{i,j}(x)]u_j \tag{4.18}$$

with

$$\begin{aligned}&f_i(0) = 0, \quad 0\le i\le p,\\ &\operatorname{rank}\mathcal{G}_0(0) = m,\\ &\mathcal{G}_0 = [g_{0,1},\ldots,g_{0,m}]\end{aligned}$$

If system dynamics (4.18) satisfies feedback linearization and pure-feedback conditions, there is a diffeomorphism $z=\phi(x)$ with $\phi(0)=0$ which transforms (4.18) into

$$\begin{aligned}\dot{z}_{i,j} &= z_{i+1,j} + \theta^T\gamma_{i,j}(z_{1,1},\ldots,z_{k_1-k_j+2},\ldots,z_{1,m},\ldots,z_{k_m-k_j+1,m}) \\ &\qquad 1\le i\le k_j-1, \quad 1\le j\le m \\ \dot{z}_{k_j,j} &= \gamma_{0,j} + \theta^T\gamma_{k_j,j}(z) + [\beta_{0,j} + \sum_{l=1}^{p}\theta_l\beta_{l,j}(z)]^T u, 1\le j\le p\end{aligned} \tag{4.19}$$

with $\gamma_{l,j}(0)=0, 0\le i\le k_j, 1\le j\le m, \det(B_0(0))\neq 0$,
where $B_0=[\beta_{0,1},\ldots,\beta_{0,m}]$ and $\sum_{j=1}^{m}k_j = n$.

Proposition 2 *A parameter independent diffeomorphism $z = \phi(x)$ exists in a neighborhood of the origin, with $\phi(0) = 0$, which transforms the system (4.18) into (4.19) if and only if around the origin*

- *the feedback linearization condition holds or the distributions*

$$\mathcal{G}_i = \text{span}\{g_{0,j}, ad_{f_0} g_{0,j}, \ldots, ad^i_{f_0} g_{0,j}\}, \quad 0 \le j \le m.$$

  are involutive and of constant rank r_i, with $r_{n-1} = n$.

- *Pure-feedback condition holds or*

$$g_{i,j} \in \mathcal{G}_0, \quad 0 \le j \le m$$
$$[X, f_i] \in \mathcal{G}_{k+1}, \ \forall X \in \mathcal{G}_k, \quad 0 \le k \le n-3, 0 \le i \le p$$

We remark that the above regulation results have their tracking counterpart and the tracking formula can be easily obtained using above formula with small modifications. In addition, similar to the single-input case, the adaptive design procedure for a multi-input system is presented in [44]. This design is applied to the VSC model in the next section.

4.6 Systematic Design of Adaptive Control for a VSC

In this section, the systematic adaptive control design for a VSC when two and three parameters are unknown is investigated. For each case, the feedback linearizable and parametric-pure-feedback conditions are checked.

4.6.1 VSC With Two Unknown Parameters

Recall the VSC dynamics with unknown parameters R and R_c

$$\begin{aligned}
\dot{x}_1 &= \omega x_2 - \frac{x_1}{L}\theta_1 + \frac{1}{L}u_1 \\
\dot{x}_2 &= -\omega x_1 - \frac{x_2}{L}\theta_1 + \frac{1}{L}u_2 \\
\dot{x}_3 &= \frac{3v_d}{C}x_1 + \frac{3v_q}{C}x_2 - \frac{2x_3}{C}\theta_2 - \frac{3}{C}x_1 u_1 - \frac{3}{C}x_2 u_2
\end{aligned} \tag{4.20}$$

where $(x_1, x_2, x_3) = (i_d, i_q, v_{dc}^2)$, $\theta_1 = R$ and $\theta_2 = 1/R_c$. The VSC dynamics (4.20) can be written as

$$\dot{x} = f_0(x) + f_1(x)\theta_1 + f_2(x)\theta_2 + g_{0,1}(x)u_1 + g_{0,2}(x)u_2$$

where

$$f_0(x) = [\omega x_2, -\omega x_1, \frac{3v_d}{C}x_1 + \frac{3v_q}{C}x_2]^T, \quad f_1(x) = [\frac{-x_1}{L}, \frac{-x_2}{L}, 0]^T,$$
$$f_2(x) = [0, 0, -\frac{2}{C}x_3]^T, \quad g_1 = [\frac{1}{L}, 0, -\frac{3}{C}x_1]^T, \quad g_2 = [0, \frac{1}{L}, -\frac{3}{C}x_2]^T$$

It can be shown that the system $\dot{x} = f_0(x) + g_{0,1}(x)u_1 + g_{0,2}(x)u_2$ is feedback linearizable via the diffeomorphism

$$z_1 = Cx_3 + \frac{3}{2}L(x_1^2 + x_2^2)$$
$$z_2 = 3v_d x_1 + 3v_q x_2$$
$$z_3 = x_3$$

Therefore, the adaptive control tracking output is $y_r = [y_{1r}, y_{2r}] = [z_{1r}, z_{3r}]^T$. Next, the system equations in the z-coordinate is derived as

$$\begin{aligned}
\dot{z}_1 &= C\dot{x}_3 + 3L(x_1\dot{x}_1 + x_2\dot{x}_2) \\
&= C(\frac{3v_d}{C}x_1 + \frac{3v_q}{C}x_2 - \frac{2x_3}{C}\theta_2 - \frac{3}{C}x_1u_1 - \frac{3}{C}x_2u_2) + 3L[x_1(\omega x_2 - \frac{x_1}{L}\theta_1 \\
&\quad + \frac{1}{L}u_1) + x_2(-\omega x_1 - \frac{x_2}{L}\theta_1 + \frac{1}{L}u_2)] \\
&= 3v_d x_1 + 3v_q x_2 + 3(x_1^2 + x_2^2)\theta_1 + (-2x_3)\theta_2
\end{aligned}$$

Similarly,

$$\begin{aligned}
\dot{z}_2 &= 3v_d[\omega x_2 - \frac{x_1}{L}\theta_1 + \frac{1}{L}u_1] + 3v_q[-\omega x_1 - \frac{x_2}{L}\theta_1 + \frac{1}{L}u_2] \\
&= 3\omega(v_d x_1 - v_q x_2) - \frac{1}{L}(3v_d x_1 + 3v_q x_2)\theta_1 + \frac{1}{L}(v_d u_1 + v_q u_2)
\end{aligned}$$

$$\dot{z}_3 = \dot{x}_3 = \frac{3v_d x_1 + 3v_q x_2}{C} - \frac{2x_3}{C}\theta_2 - \frac{3(x_1u_1 + x_2u_2)}{C}$$

where

$$3(x_1^2 + x_2^2) = [3(x_1^2 + x_2^2) + Cx_3] - Cx_3 = z_1 - Cz_3$$

Therefore, the dynamics in z-coordinate are

$$\begin{aligned}
\dot{z}_1 &= z_2 + \theta_1[z_1 - Cz_3] - 2z_3\theta_2 \\
\dot{z}_2 &= 3\omega(v_d x_1 - v_q x_2) - \frac{1}{L}z_2\theta_1 + \frac{3}{L}[v_d u_1 + v_q u_2] \\
\dot{z}_3 &= \frac{1}{C}z_2 - \frac{2}{C}z_3 - \frac{3}{C}(x_1u_1 + x_2u_2)
\end{aligned}$$

or

$$\dot{z}_1 = z_2 + \theta^T \gamma_1(z_1, z_3)$$
$$\dot{z}_2 = \gamma_{0,2}(z) + \theta^T \gamma_2(z_2) + \beta_2^T(x)u$$
$$\dot{z}_3 = \gamma_{0,3}(z) + \beta_3^T(x)u$$

where

$$\gamma_1(z_1, z_3) = [z_1 - Cz_3, -2z_3]^T, \quad \beta_2 = [\frac{3}{L}v_d, \frac{3}{L}v_q]^T$$
$$\gamma_{0,2}(z) = 3\omega(v_d x_1 - v_q x_2), \quad \gamma_{0,3} = \frac{1}{C}z_2 - \frac{2}{C}z_3$$
$$\gamma_2(z_2) = [-\frac{1}{L}z_2, 0]^T, \quad \beta_3(x) = [-\frac{3}{C}x_1, -\frac{3}{C}x_2]^T$$

If we define $\zeta_1 = z_1 - y_{1r}$ and $\zeta_3 = z_3 - y_{2r}$, we have

$$\dot{\zeta}_1 = z_2 + \theta^T \gamma_1(z_1, z_3) - \dot{y}_{1r} \tag{4.21}$$

Let us consider $\hat{\theta}_a$ an estimate of θ and define a new state ζ_2 as

$$\zeta_2 = k_1\zeta_1 + z_2 + \hat{\theta}_a^T \gamma_1(z_1, z_3) - \dot{y}_{1r} \tag{4.22}$$

where $k_1 > 0$. Substitute (4.22) into (4.21) to obtain

$$\dot{\zeta}_1 = -k_1\zeta_1 + \zeta_2 + (\theta - \hat{\theta}_a)^T \omega_1(\zeta_1, z_3, y_{1r}) - \dot{y}_{1r}$$

The update law for $\hat{\theta}_a$ is

$$\dot{\hat{\theta}}_a = \zeta_1\gamma_1(z_1, z_3) = \zeta_1\omega_1(\zeta_1, \zeta_3, y_r) \tag{4.23}$$

Using the definition for ζ_1, ζ_2 and $\dot{\hat{\theta}}_a$, $\dot{\zeta}_2$ can be written

$$\begin{aligned}
\dot{\zeta}_2 &= k_1[-k_1\zeta_1 + \zeta_2 + (\theta - \hat{\theta}_a)^T\omega_1(\zeta_1, z_3, y_{1r})] + [\gamma_{0,2}(z) + \theta^T\gamma_2(z_2) + \beta_2^T(x)u] \\
&\quad + \zeta_1\omega_1(\zeta_1, z_3, y_{1r})\gamma_1(z_1, z_3) + \hat{\theta}_a^T[\frac{\partial\gamma_1}{\partial z_1}(z_2 + \theta^T\gamma_1) + \frac{\partial\gamma_1}{\partial z_3}(\gamma_{0,3}(z) + \beta_3(x)^T u)] - \ddot{y}_{1r} \\
&= -k_1^2\zeta_1 + k_1\zeta_2 + k_1\theta^T\omega_1 - k_1\hat{\theta}_a^T\omega_1 + \gamma_{0,2} + \theta^T\gamma_2 + \beta_2^T u \\
&\quad + \zeta_1\omega_1^2 + \hat{\theta}_a^T[1,0]^T(z_2 + \theta^T\gamma_1) + \hat{\theta}_a^T[-C,-2]^T(\gamma_{0,3} + \beta_3^T u) - \ddot{y}_{1r} \\
&= (-k_1^2\zeta_1 + k_1\zeta_2 - k_1\hat{\theta}_a^T\omega_1 + \gamma_{0,2} + \zeta_1\omega_1^2 + \hat{\theta}_a^T[1,0]^T z_2 + \hat{\theta}_a^T[-C,2]^T\gamma_{0,3}) \\
&\quad + \theta^T(\gamma_2 + k_1\omega_1 + \hat{\theta}_a^T[1,0]^T\omega_1) + (\beta_2^T + \hat{\theta}_a^T[-C,2]^T\beta_3^T)u - \ddot{y}_{1r}
\end{aligned}$$

Therefore,

$$\dot{\zeta}_2 = \phi_{21}(\zeta, \hat{\theta}) + \theta^T\phi_{22}(\zeta, \hat{\theta}) + \psi(\zeta, \hat{\theta})u$$
$$\dot{\zeta}_3 = \gamma_3(\zeta) + \beta_3(\zeta)^T u$$

and the system dynamics in the new coordinates is

$$\dot{\zeta}_1 = -k_1\zeta_1 + \zeta_2 + \theta^T\omega_1(\zeta_1, z_3, y_{1r}) - \hat{\theta}_a^T\omega_1(\zeta_1, z_3, y_{1r})$$
$$\dot{\zeta}_2 = \phi_{21}(\zeta, \hat{\theta}_a, y_r, \dot{y}_r, \ddot{y}_r) + \theta^T\phi_{22}(\zeta, \hat{\theta}_a, y_r, \dot{y}_r, \ddot{y}_r) + \psi_2(\zeta, \hat{\theta}_a)u$$
$$\dot{\zeta}_3 = \gamma_3(\zeta, y_r) + \beta_3^T(\zeta, y_r)u$$

We consider $\hat{\theta}_b$ as a new estimate of θ and define the control u as

$$u = -\begin{pmatrix}\psi_2(\zeta, \hat{\theta}_a)\\ \beta_3(\zeta, y_r)^T\end{pmatrix}^{-1}\begin{pmatrix}k_2\zeta_2\\ k_3\zeta_3\end{pmatrix} - \begin{pmatrix}\phi_{21}(\zeta, \hat{\theta}_a, y_r, \dot{y}_r, \ddot{y}_r)\\ \gamma_3(\zeta, y_r)\end{pmatrix} - \begin{pmatrix}\phi_{22}(\zeta, \hat{\theta}_a, y_r, \dot{y}_r, \ddot{y}_r)\\ 0\end{pmatrix}\hat{\theta}_b^T \tag{4.24}$$

Hence, the closed loop dynamics is

$$\dot{\zeta} = \begin{pmatrix}-k_1\zeta_1 + \zeta_2 + (\theta - \hat{\theta}_a)\gamma_1\\ -k_2\zeta_2 + (\theta - \hat{\theta}_b)\phi_{22}(\zeta, \hat{\theta}_a, y_r, \dot{y}_r, \ddot{y}_r)\\ -k_3\gamma_3\end{pmatrix}$$

the update law for $\hat{\theta}_b$ is

$$\dot{\hat{\theta}}_b = \zeta_2\phi_{22}(\zeta, \hat{\theta}_a, y_r, \dot{y}_r, \ddot{y}_r) \tag{4.25}$$

The control input (4.24) and parameter update laws (4.23) and (4.25) guarantee that the closed-loop error dynamics is stable [44].

4.6.2 VSC With Three Unknown Parameters

For the case when $\theta_3 = L$ is unknown the VSC dynamics are

$$\dot{x} = \underbrace{\begin{pmatrix}\omega x_2\\ -\omega x_1\\ \frac{3}{C}(v_d x_1 + v_q x_2)\end{pmatrix}}_{f_0} + \underbrace{\begin{pmatrix}-x_1\\ -x_2\\ 0\end{pmatrix}}_{f_1}\theta_1 + \underbrace{\begin{pmatrix}0\\ 0\\ x_3\end{pmatrix}}_{f_2}\theta_2$$
$$+ \underbrace{\begin{pmatrix}0\\ 0\\ -\frac{3x_1}{C}\end{pmatrix}}_{g_{0,1}}u_1 + \underbrace{\begin{pmatrix}0\\ 0\\ -\frac{3x_2}{C}\end{pmatrix}}_{g_{0,2}}u_2 + \underbrace{\begin{pmatrix}0\\ 0\\ 1\end{pmatrix}}_{g_{1,3}}u_1\theta_3 + \underbrace{\begin{pmatrix}0\\ 1\\ 0\end{pmatrix}}_{g_{2,3}}u_2\theta_3$$

or

$$\dot{x} = f_0(x) + f_1(x)\theta_1 + f_2(x)\theta_2 + (g_{0,1}(x) + g_{1,3}(x)\theta_3)u_1 + (g_{0,2} + g_{2,3}\theta_3)u_2$$

We have $\mathcal{G}_0 = \text{span}\{g_{0,1}, g_{0,2}\}$, $\mathcal{G}_1 = \text{span}\{g_{0,1}, g_{0,2}, ad_f g_{0,1}, ad_f g_{0,2}\}$ and $\text{rank}\,\mathcal{G}_0 = \text{rank}\,\mathcal{G}_1 = 1$ for $x_1 \neq 0$ and $x_2 \neq 0$. Therefore, $\mathcal{G}_i$ is not constant rank $i+1$ and the linearizability condition for Proposition 2 is not satisfied.

4.7 Summary

Since the focus in the rest of the thesis is on the adaptive control of a VSC, this chapter starts with a review of adaptive control history. Different types of adaptive control are also summarized. Next, a systematic method for designing an adaptive control for regulation of a linearly parameterized system is reviewed. At last, this design is applied to a two parameter uncertainty problem for the VSC. It is shown that the theory is not admissible for uncertainty in three parameters. Therefore, other adaptive control approaches are investigated for the VSC with three unknown parameters in the following chapters.

Chapter 5

Adaptive PI Vector Control for Power Factor Correction

Improvement of vector control is investigated in this chapter in which an adaptive PI vector controller is designed to provide PFC. The method relies on a third order nonlinear model of the VSC which accounts for uncertainty in system parameters. The proposed method ensures asymptotic tracking of the q-axis current using an inner loop which contains two PI (Proportional-Integral) controllers which have adaptive decoupling terms. An outer loop PI controller's output defines the reference for the d-axis current control. The asymptotic stability of the closed-loop is proven using Lyapunov's method. The performance of the proposed method is evaluated in the simulation, and results show improved performance and ease of controller tuning.

5.1 Adaptive PI Vector Control of a VSC

As discussed in the previous chapter, the current dynamics in the dq frame are decoupled in the classical vector control strategy. However, this decoupling requires an accurate knowledge of the inductance parameter L. Although the integral term in the PI control compensates for steady state coupling disturbances, the transient system performance will be degraded. In this section, an adaptive PI vector control is proposed which guarantees the asymptotic decoupling of the current error dynamics with an uncertain inductance parameter.

Recalling the VSC bilinear model in dq frame from the previous chapter

$$\begin{aligned}\frac{di_d}{dt} &= -\frac{R}{L}i_d + \omega i_q + \frac{v_d}{L} - \frac{e_d}{L} \\ \frac{di_q}{dt} &= -\frac{R}{L}i_q - \omega i_d + \frac{v_q}{L} - \frac{e_q}{L} \\ \frac{dv_{dc}}{dt} &= \frac{3}{2}\cdot\frac{e_d i_d + e_q i_q}{C v_{dc}} - \frac{v_{dc}}{CR_c}\end{aligned} \tag{5.1}$$

We define e_d and e_q as

$$e_d = v_d + \hat{L}\omega i_q - v_1$$

$$e_q = v_q - \hat{L}\omega i_d - v_2$$

where $\hat{L}$ is the estimated value of the inductance. Therefore, the current dynamics is

$$\begin{aligned}\frac{di_d}{dt} &= -\frac{R}{L}i_d + \omega i_q\frac{\tilde{L}}{L} + \frac{v_1}{L} \\ \frac{di_q}{dt} &= -\frac{R}{L}i_q - \omega i_d\frac{\tilde{L}}{L} + \frac{v_2}{L}\end{aligned}$$

The new inputs v_1 and v_2 are defined using the PI control

$$v_1 = k_{p_d}(i_d^* - i_d) + k_{i_d}\int_0^t (i_d^* - i_d)d\tau$$

$$v_2 = k_{p_q}(i_q^* - i_q) + k_{i_q}\int_0^t (i_q^* - i_q)d\tau$$

Hence, the closed-loop current dynamics are

$$\begin{aligned}\frac{di_d}{dt} &= -\frac{R}{L}i_d + \omega i_q\frac{\tilde{L}}{L} + \frac{k_{p_d}}{L}(i_d^* - i_d) + \frac{k_{i_d}}{L}\int_0^t (i_d^* - i_d)d\tau \\ \frac{di_q}{dt} &= -\frac{R}{L}i_q - \omega i_d\frac{\tilde{L}}{L} + \frac{k_{p_q}}{L}(i_q^* - i_q) + \frac{k_{i_q}}{L}\int_0^t (i_q^* - i_q)d\tau\end{aligned}$$

where $\tilde{L} = L - \hat{L}$. The reference for i_d is the output of the PI compensator for dc voltage

$$I_d^*(s) = \left(k_{p_v} + \frac{k_{i_v}}{s}\right)(v_{dc}^* - V_{dc}) \tag{5.2}$$

It is assumed that the dc voltage dynamics is much slower than the time scale of the current dynamics. Therefore, in designing the inner loop control, the current reference values i.e., i_d^* and i_q^* are assumed to be constant. We define $(\tilde{i}_d, \tilde{i}_q) = (i_d^* - i_d, i_q^* - i_q)$ so that

$$\begin{aligned}-\frac{di_d}{dt} = \frac{d\tilde{i}_d}{dt} &= -\frac{R + k_{p_d}}{L}\tilde{i}_d - \omega i_q\frac{\tilde{L}}{L} - \frac{k_{i_d}}{L}\int_0^t \tilde{i}_d d\tau + \frac{R}{L}i_d^* \\ -\frac{di_q}{dt} = \frac{d\tilde{i}_q}{dt} &= -\frac{R + k_{p_q}}{L}\tilde{i}_q + \omega i_d\frac{\tilde{L}}{L} - \frac{k_{i_q}}{L}\int_0^t \tilde{i}_q d\tau + \frac{R}{L}i_q^*\end{aligned} \tag{5.3}$$

To eliminate the integrator terms in (5.3), we define new error states as

$$e_1 = \int_0^t \tilde{i}_d d\tau - \frac{R}{k_{i_d}} i_d^*, \quad e_2 = \tilde{i}_d,$$
$$e_3 = \int_0^t \tilde{i}_q d\tau - \frac{R}{k_{i_q}} i_q^*, \quad e_4 = \tilde{i}_q$$

Therefore, the current dynamics (5.3) can be expressed as

$$\begin{aligned}
\dot{e}_1 &= e_2 \\
\dot{e}_2 &= -\frac{R + k_{p_d}}{L} e_2 - \omega i_q \frac{\tilde{L}}{L} - \frac{k_{i_d}}{L} e_1 \\
\dot{e}_3 &= e_4 \\
\dot{e}_4 &= -\frac{R + k_{p_q}}{L} e_4 + \omega i_d \frac{\tilde{L}}{L} - \frac{k_{i_q}}{L} e_3
\end{aligned}$$

With the parameter error defined as $\tilde{\theta} = \tilde{L}/L$, the error dynamics can be written

$$\dot{e} = \Psi e + \Gamma^T \tilde{\theta} \tag{5.4}$$

where

$$\Psi = \begin{bmatrix} \Psi_1 & 0 \\ 0 & \Psi_2 \end{bmatrix}$$

and

$$\Psi_1 = \begin{bmatrix} 0 & 1 \\ -\frac{k_{i_d}}{L} & -\frac{R+k_{p_d}}{L} \end{bmatrix}, \quad \Psi_2 = \begin{bmatrix} 0 & 1 \\ -\frac{k_{i_q}}{L} & -\frac{R+k_{p_q}}{L} \end{bmatrix}$$
$$\Gamma = \begin{bmatrix} 0 & -\omega i_q & 0 & +\omega i_d \end{bmatrix}$$

In order to analyze the convergence of the tracking error, the following Lyapunov function candidate is considered

$$V = e^T P e + \Lambda^{-1} \tilde{\theta}^2 \tag{5.5}$$

where $\Lambda > 0$ and $P \in \mathbb{R}^{4\times 4}$ is the symmetric positive definite matrix defined as

$$P = \begin{bmatrix} P_1 & 0 \\ 0 & P_2 \end{bmatrix}$$

where P_i, $i = 1, 2$ are solutions of

$$\Psi_i^T P_i + P_i \Psi_i = -Q_i, \quad i = 1, 2 \tag{5.6}$$

where $Q_i \in \mathbb{R}^{2\times 2}$, $i = 1, 2$ are symmetric positive definite matrices. Since Ψ_i is Hurwitz, there exists a unique symmetric positive definite matrix P_i which

satisfies (5.6). The derivative of (5.5) along the current error dynamics (5.4) is

$$\dot{V} = e^T(\Psi^T P + P\Psi)e + 2e^T P\Gamma\tilde{\theta} + 2\Lambda^{-1}\dot{\tilde{\theta}}\tilde{\theta} \tag{5.7}$$

Hence, taking a parameter update law

$$\dot{\hat{L}}/L = -\dot{\tilde{\theta}} = \Lambda\Gamma Pe \tag{5.8}$$

and substituting it into (5.7) yields

$$\dot{V} = -e^T Qe \leq 0 \tag{5.9}$$

where Q is a symmetric positive matrix

$$Q = \begin{bmatrix} Q_1 & 0 \\ 0 & Q_2 \end{bmatrix}$$

Since V is positive definite and radially unbounded, the equilibrium $z = (e^T, \tilde{L})^T = 0$ is globally uniformly stable and the solution $(e^T, \tilde{L})$ of (5.4) and (5.8) dynamics are uniformly bounded for any initial condition provided $v_{dc}(t) > 2v_d, t \geq 0$. Integration of (5.9) with respect to time gives

$$\int_0^t e^T(\tau)Qe(\tau)\,d\tau = -\int_0^t \dot{V}(\tau)\,d\tau = V(0) - V(t)$$

which implies

$$\lim_{t\to\infty}\int_0^t e^T(\tau)Qe(\tau)\,d\tau = V(0) - V(\infty) < \infty$$

since z is bounded. According to Barbalat's Lemma we conclude $\lim_{t\to\infty}||e|| = 0$ or the tracking error is asymptotically stable [44, 54]. The conditions for parameter estimate error convergence follow from Matrosov's Theorem [54, 84]. A sufficient condition is given by

$$\Gamma(i^*, t)\Gamma(i^*, t)^T = \omega^2((i_d^*)^2 + (i_q^*)^2) > 0$$

We remark that although parameter error remains bounded, convergence is not required to achieve asymptotic trajectory tracking. A block diagram of adaptive PI vector control is shown in Fig. 5.1.

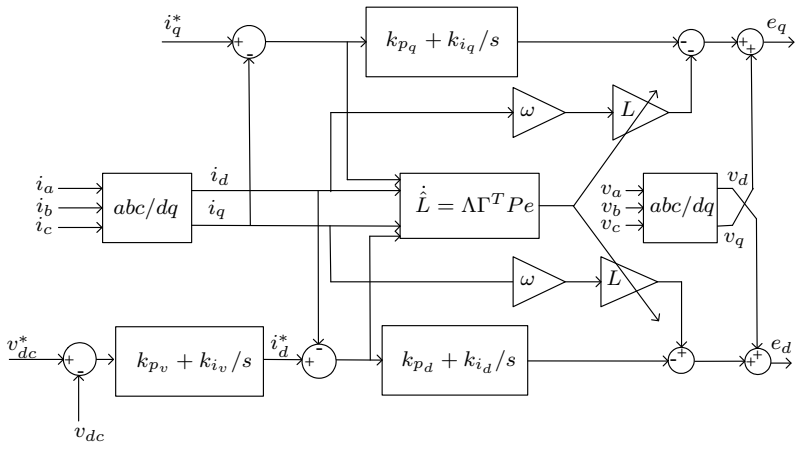

Figure 5.1: Block diagram of adaptive PI vector control

5.2 Stability of dc Voltage Dynamics

As mentioned earlier, the steady-state effect of the ac side resistor losses P_R can be included in the effective dc side resistance R_c. Therefore, as in [17] the dc dynamics in (5.1) can be rewritten

$$\frac{dv_{dc}}{dt} = \frac{3}{2} \cdot \frac{v_d i_d + v_q i_q}{C v_{dc}} - \frac{v_{dc}}{C R_c}$$

If we assume that the ac supply is balanced then $v_q = 0$. The dc voltage is indirectly controlled by the current i_d using the PI controller (5.2). If we assume the current loop dynamics are significantly faster than dc voltage dynamics then

$$\frac{dv_{dc}}{dt} = \frac{3v_d}{2} \cdot \frac{k_{p_v}\tilde{v}_{dc} + k_{i_v}\int_0^t \tilde{v}_{dc} d\tau}{C v_{dc}} - \frac{v_{dc}}{C R_c} \tag{5.10}$$

where $\tilde{v}_{dc} = v_{dc}^* - v_{dc}$. Defining $(x_1, x_2) = \left(\int_0^t \tilde{v}_{dc} d\tau - (2{v_{dc}^*}^2)/(3R_c k_{i_v} v_d), \tilde{v}_{dc} \right)$ then (5.10) can be written as

$$\begin{aligned} \dot{x}_1 &= x_2 \\ \dot{x}_2 &= \frac{k_{v_d}}{v_{dc}^* - x_2}(-k_{i_v} x_1 - \bar{k}_{p_v} x_2) - \frac{x_2}{C R_c} \end{aligned} \tag{5.11}$$

in which $k_{v_d} = (3v_d)/(2C)$ and $\bar{k}_{p_v} = k_{p_v} + (2v_{dc}^*)/(3v_d R_c)$. It is assumed that $v_{dc} > 2v_d$, therefore $v_{dc}^* - x_2 > 0$. It can be shown that (5.11) has an equilibrium point at the origin. A Lyapunov stability analysis is used to prove asymptotic stability. We use a variable gradient method to compute a Lyapunov function

V for (5.11). That is, we take $g(x) = \partial V/\partial x$ and choose g such that it is the gradient of a positive definite function V and $\dot{V}$ is negative definite. That is, we take $g(x) = [g_1(x), g_2(x)]$ and

$$\begin{aligned}
&\frac{\partial g_1(x)}{\partial x_2} = \frac{\partial g_2(x)}{\partial x_1} \\
&\dot{V} = g_1(x)x_2 - g_2(x)(\frac{k_{v_d}}{v^*_{dc} - x_2}(-k_{i_v}x_1 - \bar{k}_{p_v}x_2) - \frac{x_2}{CR_c}) < 0 \text{ for } x \neq 0 \\
&V(x) = \int_0^{x_1} g_1(y_1)dy_1 + \int_0^{x_2} g_2(y_2)dy_2 > 0 \text{ for } x \neq 0
\end{aligned} \tag{5.12}$$

Taking g of the form

$$g(x) = \begin{bmatrix} \alpha(x)x_1 + \beta(x)x_2 \\ \gamma(x)x_1 + \eta(x)x_2 \end{bmatrix}$$

where scalar functions α, β, γ and η are to be determined, constraint (5.12) is

$$\beta(x) + \frac{\partial \alpha(x)}{\partial x_2}x_1 + \frac{\partial \beta(x)}{\partial x_2}x_2 = \gamma(x) + \frac{\partial \gamma(x)}{\partial x_1}x_1 + \frac{\partial \eta(x)}{\partial x_1}x_2$$

The derivative $\dot{V}$ is given by

$$\begin{aligned}
\dot{V} = &\left[\alpha(x) - \frac{k_{v_d}}{v^*_{dc} - x_2}\left(\bar{k}_{p_v}\gamma(x) + k_{i_v}\eta(x)\right) - \frac{1}{CR_c}\gamma(x)\right]x_1x_2 \\
&- \left[\frac{k_{v_d}}{v^*_{dc} - x_2}k_{i_v}\gamma(x)\right]x_1^2 - \left[\frac{k_{v_d}}{v^*_{dc} - x_2}\bar{k}_{p_v}\eta(x) + \frac{1}{CR_c}\eta(x) - \beta(x)\right]x_2^2
\end{aligned} \tag{5.13}$$

To cancel the indefinite terms in (5.13) and satisfy (5.12) we take

$$\alpha(x) = k_{v_d}k_{i_v},\ \beta(x) = 0,\ \gamma(x) = 0,\ \eta(x) = v^*_{dc} - x_2$$

Hence,

$$\dot{V} = -(k_{v_d}\bar{k}_{p_v} + \frac{1}{CR_c}(v^*_{dc} - x_2))x_2^2 \leq 0$$

The expression for g is therefore

$$g(x) = \begin{bmatrix} k_{v_d}k_{i_v}x_1 \\ (v^*_{dc} - x_2)x_2 \end{bmatrix}$$

Integration yields the Lyapunov function

$$\begin{aligned}
V(x) &= \int_0^{x_1}(k_{v_d}k_{i_v}y_1)dy_1 + \int_0^{x_2}(v^*_{dc}y_2 - y_2^2)dy_2 \\
&= \frac{1}{2}k_{v_d}k_{i_v}x_1^2 + \frac{1}{2}v^*_{dc}x_2^2 - \frac{1}{3}x_2^3 = \frac{1}{2}k_{v_d}k_{i_v}x_1^2 + \left(\frac{1}{6}v^*_{dc} + \frac{1}{3}(v^*_{dc} - x_2)\right)x_2^2
\end{aligned}$$

Let $D = \{(x_1, x_2)^T \in \mathbb{R}^2 : (v_{dc}^* - x_2) > 0\}$ where V is positive definite in D and $\dot{V}$ is negative semidefinite. Defining $S = \{(x_1, x_2)^T \in D : \dot{V} = 0\}$ and since

$$\dot{V} = 0 \Rightarrow x_2 = 0 \Rightarrow \dot{x}_2 = 0 \Rightarrow x_1 = 0$$

this implies the only point in S is the origin which is an invariant solution. Thus by LaSalle's Theorem [71] the origin is asymptotically stable.

5.3 Simulation Results

Simulations of the adaptive PI vector control and classical vector control are performed in MATLAB/Simulink. The controls are applied to the third order nonlinear model of the VSC (5.1). The q-axis current reference varies between -3 A and 3 A, and the dc voltage reference changes between 170 V and 200 V. The q-axis current and dc voltage references are varied at different time instances.

5.3.1 Classical Vector Control with Parameter Uncertainties

As previously mentioned, vector control requires knowledge of the terms ωi_q and $-\omega i_d$ which are canceled in the i_d and i_q dynamics. This cancelation can only be performed exactly if L is known. Any deviation of L from its nominal value affects control performance [12]. To investigate the effect of uncertainty in L we take its value as three times the nominal inductance. As seen in Fig. 5.2, the system tracking performance is degraded. The control inputs are saturated in transient when the references change. On the other hand, we will demonstrate in Section 5.3.2 that the proposed adaptive PI vector control can achieve improved performance.

5.3.2 Adaptive PI Vector Control with Parameter Uncertainties

The performance of adaptive PI vector control when there is an uncertainty in the inductance value is investigated in this section. The adaptive PI vector

controller gains are provided in Table 5.1. As shown in Fig. 5.3(a) the controller achieves good trajectory tracking. At the beginning of the simulation the outputs are similar to the classical vector control. However, the performance significantly improves in a few seconds. It can be seen in Fig. 5.3(b) that the control inputs quickly become unsaturated. It is clear that control performance, which depends on the estimated value of inductance, improves with time as this estimate becomes more accurate. Fig. 5.3(b) also shows the convergence of the inductance estimate to its actual value, i.e., 2 mH. The matrices P_1 and P_2 are obtained using (5.6) with $Q_i = -I$.

5.4 Summary

In this chapter an adaptive control system is developed which ensures PFC. In comparison with the classical vector control, this method has adaptive decoupling terms in its current loops which account for uncertainty in the system parameters. The performance of the proposed controller is evaluated in simulation and the benefit of adapting the inductance estimate is demonstrated. In the next chapter, two other adaptive methods, adaptive current control and full adaptive control, for a VSC is proposed. Adaptive current control structure is similar to vector control except that it does not have integration terms in its current loop. We note that the decoupling of the current and voltage loops is considered in designing the controller for adaptive current control and adaptive PI vector control while this is not the case in designing the full adaptive control.

Table 5.1: Adaptive PI vector controller gains used in simulation

Gains	Value
(k_{dp}, k_{di})	$(0.04\ \text{V/A}, 0.2\ \text{V/(A.s)})$
(k_{qp}, k_{qi})	$(2\ \text{V/A}, 60\ \text{V/(A.s)})$
(k_{vp}, k_{vi})	$(1\ \text{A/V}, 4\ \text{A/(V.s)})$
Λ	10^{-7}

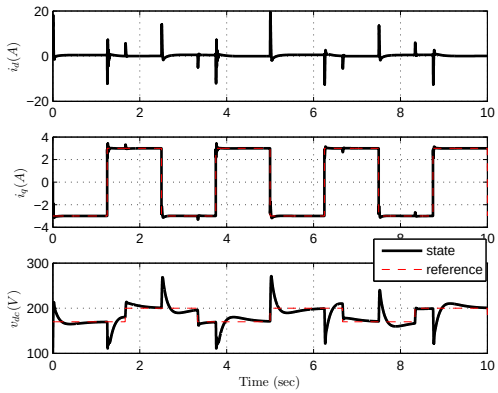

(a) trajectories of state and reference

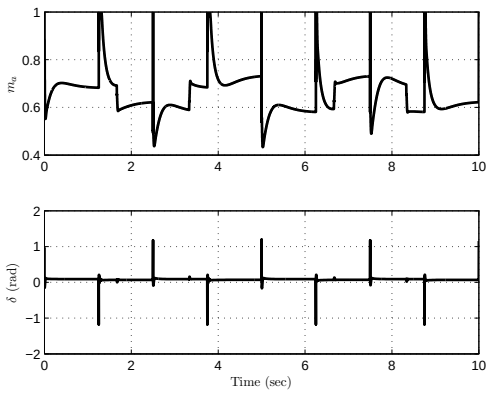

(b) control inputs m_a and δ

Figure 5.2: Simulation results of vector control using VSC nonlinear model with parameter uncertainties

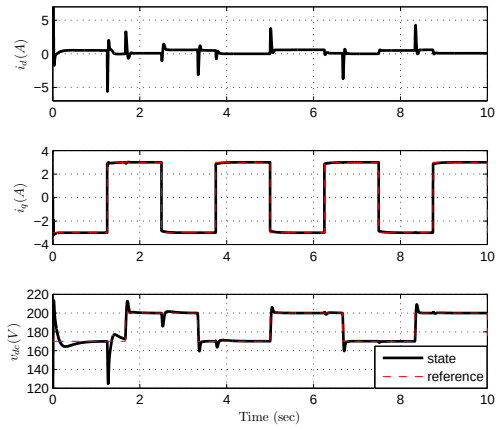

(a) trajectories of state and reference

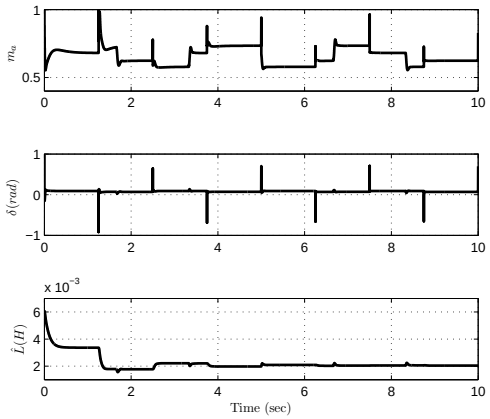

(b) control inputs and inductance estimate

Figure 5.3: Simulation results of adaptive PI vector control using VSC nonlinear model with parameter uncertainties

Chapter 6

Adaptive Control of VSC for Power Factor Correction

In this chapter two adaptive controllers are designed to provide PFC using a VSC. The proposed adaptive controls account for uncertainty in the VSC circuit parameters R, L and R_c. The chapter is organized as follows: first, the adaptive current control with PI voltage control is presented in Section 6.1, next the so-called *full* adaptive control is presented in Section 6.2. Finally, simulation validations demonstrate the full adaptive method's performance.

6.1 Adaptive Current Control of VSC with Voltage PI Controller

Let us first define non-zero parameters $\theta_1 = L$, $\theta_2 = R$ and denote their estimates $\hat{\theta}_i$, $i = 1, 2$ and the parameter estimate error is $\tilde{\theta}_i = \theta_i - \hat{\theta}_i, i = 1, 2$, with $\tilde{\theta} = (\frac{\tilde{\theta}_1}{\theta_1}, \frac{\tilde{\theta}_2}{\theta_1})^T$. The tracking error is denoted $\tilde{x} = (\tilde{x}_1, \tilde{x}_2, \tilde{x}_3)^T$ with $\tilde{x}_i = x_i - x_{ir}$ where x_{ir} stands for reference trajectory. Recalling the VSC linear model

$$\dot{x} = Ax + Bu \tag{6.1}$$

where

$$A = \begin{bmatrix} -R/L & \omega & 0 \\ -\omega & -R/L & 0 \\ 1 & v_q/v_q & -2/(CR_c) \end{bmatrix}, B = \begin{bmatrix} 1/L & 0 \\ 0 & 1/L \\ 0 & 0 \end{bmatrix}$$

and

$$x = (x_1, x_2, x_3)^T = (i_d, i_q, \frac{C}{3v_d} v_{dc}^2)^T, \quad u = (u_1, u_2)^T = (v_d - e_d, v_q - e_q)^T$$

Taking control input

$$u_2 = \hat{L}\left[\omega x_1 + \frac{\hat{R}}{\hat{L}}x_2 + \dot{x}_{2r} - k_2\tilde{x}_2\right]$$
$$= \hat{R}x_2 - \hat{L}\underbrace{[-\omega x_1 - \dot{x}_{2r} + k_2\tilde{x}_2]}_{\alpha_2(x,t)} = \hat{R}x_2 - \hat{L}\alpha_2(x,t)$$

where k_2 is a positive constant and substituting u_2 into the q-axis current dynamics gives

$$\dot{\tilde{x}}_2 = \dot{x}_2 - \dot{x}_{2r} = \alpha_2 - k_2\tilde{x}_2 + \dot{x}_{2r} - \frac{R}{L}x_2 + \frac{u_2}{L} - \dot{x}_{2r}$$
$$= -\frac{\tilde{R}}{L}x_2 + \alpha_2\left(1 - \frac{\hat{L}}{L}\right) - k_2\tilde{x}_2 \tag{6.2}$$
$$= \frac{\tilde{R}}{L}\beta_2 + \frac{\tilde{L}}{L}\alpha_2 - k_2\tilde{x}_2$$

in which $\beta_2(x) = -x_2$, $\tilde{R} = R - \hat{R}$ and $\tilde{L} = L - \hat{L}$. A similar control expression is taken for u_1

$$u_1 = \hat{L}\left[-\omega x_2 + \frac{\hat{R}}{\hat{L}}x_2 + \dot{x}_{1r} - k_1\tilde{x}_1\right]$$
$$= \hat{R}x_1 - \hat{L}\underbrace{[\omega x_2 - \dot{x}_{1r} + k_1\tilde{x}_1]}_{\alpha_1(x,t)} = \hat{R}x_1 - \hat{L}\alpha_1(x,t)$$

where $k_1 > 0$. Substituting u_1 into the d-axis current dynamics gives

$$\dot{\tilde{x}}_1 = \frac{\tilde{R}}{L}\beta_1 + \frac{\tilde{L}}{L}\alpha_1 - k_1\tilde{x}_1 \tag{6.3}$$

in which $\beta_1(x) = -x_1$. Summarizing the error dynamics gives

$$\underbrace{\begin{bmatrix}\dot{\tilde{x}}_1\\ \dot{\tilde{x}}_2\end{bmatrix}}_{\dot{\tilde{x}}} = \underbrace{\begin{bmatrix}-k_1 & 0\\ 0 & -k_2\end{bmatrix}}_{\Psi}\underbrace{\begin{bmatrix}\tilde{x}_1\\ \tilde{x}_2\end{bmatrix}}_{\tilde{x}} + \underbrace{\begin{bmatrix}\alpha_1 & \beta_1\\ \alpha_2 & \beta_2\end{bmatrix}}_{\Gamma^T}\underbrace{\begin{bmatrix}\tilde{L}/L\\ \tilde{R}/L\end{bmatrix}}_{\tilde{\theta}}$$

where

$$\alpha_1(x,t) = \omega x_2 + k_1\tilde{x}_1 - \dot{x}_{1r}$$
$$\alpha_2(x,t) = -\omega x_1 - \dot{x}_{2r} + k_2\tilde{x}_2$$
$$\beta_1(x,t) = -x_1$$
$$\beta_2(x,t) = -x_2$$

Therefore with proper choices of VSC inputs i.e., $u_1(x, \hat{\theta}, t)$ and $u_2(x, \hat{\theta}, t)$ the tracking error dynamics have the form

$$\dot{\tilde{x}} = \Psi\tilde{x} + \Gamma^T(x, \hat{\theta}, t)\tilde{\theta} \tag{6.4}$$

where $\tilde{\theta} = (\tilde{L}/L, \tilde{R}/L)^T$; $\Psi \in \mathbb{R}^{2\times 2}$ is a constant Hurwitz matrix; $\Gamma(x, \hat{\theta}, t) \in \mathbb{R}^{2\times 2}$ is a smooth function uniformly bounded in t [44, 69].

In order to analyze the convergence of the tracking error we consider the quadratic Lyapunov function

$$V = \tilde{x}^T P\tilde{x} + \tilde{\theta}^T\Lambda^{-1}\tilde{\theta} \tag{6.5}$$

where $\Lambda \in \mathbb{R}^{2\times 2}$ is a symmetric positive definite matrix and $P \in \mathbb{R}^{2\times 2}$ is the symmetric positive definite solution of

$$\Psi^T P + P\Psi = -Q \tag{6.6}$$

where $Q \in \mathbb{R}^{2\times 2}$ is a symmetric positive definite matrix. Since Ψ is Hurwitz, there exists a unique symmetric positive definite matrix P which satisfies (6.6). The derivative of (6.5) along the error dynamics (6.4) is

$$\dot{V} = \tilde{x}^T(\Psi^T P + P\Psi)\tilde{x} + 2\tilde{x}^T P\Gamma^T\tilde{\theta} + 2\dot{\tilde{\theta}}^T\Lambda^{-1}\tilde{\theta} \tag{6.7}$$

Hence, taking a parameter update law

$$\dot{\tilde{\theta}} = -\Lambda\Gamma P\tilde{x} \tag{6.8}$$

and substituting it into (6.7) yields

$$\dot{V} = -\tilde{x}^T Q\tilde{x} \leq 0 \tag{6.9}$$

Since V is positive definite and radially unbounded, the equilibrium $z = (\tilde{x}^T, \tilde{\theta}^T)^T = 0$ is globally uniformly stable and the solution $(\tilde{x}, \tilde{\theta})$ of (6.4) and (6.8) dynamics are uniformly bounded for any initial condition provided $v_{dc} > 2v_d$. Integration of (6.9) with respect to time gives

$$\int_0^t \tilde{x}^T(\tau)Q\tilde{x}(\tau)\, d\tau = -\int_0^t \dot{V}(\tau)\, d\tau = V(0) - V(t) \tag{6.10}$$

which implies

$$\lim_{t\to\infty}\int_0^t \tilde{x}^T(\tau)Q\tilde{x}(\tau)\,d\tau = V(0) - V(\infty) < \infty \tag{6.11}$$

since z is bounded, according to Barbalat's Lemma we conclude $\lim_{t\to\infty}||\tilde{x}|| = 0$ or the tracking error is asymptotically stable [71].

In order to simplify the implementation of the parameter update law (6.8) we take Λ and P diagonal:

$$P = \begin{bmatrix} P_1 & 0 \\ 0 & P_2 \end{bmatrix}, \quad \Lambda = \begin{bmatrix} \Lambda_1 & 0 \\ 0 & \Lambda_2 \end{bmatrix}$$

where $P_i, \Lambda_i > 0, i = 1, 2$. This simple choice of P satisfies (6.6) for any Q. Therefore, the parameter update law is

$$\begin{aligned} \dot{\hat{L}} &= \Lambda_{11}(\alpha_1 P_1 \tilde{x}_1 + \alpha_2 P_2 \tilde{x}_2) \\ \dot{\hat{R}} &= \Lambda_{22}(\beta_1 P_1 \tilde{x}_1 + \beta_2 P_2 \tilde{x}_2) \end{aligned} \tag{6.12}$$

If we assume the ac supply is balanced then v_q is zero. The dc voltage is indirectly controlled with the current i_d. The simplified dc voltage dynamics is

$$\dot{\tilde{x}}_3 = (\tilde{x}_1 + x_{1r}) - \frac{2}{CR_c}x_3 - \dot{x}_{3r}$$

Taking

$$x_{1r} = -\left(k_3\tilde{x}_3 + k_4\int_0^t \tilde{x}_3 \mathrm{d}\tau\right)$$

where $k_i > 0, i = 3, 4$ gives the tracking dynamics

$$\dot{\tilde{x}}_3 = -k_3\tilde{x}_3 - k_4\int_0^t \tilde{x}_3 \mathrm{d}\tau + \frac{3v_d}{C}\tilde{x}_1 - \frac{2x_3}{CR_c} \tag{6.13}$$

It is obvious that if we assume the current loop is significantly faster than the dc voltage loop and dc voltage reference is constant, $\lim_{t\to\infty}||\tilde{x}_3|| = 0$.

6.2 Full Adaptive Control Design

In this section we define parameters $\theta_1 = L$, $\theta_2 = R$, $\theta_3 = 1/R_c$ and denote their estimates $\hat{\theta}_i$, $i = 1, 2, 3$ and the parameter estimate error is $\tilde{\theta}_i = \theta_i - \hat{\theta}_i, i = 1, 2, 3$, with $\tilde{\theta} = (\frac{\tilde{\theta}_1}{\theta_1}, \frac{\tilde{\theta}_2}{\theta_1}, \tilde{\theta}_3)^T$. The tracking error is denoted $\tilde{x} = (\tilde{x}_1, \tilde{x}_2, \tilde{x}_3)^T$ with $\tilde{x}_i = x_i - x_{ir}$ where x_{ir} stands for the reference trajectory. With proper

choices of VSC inputs i.e., $u_1(x,\hat{\theta},t)$ and $u_2(x,\hat{\theta},t)$ the tracking error dynamics have the form

$$\dot{\tilde{x}} = \Psi\tilde{x} + \Gamma^T(x,\hat{\theta},t)\tilde{\theta} \tag{6.14}$$

where $\Psi \in \mathbb{R}^{3\times 3}$ is a constant Hurwitz matrix; $\Gamma(x,\hat{\theta},t) \in \mathbb{R}^{3\times 3}$ is a smooth function uniformly bounded in t [44, 69]. Taking the linearizing control

$$u_2 = -\alpha_2\hat{\theta}_1 + x_2\hat{\theta}_2 \tag{6.15}$$

where $\alpha_2 = -\omega x_1 - \dot{x}_{2r} + k_2(x_2 - x_{2r})$ in which k_2 is a positive controller gain. Substituting this control into the q-axis current dynamics gives

$$\dot{\tilde{x}}_2 = -k_2\tilde{x}_2 + \alpha_2\frac{\tilde{\theta}_1}{\theta_1} + \beta_2\frac{\tilde{\theta}_2}{\theta_1}$$

where we have defined $\beta_2 = -x_2$. Next, the dc voltage tracking error dynamics are considered and can be used to define a reference for the d-axis current

$$\dot{\tilde{x}}_3 = \tilde{x}_1 + x_{1r} + \frac{v_q}{v_d}x_2 - \frac{2\theta_3}{C}x_3 - \dot{x}_{3r}$$

Taking

$$x_{1r} = -\left(\frac{v_q}{v_d}x_2 + \gamma_3\hat{\theta}_3 - \dot{x}_{3r} + k_3(x_3 - x_{3r})\right) \tag{6.16}$$

where $\gamma_3 = -2x_3/C$, gives the tracking dynamics

$$\dot{\tilde{x}}_3 = -k_3\tilde{x}_3 + \tilde{x}_1 + \gamma_3\tilde{\theta}_3$$

Using (6.16) and the input

$$u_1 = -\alpha_1\hat{\theta}_1 + x_1\hat{\theta}_2 \tag{6.17}$$

we obtain the d-axis tracking error dynamics

$$\dot{\tilde{x}}_1 = -k_1\tilde{x}_1 + \left(\alpha_1 + \frac{v_q}{v_d}\alpha_2\right)\frac{\tilde{\theta}_1}{\theta_1} + \left(\beta_1 + \frac{v_q}{v_d}\beta_2\right)\frac{\tilde{\theta}_2}{\theta_1} + \gamma_1\tilde{\theta}_3$$

where

$$\begin{aligned}\alpha_1 = {} & \omega x_2 + \hat{\xi}_3(x_1 + \gamma_3\hat{\theta}_3) + \gamma_3\dot{\hat{\theta}}_3 - k_3\dot{x}_{3r} - \ddot{x}_{3r} \\ & + k_1(x_1 - x_{1r}) + \frac{v_q}{v_d}\left(-k_2(x_2 - x_{2r}) + \hat{\xi}_3 x_2 + \dot{x}_{2r}\right),\end{aligned}$$

$$\beta_1 = -x_1, \quad \hat{\xi}_3 = k_3 - \frac{2\hat{\theta}_3}{C}, \quad \gamma_1 = \hat{\xi}_3\gamma_3$$

Hence, the error dynamics is in form (6.14) with

$$\Psi = \begin{bmatrix} -k_1 & 0 & 0 \\ 0 & -k_2 & 0 \\ 1 & 0 & -k_3 \end{bmatrix}, \Gamma = \begin{bmatrix} \alpha_1 + (v_q/v_d)\alpha_2 & \alpha_2 & 0 \\ \beta_1 + (v_q/v_d)\beta_2 & \beta_2 & 0 \\ \gamma_1 & 0 & \gamma_3 \end{bmatrix}$$

In order to analyze the convergence of the tracking error we consider the quadratic Lyapunov function

$$V = \tilde{x}^T P \tilde{x} + \tilde{\theta}^T \Lambda^{-1} \tilde{\theta} \tag{6.18}$$

where $\Lambda \in \mathbb{R}^{3\times 3}$ is a symmetric positive definite matrix and $P \in \mathbb{R}^{3\times 3}$ is the symmetric positive definite solution of

$$\Psi^T P + P\Psi = -Q \tag{6.19}$$

where $Q \in \mathbb{R}^{3\times 3}$ is a symmetric positive definite matrix. Since Ψ is Hurwitz, there exists a unique symmetric positive definite matrix P which satisfies (6.19). The derivative of (6.18) along the error dynamics (6.14) is

$$\dot{V} = \tilde{x}^T(\Psi^T P + P\Psi)\tilde{x} + 2\tilde{x}^T P\Gamma^T \tilde{\theta} + 2\dot{\tilde{\theta}}^T \Lambda^{-1}\tilde{\theta} \tag{6.20}$$

Hence, taking a parameter update law

$$\dot{\tilde{\theta}} = -\Lambda\Gamma P\tilde{x} \tag{6.21}$$

and substituting it into (6.20) yields

$$\dot{V} = -\tilde{x}^T Q\tilde{x} \leq 0 \tag{6.22}$$

Since V is positive definite and radially unbounded, the equilibrium $z = (\tilde{x}^T, \tilde{\theta}^T)^T = 0$ is globally uniformly stable and the solution $(\tilde{x}, \tilde{\theta})$ of (6.14) and (6.21) dynamics are uniformly bounded for any initial condition provided $v_{dc}(t) > 2v_d, t \geq 0$. Integration of (6.22) with respect to time gives

$$\int_0^t \tilde{x}^T(\tau)Q\tilde{x}(\tau)\, d\tau = -\int_0^t \dot{V}(\tau)\, d\tau = V(0) - V(t) \tag{6.23}$$

which implies

$$\lim_{t\to\infty} \int_0^t \tilde{x}^T(\tau)Q\tilde{x}(\tau)\, d\tau = V(0) - V(\infty) < \infty \tag{6.24}$$

since z is bounded, according to Barbalat's Lemma we conclude $\lim_{t\to\infty} ||\tilde{x}|| = 0$ or the tracking error is asymptotically stable [71].

The conditions for parameter estimate error convergence follow from Matrosov's Theorem [54, 84]. A sufficient condition is given by

$$\Gamma(x_r, \tilde{\theta}, t)^T \Gamma(x_r, \tilde{\theta}, t) > 0$$

We remark that although parameter error must remain bounded, convergence is not required to achieve asymptotic trajectory tracking.

In order to simplify the implementation of the parameter update law (6.21) we take Λ and P diagonal:

$$P = \begin{bmatrix} P_1 & 0 & 0 \\ 0 & P_2 & 0 \\ 0 & 0 & P_3 \end{bmatrix}, \quad \Lambda = \begin{bmatrix} \Lambda_1 & 0 & 0 \\ 0 & \Lambda_2 & 0 \\ 0 & 0 & \Lambda_3 \end{bmatrix}$$

where $P_i, \Lambda_i > 0, i = 1, 2, 3$. This simple choice of P satisfies (6.19) for any Q. Therefore, the parameter update law is

$$\begin{aligned} \dot{\hat{\theta}}_1 &= -\dot{\tilde{\theta}}_1 = \Lambda_1 \left((\alpha_1 + \frac{v_q}{v_d}\alpha_2) P_1 \tilde{x}_1 + \alpha_2 P_2 \tilde{x}_2 \right) \\ \dot{\hat{\theta}}_2 &= -\dot{\tilde{\theta}}_2 = \Lambda_2 \left((\beta_1 + \frac{v_q}{v_d}\beta_2) P_1 \tilde{x}_1 + \beta_2 P_2 \tilde{x}_2 \right) \\ \dot{\hat{\theta}}_3 &= -\dot{\tilde{\theta}}_3 = \Lambda_3 \left(\gamma_1 P_1 \tilde{x}_1 + \gamma_3 P_3 \tilde{x}_3 \right) \end{aligned} \tag{6.25}$$

We remark that the same technique and procedure can be used when the value for capacitance C is not known. In this case, the adaptive control would include an additional parameter. A block diagram of adaptive control system is shown in Fig. 6.1.

From (6.14) and (6.25) there are nine gains k_i, P_i, Λ_i to be chosen which affect the transient closed-loop response. We establish approximate values for these gains based on a linearization of the closed-loop system (6.14) and (6.21) about an equilibrium point $z = 0$:

$$\dot{z} = A_c z$$

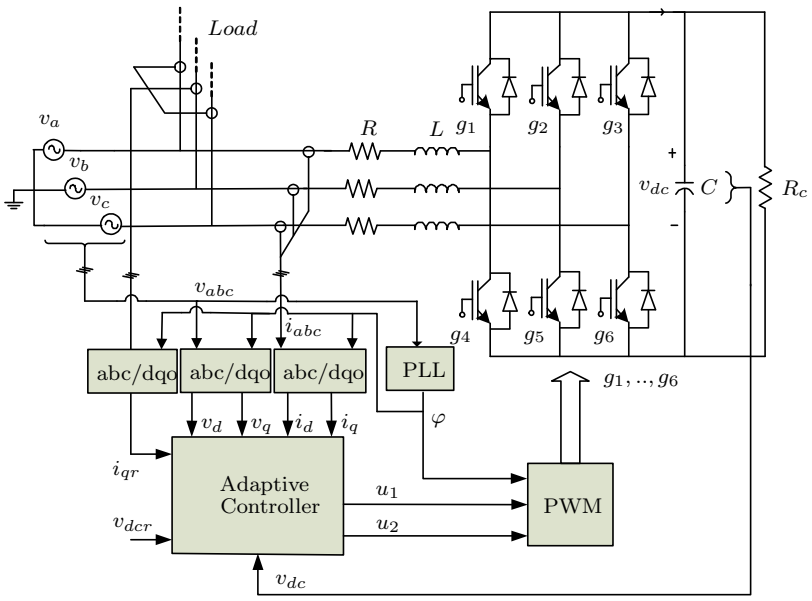

Figure 6.1: VSC adaptive control (ADC) block diagram

where

$$A_c = \begin{bmatrix} \Psi & A_{c12} \\ -\Lambda\, A_{c12}^T\, P & 0 \end{bmatrix},$$

$$A_{c12} = \begin{bmatrix} (1 - v_q/v_d)\omega x_{2r} & \gamma_{3r}\theta_3 & \xi_3\gamma_{3r} \\ (v_q/v_d)\omega x_{2r} + \omega\gamma_{3r}\theta_3 & -x_{2r} & 0 \\ 0 & 0 & \gamma_{3r} \end{bmatrix},$$

$$\xi_3 = k_3 - \frac{2\theta_3}{C}, \quad \gamma_{3r} = -\frac{2x_{3r}}{C}$$

The characteristic polynomial of A_c can be used to obtain controller gains which approximately provide the desired transient performance. To account for nonlinearity, modeling errors, and disturbances we adjust the gains experimentally. The convergence rate of the parameter estimate and tracking error can be adjusted with Λ_i and k_i gains, respectively. This can be seen from the tracking error dynamics for zero parameter error, i.e., $\dot{\tilde{x}} = \Psi\tilde{x}$. Hence, k_i directly controls the rate of convergence of $\tilde{x}_i$ and can be adjusted accordingly. The convergence rate for $\tilde{\theta}_i$ can be adjusted with Λ_i with larger Λ_i providing faster convergence. Gains P_i scale the tracking errors forcing the parameter estimate error dynamics. It should be noted that larger values of Λ_i, P_i and k_i generally lead to larger amplitude control signals and faster transient performance. However, since the PWM modulation index m_a is bounded, transient

response can only be so fast.

A block diagram of the control algorithm is shown in Fig. 6.2. At each iteration first x_{1r} is computed using (6.16) which requires the VSC state, the reference q-axis current and dc voltage, and the parameter estimate $\hat{\theta}$. Next, the state reference x_r including calculated x_{1r} along with x and $\hat{\theta}$ give the control output u via (6.15) and (6.17). Finally, $\hat{\theta}$ is updated using (6.25). The parameter update is initialized as $\hat{\theta}(0) = \hat{\theta}_o$.

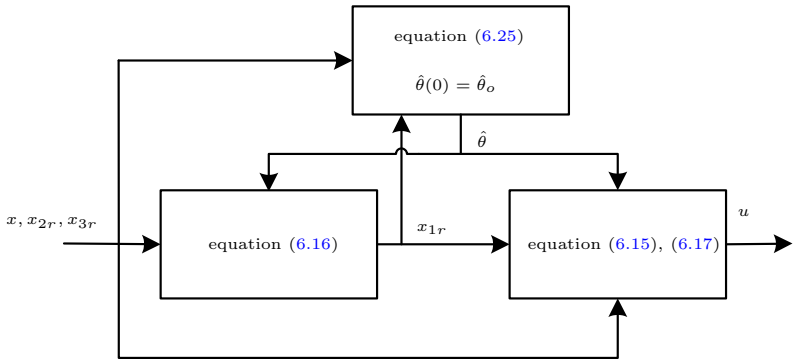

Figure 6.2: VSC adaptive control algorithm

6.3 Simulation Results

Simulation of the adaptive control is performed in Simulink/MATLAB. The nonlinear model and nonlinear Simulink SimPowerSystems Library switched model are used in simulation to verify robustness to the model error Δ. The initial values of VSC parameters are taken as $(0.5L, 1.5R, 2/\bar{R}_c)$ where L, R and $\bar{R}_c$ are the nominal values. System nominal parameter values and controller gains are shown in Table 3.1 and Table 6.1, respectively.

Table 6.1: Adaptive controller gains used in simulation

Gains	Value
(k_1, k_2, k_3)	$(600, 900, 200)$ 1/s
(P_1, P_2, P_3)	$(10^{-6}$ V·s^2/A^3, 10^{-5} V/(A^3· s), 0.5 1/(V^2· s^2)
$(\Lambda_1, \Lambda_2, \Lambda_3)$	$(70, 10^6, 0.06)$

6.3.1 Adaptive Control Using VSC Nonlinear Average Model

The q-axis current reference changes between -3 A and 3 A, and the dc voltage reference changes between 170 V and 200 V. Fig. 6.3 and Fig. 6.4 verify the controller's good tracking performance. The parameter convergence is shown in Fig. 6.5 where all three parameter errors converge to zero, i.e., all parameter estimates converge to their actual values. The control inputs modulation index m_a and phase shift δ are depicted in Fig. 6.6. It is clear from this figure the inputs stay within their bounds. We remark that step reference changes initially affect all system variables including system state and estimated parameters. The effect of this change is attenuated rapidly and zero steady state tracking error is achieved.

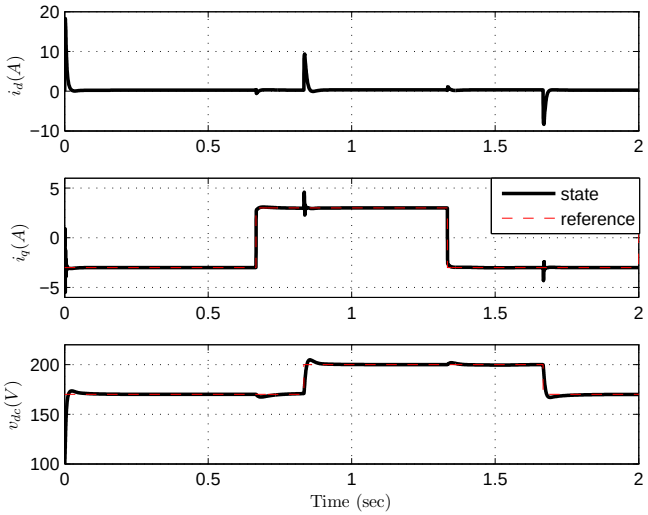

Figure 6.3: Simulation results of adaptive control using VSC nonlinear model: VSC state and desired reference trajectories

To observe the performance of the controller in transient, a close-up view of the VSC state trajectories are given in Figs. 6.7 and 6.8. It can be concluded that rise times are less than 100 ms and 10 ms for v_{dc} and i_q, respectively. The control gains were chosen such that dc voltage transients were optimized to have minimum overshoot and fastest response given the control input constraints.

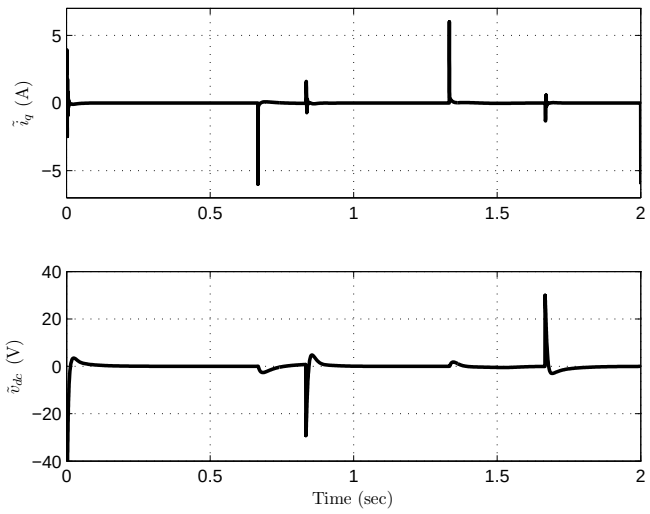

Figure 6.4: Simulation results of adaptive control using VSC nonlinear model: trajectory of tracking error

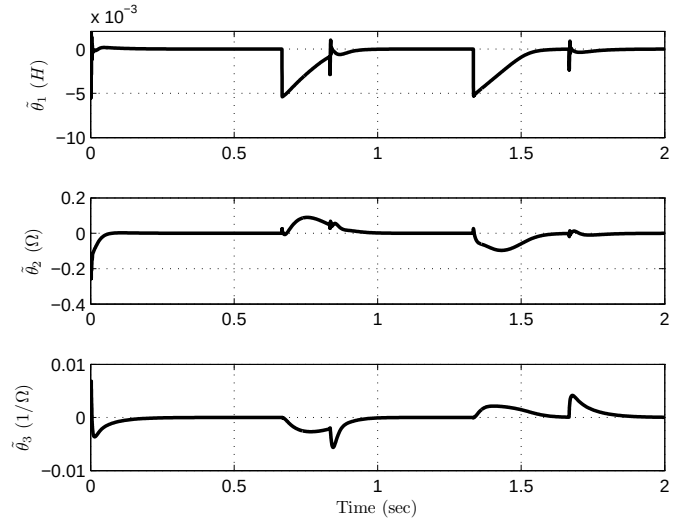

Figure 6.5: Simulation results of adaptive control using VSC nonlinear model: parameter estimate error

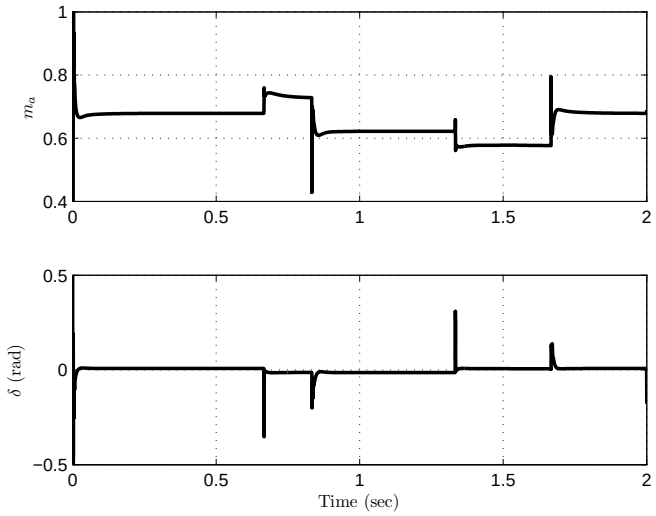

Figure 6.6: Simulation results of adaptive control using VSC nonlinear model: control inputs m_a and δ

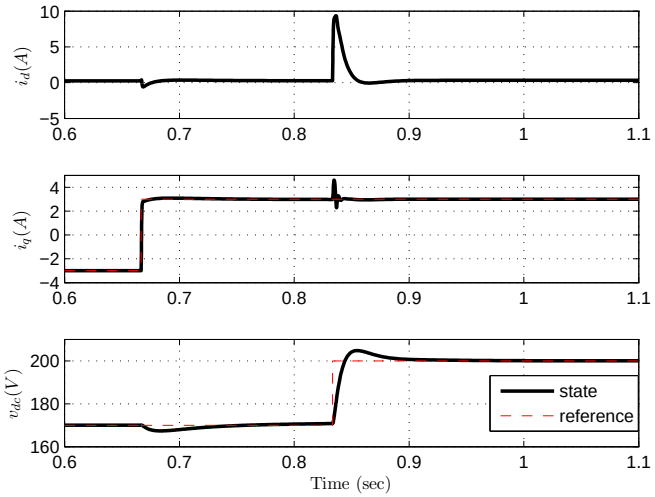

Figure 6.7: Simulation results of adaptive control using VSC nonlinear model: zoom in view of VSC state and desired reference trajectories

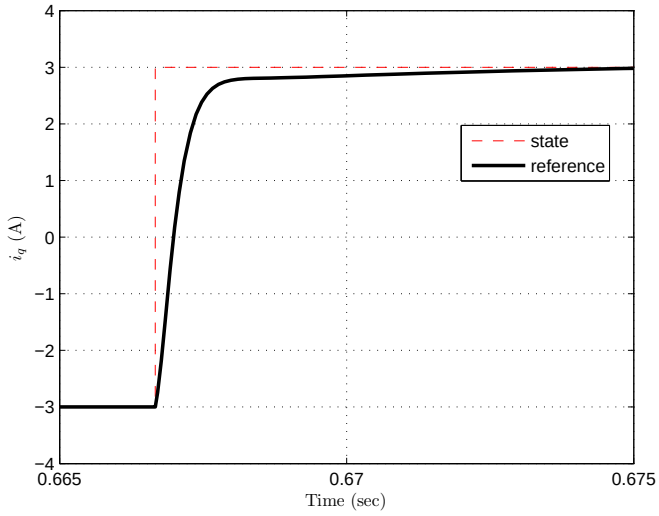

Figure 6.8: Simulation results of adaptive control using VSC nonlinear model: zoom in view of VSC q-axis current and desired reference trajectory

6.3.2 Adaptive Control with DC Load Change

The performance of the VSC employed as an ac-dc converter, with variable dc load R_c, is investigated in this subsection. At the start of simulation initial value for R_c is considered as 10 $\bar{R}_c$ and after 1 second, it is changed to $\bar{R}_c/10$ (Fig. 6.9). To further examine for the performance of the controller, the q-axis current and dc voltage references are varied at different time instances. As shown in Figs. 6.10–6.12, the controller performs well in dealing with the sudden dc load current increase and the parameter estimates converge to their actual values. Control inputs are well behaved and vary smoothly in their unsaturated ranges. Fig 6.10 shows the expected d-axis current increase to compensate for the load rise. We remark that filtered results are provided in this subsection and the next to show the VSC outputs without their high frequency harmonics. This makes it easier to verify that the q-axis current and dc voltage converge to their desired references. The filters are first order low pass with a cut-off frequency of $\omega_c = 1500$ rad/s.

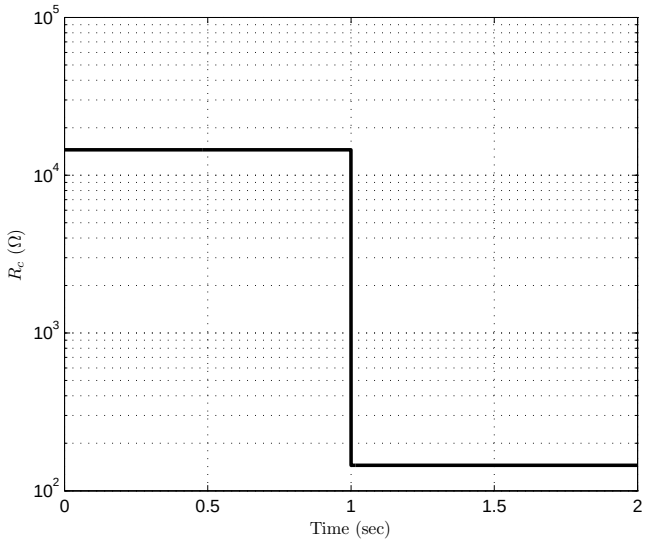

Figure 6.9: Adaptive control simulation results using nonlinear model with change in dc load: dc link load change

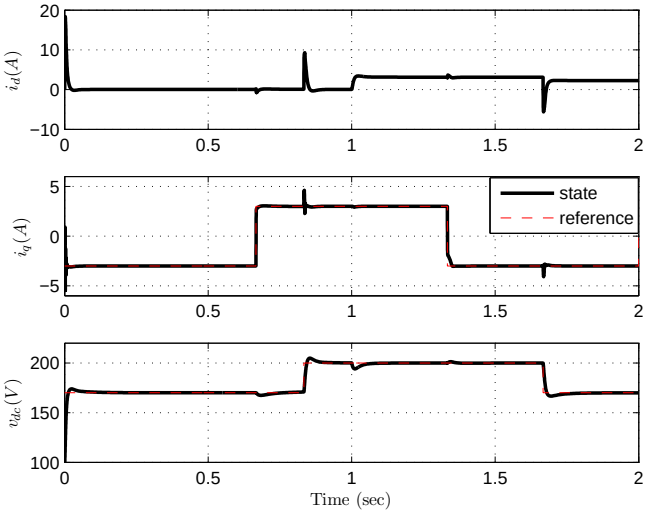

Figure 6.10: Adaptive control simulation results using nonlinear model with change in dc load: VSC state and desired reference trajectories

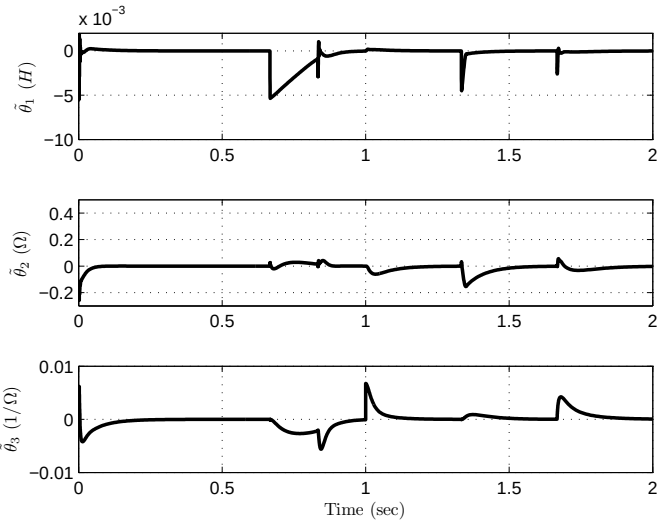

Figure 6.11: Adaptive control simulation results using nonlinear model with change in dc load: parameter estimate error

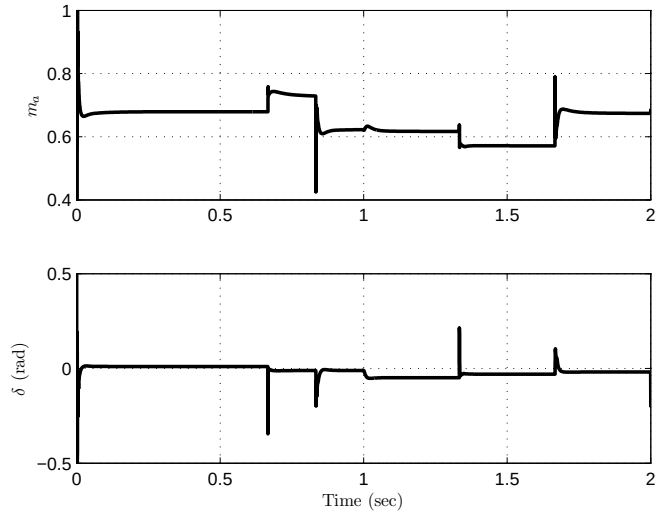

Figure 6.12: Adaptive control simulation results using nonlinear model with change in dc load: control inputs m_a and δ

6.3.3 Adaptive Control Using Switched Model with RL Load

The performance of the adaptive controller applied on a switched model of the VSC with RL load added is investigated in this subsection. A balanced three phase RL load is connected to the ac source and the load current is used to generate q-axis current reference trajectory. The PWM carrier frequency used is 10^4 Hz which is the same value used in the experimental setup. The dc voltage reference is changed between levels 170 V and 200 V. Each phase of the three phase load consists of a 12 Ω resistor in parallel with an inductive load $(3.6 + j\omega 0.047)\Omega$. The reference $i_{qr} = -i_{qL}$ ensures source zero q-axis current at the ac source. The simulation results are captured for 200 ms which is enough time for signals to reach steady state. Figs. 6.13 and 6.14 demonstrate good tracking performance for i_q and v_{dc}, and the control signals remain in their unsaturated ranges.

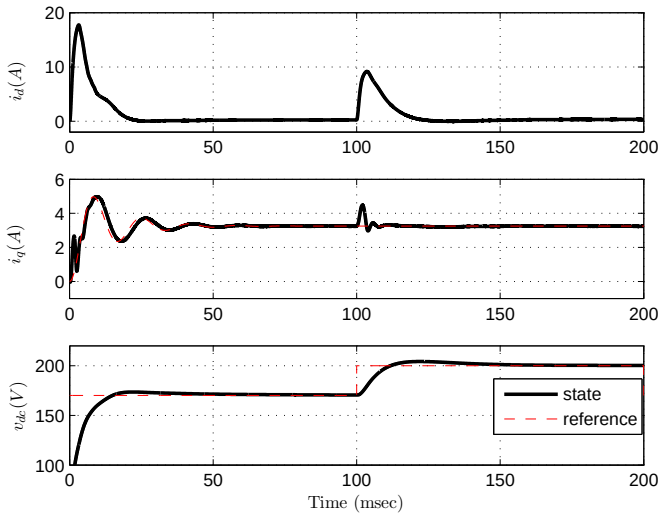

Figure 6.13: Simulation results of adaptive control using VSC nonlinear switched model with RL load: VSC state and desired reference trajectories

The rise time for v_{dc} is less than 50 ms. The parameters estimates converge to values close to zero to compensate system uncertainty. The current and voltage for phase-a of the ac source are shown in Fig. 6.16; the power factor is regulated to one. The dc voltage reference is changed at both $t = 0$ and

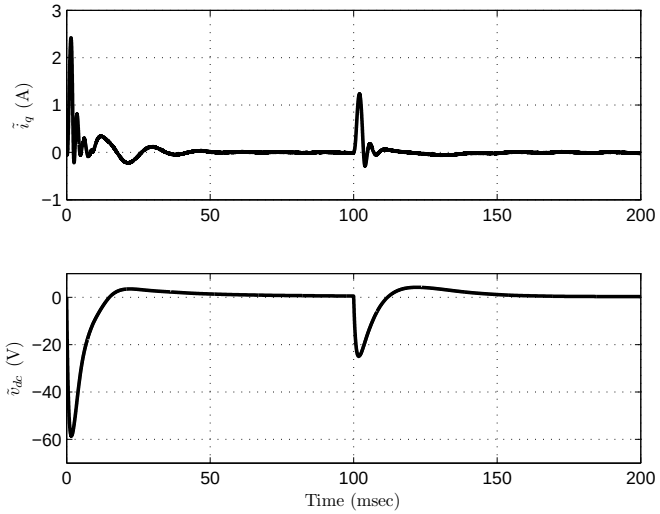

Figure 6.14: Simulation results of adaptive control using VSC nonlinear switched model with RL load: control inputs m_a and δ

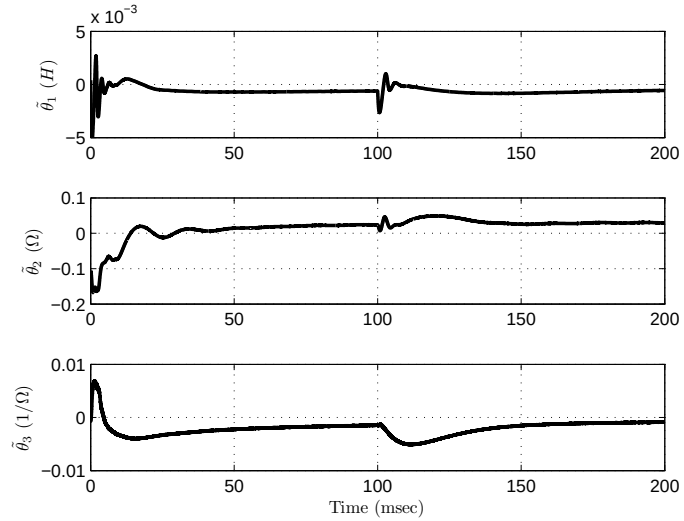

Figure 6.15: Simulation results of adaptive control using VSC nonlinear switched model with RL load: parameter estimate error

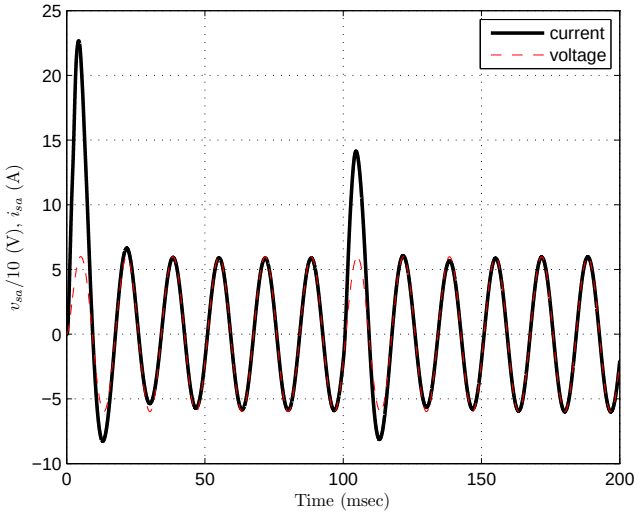

Figure 6.16: Simulation results of adaptive control using VSC nonlinear switched model with RL load: source phase current and voltage

$t = 100$ ms. Therefore, the d-axis current i_d as well as the ac source current i_{sa} change quickly to compensate for this change and to quickly drive the dc voltage to its reference value. The overshoots in i_{sa} can be reduced with a different choice of control gains k_i but this leads to slower dc voltage tracking.

6.3.4 VSC Switched Model and Imbalanced Source

An imbalanced source is considered in this section where phase-a of the ac source voltage is phase shifted by $\pi/8$. As shown in Fig. 6.17, the v_o component in the dqo frame is non-zero and also v_d and v_q have sinusoidal components with frequency twice that of the source.

From Fig. 6.18, it is clear that the controller performs well with an unbalanced source with performance roughly the same as the balanced case. The details of the transient performance is shown over 500 msec in Figs. 6.19 and 6.20. The control input also contains sinusoidal components with frequency twice the ac source frequency; this effectively compensates for the sinusoidal changes in v_{dqo}.

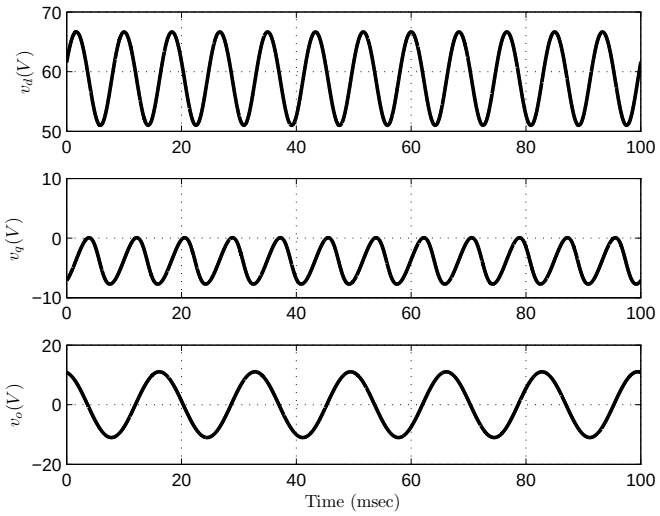

Figure 6.17: Simulation results of adaptive control using VSC nonlinear switched model with imbalanced ac source: zoom in view ac source components in dqo frame

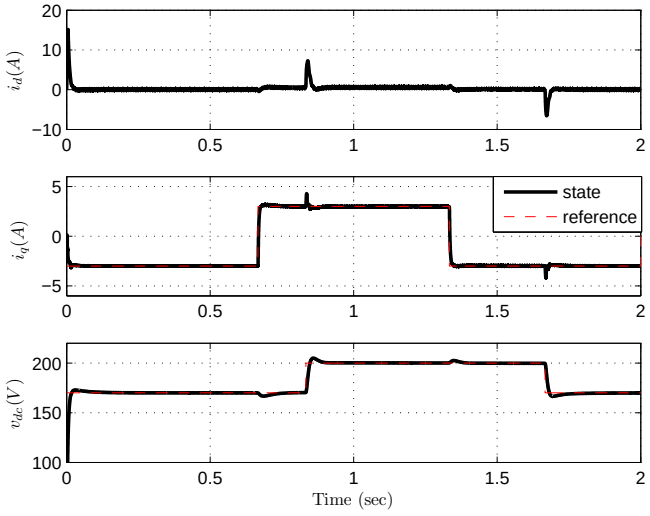

Figure 6.18: Simulation results of adaptive control using VSC nonlinear switched model with imbalanced ac source: VSC state and desired reference trajectories

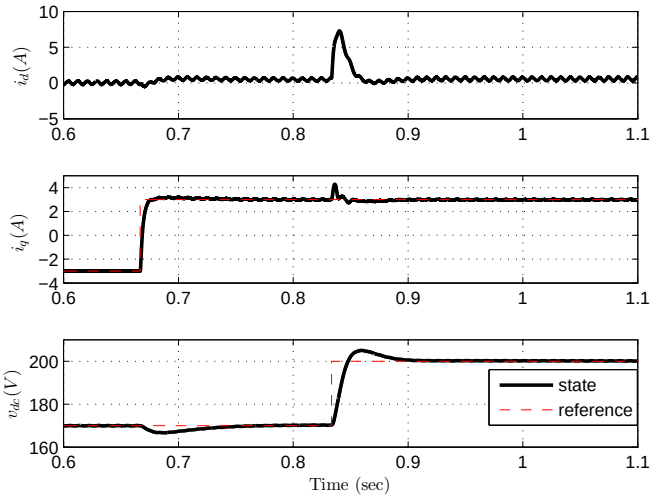

Figure 6.19: Simulation results of adaptive control using VSC nonlinear switched model with imbalanced ac source: zoom in view VSC state and desired reference trajectories

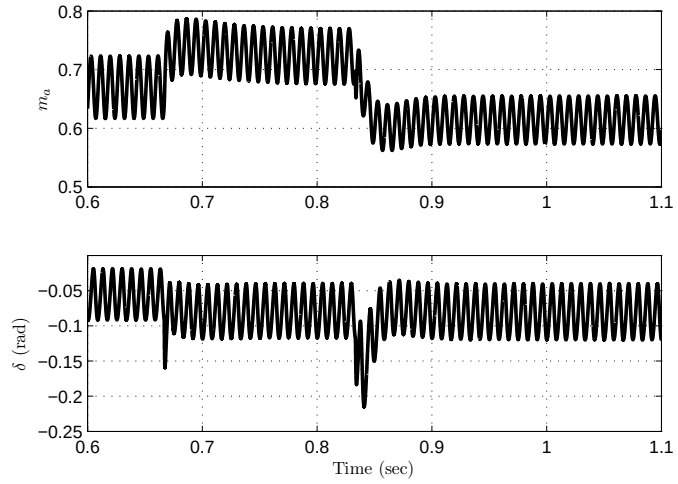

Figure 6.20: Simulation results of adaptive control using VSC nonlinear switched model with imbalanced ac source: zoom in view control inputs m_a and δ

6.4 Summary

This chapter presents two adaptive controls for PFC which directly account for uncertainty in VSC circuit parameters. The first approach uses adaptive current control combined with a PI dc voltage control. The second approach provides a so-called *full* adaptive control. The former controller accounts for uncertainty in the parameters R and L while in the later also R_c is included as an additional unknown parameter. To our knowledge, this is the first time the control of a VSC with three unknown parameters is investigated in literature. Simulations validate the performance of the full adaptive controller.

Chapter 7

Harmonic Compensation using a Shunt Active Power Filter

The harmonic and reactive power compensation in a power system using a three-phase shunt active power filter (SAPF) is investigated in this chapter. Two designs are presented: a traditional PI control and an adaptive control. The difference between these techniques lies in their current and voltage control. The proposed adaptive controller is designed based on the approximate third order nonlinear model of the SAPF which accounts for uncertainty in R and L. The dc voltage of the SAPF is regulated using a PI controller which generates the bias reference for d-axis current. The summation of this bias reference and the load d-axis current harmonics gives the d-axis current reference. The q-axis reference is set to be equal to the negative of the load q-axis current. The proposed method ensures asymptotic tracking of the d- and q-axis current reference trajectories while keeping the dc voltage at the desired reference. Since there are no integrator terms in the full adaptive control proposed in Chapter 6, the performance of the full adaptive control for harmonics elimination is poor. On the other hand, adding integrator terms to the full adaptive control further increases the number of control parameters and therefore the complexity of the full adaptive control. The proposed adaptive control in this chapter is equipped with three integrator terms to ease the tracking of the current harmonics with simple control structure. The chapter is organized as follow; first the PI and adaptive control techniques for the current control loop are presented in Section 7.1. The dc voltage PI control is explained in

Section 7.2. Finally, the simulation results in Section 7.3 demonstrate the controllers' performance and show the benefits of the adaptive control.

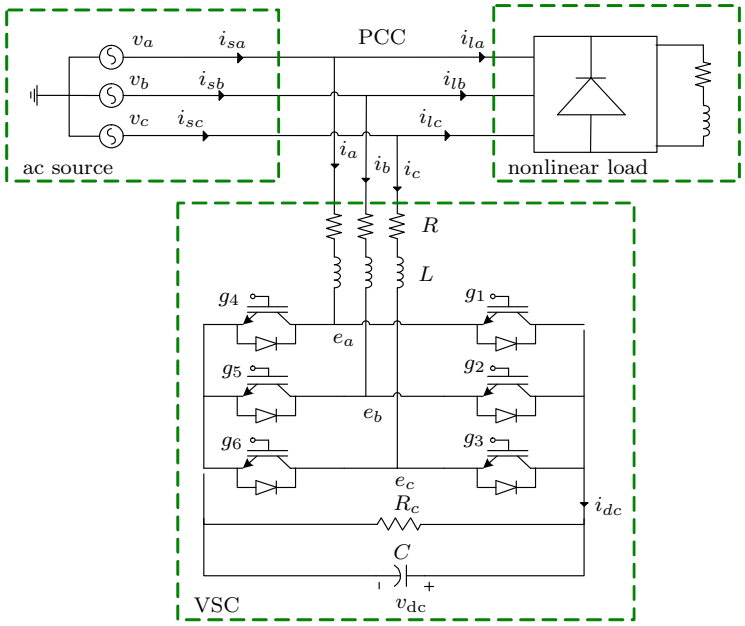

Figure 7.1: Voltage source converter for PFC and harmonic elimination

7.1 Current Control of a Three Phase Shunt Active Power Filter

Fig. 7.1 shows an SAPF used for PFC and harmonic elimination. A SAPF is a controlled current source which is in parallel with a nonlinear load. A SAPF compensates the unwanted unbalanced, harmonics and reactive load current components. In [46, 13], a nonlinear technique is proposed for harmonic and reactive current compensation and dc voltage regulation. This PI based control has two loops i.e., an inner current loop and an outer dc voltage loop. In this section, the current control technique in [46, 13] is presented in Subsection 7.1.1. Although the PI control has simple form and can be readily adopted in practice, its robust performance to model error can be of concern. An adaptive current control method is proposed in Subsection 7.1.2 which improves robustness to model error. Dc voltage regulation for both cases is discussed in Section 7.2.

7.1.1 PI Based Current Loop Control

Recalling the VSC current dynamics

$$\begin{aligned} L\frac{di_d}{dt} + Ri_d &= L\omega i_q + v_d - e_d \\ L\frac{di_q}{dt} - Ri_q &= -L\omega i_d + v_q - e_q \end{aligned} \tag{7.1}$$

and defining new inputs u_d and u_q as

$$\begin{aligned} u_d &= L\omega i_q + v_d - e_d \\ u_q &= -L\omega i_d + v_q - e_q \end{aligned} \tag{7.2}$$

where u_d, u_q are the outputs from the PI compensators of i_d and i_q, respectively. Substituting (7.2) into current dynamics (7.1) gives the decoupled equations

$$\begin{aligned} \frac{di_d}{dt} + \frac{R}{L}i_d &= u_d \\ \frac{di_q}{dt} + \frac{R}{L}i_q &= u_q \end{aligned} \tag{7.3}$$

Hence, we can independently control i_d and i_q. We define u_d and u_q

$$\begin{aligned} u_d &= k_{p_d}(i_d^* - i_d) + k_{i_d}\int_0^t (i_d^* - i_d)d\tau \\ u_q &= k_{p_q}(i_q^* - i_q) + k_{i_q}\int_0^t (i_q^* - i_q)d\tau \end{aligned} \tag{7.4}$$

where $(\cdot)^*$ denotes a desired reference value. In frequency domain we have

$$\begin{aligned} U_d(s) &= \left(k_{p_d} + \frac{k_{i_d}}{s}\right)(I_d^* - I_d) \\ U_q(s) &= \left(k_{p_q} + \frac{k_{i_q}}{s}\right)(I_q^* - I_q) \end{aligned}$$

From (7.3) and (7.4), the closed-loop transfer function of current dynamics is

$$\begin{aligned} \frac{I_d}{I_d^*} &= \frac{k_{p_d}s + k_{i_d}}{s^2 + (R/L + k_{p_d})s + k_{i_d}} \\ \frac{I_q}{I_q^*} &= \frac{k_{p_q}s + k_{i_q}}{s^2 + (R/L + k_{p_q})s + k_{i_q}} \end{aligned} \tag{7.5}$$

The closed-loop dynamics (7.5) consists of two second order linear systems with zeros at $z_d = -k_{i_d}/k_{p_d}$ and $z_q = -k_{i_q}/k_{p_q}$. The zeros terms in (7.5) can

be canceled with standard first order filters $G_d(s)$ and $G_q(s)$ if their poles are placed on the zeros.

$$G_d(s) = \frac{1}{k_{p_d}/k_{i_d}s + 1}$$
$$G_q(s) = \frac{1}{k_{p_q}/k_{i_q}s + 1}$$

Therefore, the choice of parameters for the PI controllers is straightforward. If we assume the closed-loop damping ratio ζ and natural undamped frequency w_n, the PI control parameters are

$$k_{p_d} = 2\zeta_d\omega_{n_d}L - R, \quad k_{i_d} = L\omega_{n_d}^2$$
$$k_{p_q} = 2\zeta_q\omega_{n_q}L - R, \quad k_{i_d} = L\omega_{n_q}^2$$

We note that using (7.2) and (7.4) gives e_d and e_q

$$e_d = L\omega i_q + v_d - k_{p_d}\tilde{i}_d - k_{i_d}\int_0^t \tilde{i}_d d\tau$$
$$e_q = -L\omega i_d + v_q - k_{p_q}\tilde{i}_q - k_{i_q}\int_0^t \tilde{i}_q d\tau$$

7.1.2 Adaptive Based Current Control

We recall current dynamics (7.1) and define

$$e_d = v_d + \alpha_1\hat{\theta}_1 + \beta_1\hat{\theta}_2$$
$$e_q = v_q + \alpha_2\hat{\theta}_1 + \beta_2\hat{\theta}_2$$

in which

$$\alpha_1 = \omega i_q - \dot{i}_d^* - v_1, \quad \beta_1 = -i_d$$
$$\alpha_2 = -\omega i_d - \dot{i}_q^* - v_2, \quad \beta_2 = -i_q$$

where $\theta_1 = L$, $\theta_2 = R$ and their estimates $\hat{\theta}_i$, $i = 1, 2$. The parameter estimate error is $\tilde{\theta}_i = \theta_i - \hat{\theta}_i, i = 1, 2$, with $\tilde{\theta} = (\frac{\tilde{\theta}_1}{\theta_1}, \frac{\tilde{\theta}_2}{\theta_1})^T$. The tracking error is denoted $\tilde{i} = (\tilde{i}_d, \tilde{i}_q)^T$ with $\tilde{i}_j = i_j - i_j^*, j = d, q$ where i_j^* stands for the reference trajectory. Therefore, the current dynamics are

$$\dot{\tilde{i}}_d = \alpha_1\frac{\tilde{\theta}_1}{\theta_1} + \beta_1\frac{\tilde{\theta}_2}{\theta_1} + v_1$$
$$\dot{\tilde{i}}_q = \alpha_2\frac{\tilde{\theta}_1}{\theta_1} + \beta_2\frac{\tilde{\theta}_2}{\theta_1} + v_2$$

The control inputs v_1 and v_2 are defined as

$$v_1 = -k_{p_d}\tilde{i}_d - k_{i_d}\int_0^t \tilde{i}_d d\tau$$
$$v_2 = -k_{p_q}\tilde{i}_q - k_{i_q}\int_0^t \tilde{i}_q d\tau$$

The current error dynamics are

$$\dot{\tilde{i}}_d = \alpha_1\frac{\tilde{\theta}_1}{\theta_1} + \beta_1\frac{\tilde{\theta}_2}{\theta_1} - k_{p_d}\tilde{i}_d - k_{i_d}\int_0^t \tilde{i}_d d\tau$$
$$\dot{\tilde{i}}_q = \alpha_2\frac{\tilde{\theta}_1}{\theta_1} + \beta_2\frac{\tilde{\theta}_2}{\theta_1} - k_{p_q}\tilde{i}_q - k_{i_q}\int_0^t \tilde{i}_q d\tau$$

If new variables $e_{ij}, i, j = 1, 2$ are defined as

$$e_{11} = \int_0^t \tilde{i}_d d\tau \quad e_{12} = \tilde{i}_d$$
$$e_{21} = \int_0^t \tilde{i}_q d\tau \quad e_{22} = \tilde{i}_q$$

The error dynamics are

$$\dot{e}_{11} = e_{12}$$
$$\dot{e}_{12} = -k_{i_d}e_{11} - k_{p_d}e_{12} + \alpha_1\frac{\tilde{\theta}_1}{\theta_1} + \beta_1\frac{\tilde{\theta}_2}{\theta_1}$$
$$\dot{e}_{12} = e_{22}$$
$$\dot{e}_{22} = -k_{i_q}e_{21} - k_{p_q}e_{22} + \alpha_2\frac{\tilde{\theta}_1}{\theta_1} + \beta_2\frac{\tilde{\theta}_2}{\theta_1}$$

Hence, the error dynamics can be simplified to

$$\dot{E} = \Psi E + \Gamma^T\tilde{\theta} \tag{7.6}$$

in which $E = (e_{11}\ e_{12}\ e_{21}\ e_{22})^T$

$$\Psi = \begin{bmatrix}\Psi_1 & 0\\ 0 & \Psi_2\end{bmatrix}, \quad \Psi_1 = \begin{bmatrix}0 & 1\\ -k_{i_q} & -k_{p_q}\end{bmatrix}, \quad \Psi_2 = \begin{bmatrix}0 & 1\\ -k_{i_q} & -k_{p_q}\end{bmatrix}$$

$$\Gamma = \begin{bmatrix}0 & \alpha_1 & 0 & \alpha_2\\ 0 & \beta_1 & 0 & \beta_2\end{bmatrix}$$

We take a parameter update law

$$\dot{\hat{\theta}} = -\dot{\tilde{\theta}} = \Lambda\Gamma P e \tag{7.7}$$

where $\Lambda \in \mathbb{R}^{2\times 2}$ is a symmetric positive definite matrix and $P \in \mathbb{R}^{4\times 4}$ is the solution of

$$\Psi^T P + P\Psi = -Q \tag{7.8}$$

in which $Q \in \mathbb{R}^{4\times 4}$ is a symmetric positive definite matrix. Since Ψ is Hurwitz, there exists a unique symmetric positive definite matrix P which satisfies (7.8). It can be readily shown that (7.7) guarantees that $\lim_{t\to\infty} ||E|| = 0$ or the tracking error is asymptotically stable [44, 71]. The conditions for parameter estimate error convergence follow from Matrosov's Theorem [84]. A sufficient condition is given by

$$\Gamma(x_r, \tilde{\theta}, t)\Gamma(x_r, \tilde{\theta}, t)^T > 0$$

We remark that although parameter errors remain bounded, convergence is not required to achieve asymptotic trajectory tracking. In order to simplify the implementation of the parameter update law (7.7), we take the diagonal matrices of Λ and P

$$\Lambda = \begin{bmatrix} \Lambda_1 & 0 \\ 0 & \Lambda_2 \end{bmatrix}, \quad P = \begin{bmatrix} P_d & 0 \\ 0 & P_q \end{bmatrix} \quad P_d = \begin{bmatrix} P_{d1} & 0 \\ 0 & P_{d2} \end{bmatrix} \quad P_q = \begin{bmatrix} P_{q1} & 0 \\ 0 & P_{q2} \end{bmatrix}$$

where $P_{di}, P_{qi}, \Lambda_i > 0, i = 1, 2$. Therefore, the parameter update law is

$$\begin{bmatrix} \dot{\hat{\theta}}_1 \\ \dot{\hat{\theta}}_2 \end{bmatrix} = \begin{bmatrix} \Lambda_1 \left(\alpha_1 (P_{d_1} \int_0^t \tilde{i}_d d\tau + P_{d_2} \tilde{i}_d) + \alpha_2 (P_{q_1} \int_0^t \tilde{i}_q d\tau + P_{q_2} \tilde{i}_q) \right) \\ \Lambda_2 \left(\beta_1 (P_{d_1} \int_0^t \tilde{i}_d d\tau + P_{d_2} \tilde{i}_d) + \beta_2 (P_{q_1} \int_0^t \tilde{i}_q d\tau + P_{q_2} \tilde{i}_q) \right) \end{bmatrix}$$

7.1.3 Parameter Tuning for Current Control Loop

There are 12 gains i.e. PI controller parameters and $P_{di}, P_{qi}, \Lambda_i, i = 1, 2$ to be chosen which affect the transient in the closed-loop response. To choose the PI parameters, we assume that the system parameters converge to their nominal values and hence, the closed-loop current dynamics is

$$\begin{aligned} \ddot{\tilde{i}}_d + k_{p_d} \dot{\tilde{i}}_d + k_{i_d} \tilde{i}_d = 0 \\ \ddot{\tilde{i}}_q + k_{p_q} \dot{\tilde{i}}_q + k_{i_q} \tilde{i}_q = 0 \end{aligned} \tag{7.9}$$

The closed-loop current dynamics (7.9) consists of two second order dynamics with coefficients

$$k_{p_d} = k_{p_q} = 2\zeta\omega_n, \quad k_{i_d} = k_{i_q} = \omega_n^2$$

The damping ratio is chosen $\zeta = 1$ for critical damping with no overshoot. The natural frequency ω_n of a second order standard system is related to its rise time $\omega_n \approx 1.8/Tr$. To ensure the transient is fast enough for tracking the high order harmonics components we choose $T_r = 10$ μs. We remark that the P_{di}, P_{qi} and $\Lambda_i, i = 1, 2$ values are obtained by trial and error.

7.2 DC Voltage Control Loop Control (Outer Loop)

7.2.1 Established Approach

Recalling the dc voltage dynamics

$$C\frac{dv_{dc}}{dt} = \frac{3}{2}\frac{i_d v_d + i_q v_q}{v_{dc}} - \frac{v_{dc}}{R_c} \tag{7.10}$$

An equivalent input u_{dc} is defined as

$$C\frac{dv_{dc}}{dt} + \frac{v_{dc}}{R_c} = \frac{3(i_d v_d + i_q v_q)}{2v_{dc}} = u_{dc} = k_{p_v}\tilde{v}_{dc} + k_{i_v}\int_0^t \tilde{v}_{dc}d\tau$$

where $\tilde{v}_{dc} = v_{dc}^* - v_{dc}$. Therefore, the resulting closed-loop transfer function is second order:

$$\frac{V_{dc}}{v_{dc}^*} = \frac{k_{p_v}s + k_{i_v}}{Cs^2 + (1/R_c + k_{p_v})s + k_{i_v}} = \frac{k_{p_v}}{C}\frac{s + k_{i_v}/k_{p_v}}{s^2 + (1/R_c + k_{p_v})/Cs + k_{i_v}/C}$$

If this system has natural frequency ω_{nv} and damping ratio ζ, the control gains are

$$k_{p_v} = 2C\zeta\omega_{n_v} - \frac{1}{R_c}, \quad k_{i_v} = C\omega_{n_v}^2$$

By acting on i_d, the dc voltage level is maintained at a desired level to compensate the losses in the active filter components and dc load R_c. The outer control effort can be expressed as

$$i_{do}^* = \frac{u_{dc}v_{dc} - 3/2(i_q v_q)}{3/2(v_d)}$$

Assume the three phase ac source is balanced i.e., $v_q = 0$ and the inner loop is ideal or in other words, current tracks its reference fast enough. Then the dc reference for d-axis current can be obtained as

$$i_{do}^* \approx \frac{2}{3}\frac{v_{dc}}{v_d}u_{dc}$$

7.2.2 Proposed Approach

If we recall the dc voltage dynamics (7.10) and define $v_{DC} = \frac{C}{3v_d} v_{dc}^2$, the transformed dc voltage dynamics is

$$\dot{v}_{DC} + \frac{2}{CR_c} v_{DC} = i_d + \frac{v_q}{v_d} i_q$$

Now if we define an equivalent input u_{DC}

$$\dot{v}_{DC} + \frac{2}{CR_c} v_{DC} = i_d + \frac{v_q}{v_d} i_q = u_{DC} = K_{p_v} \tilde{v}_{DC} + K_{i_v} \int_0^t \tilde{v}_{DC} d\tau$$

where $\tilde{v}_{DC} = v_{DC}^* - v_{DC}$, the closed-loop transfer function is

$$\frac{V_{DC}}{V_{DC}^*} = \frac{K_{p_v} s + K_{i_v}}{s^2 + (1/CR_c + K_{p_v})s + K_{i_v}} = K_{p_v} \frac{s + K_{i_v}/K_{p_v}}{s^2 + (1/CR_c + K_{p_v})/s + K_{i_v}}$$

If we assume that the three phase ac source is balanced i.e. $v_q = 0$ and the current loop dynamics is significantly faster than dc voltage dynamics, the d-axis bias reference i_{do}^* can be obtained

$$i_{do}^* \approx u_{DC}$$

7.2.3 Reference Current

The bias reference current i_{do}^* is added to the harmonic reference current of the d-axis current loop i_{Lh} to generate the reference current i_d^* for the d-axis current dynamics. The bias component forces the active filter to draw a current at the fundamental frequency in order to compensate for the converter switching and conduction losses. Designing the dc voltage loop to be much slower than the current control loop ensures interaction between the current and voltage loops are negligible. The fundamental components of the load currents appear as dc quantities in the synchronous reference frame rotating at the frequency ω. Therefore, these components can easily be separated from the load actual currents. The current loop references are obtained as follows:

$$i_d^* = -i_{Lh} + i_{do}^*$$

$$i_q^* = -i_{Lq}$$

where i_{Lh} and i_{Lq} are the harmonic component of load d-axis current and the q-axis load current, respectively. We take a damping ratio $\zeta = 1$ and a

rise-time specification $T_r = 40$ ms. This ensures the dc voltage response is sufficiently slow relative to the current loop while still maintaining a fast dc voltage response.

7.3 Simulation Results

Simulation of the control methods are performed in Simulink/MATLAB. The nonlinear Simulink SimPowerSystems Library switched model is used to model the system. The system nominal parameter values are shown in Table 3.1. The three phase balanced load consists of a diode rectifier which feeds an inductive load $(40 + j\omega 0.001)\Omega$. An inductive load $(40 + j\omega 0.001)\Omega$ is placed in parallel with the rectifier and is switched on and off with 150 ms period. This means a decrease in the load current at 150 ms and an increase at 300 ms. The PWM carrier frequency is 10^4 Hz. The simulation results are captured for 400 ms which is enough time for signals to reach their steady state. The dc voltage reference is set at 200 V.

7.4 Simulation Results of the SAPF

This section presents the simulation results for PI and the proposed adaptive control applied to the switched model of SAPF. The SAPF states and control inputs modulation index m_a and phase shift δ are depicted in Fig. 7.2 and Fig. 7.3, respectively. Since there are high order harmonics in the load, the system states and control signals change accordingly. It is clear that for both controllers, the dc voltage is regulated to 200 V and control inputs vary in their unsaturated range. Fig. 7.4 and Fig. 7.5 provide close up view of the signals. It is clear that SAPF currents in the dq frame track their references. The SAPF ac output currents are depicted in Fig. 7.6; they vary over a suitable range. The frequency spectrum of phase-a of the three phase load and ac source currents are given in Fig. 7.7 and Fig. 7.8 respectively. For PI control case, the THD of the load phase-a current is 24.54% while the ac source phase-a current has the THD of 7.35%. For the adaptive control, the THD of the load phase-a current is 24.54% as before whereas the ac source phase-a current

THD is 2.62%. For this case, the THD of the load phase-a current is almost 3 times smaller than the THD obtained using PI controller which demonstrates the benefits of the adaptive control. The PI and adaptive controller gains are given in Table 7.1 and Table 7.2, respectively.

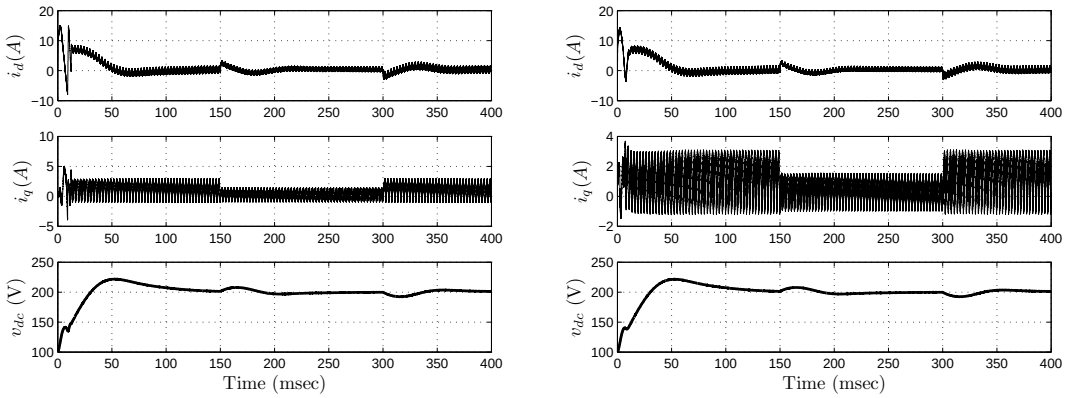

(a) SAPF PI control (b) SAPF adaptive control

Figure 7.2: Simulation results of PI and adaptive control using SAPF nonlinear switched model: state trajectories

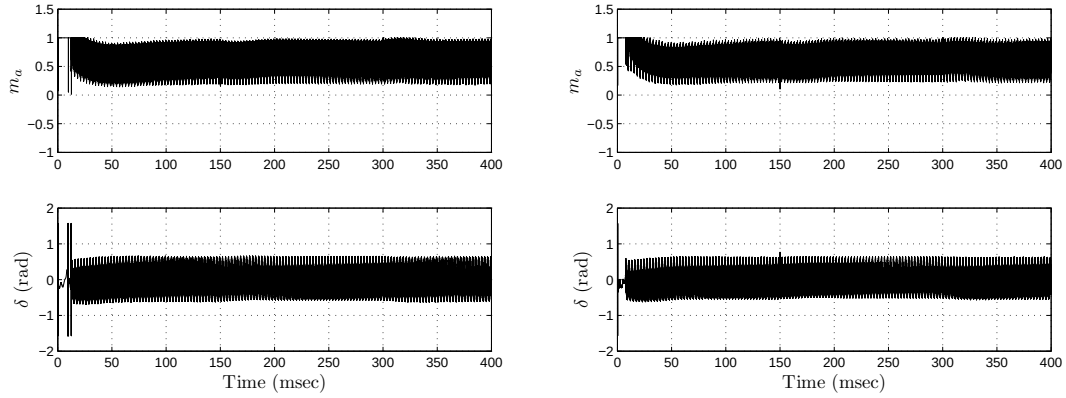

(a) SAPF PI control (b) SAPF adaptive control

Figure 7.3: Simulation results of PI and adaptive control using SAPF nonlinear switched model: control inputs m_a and δ

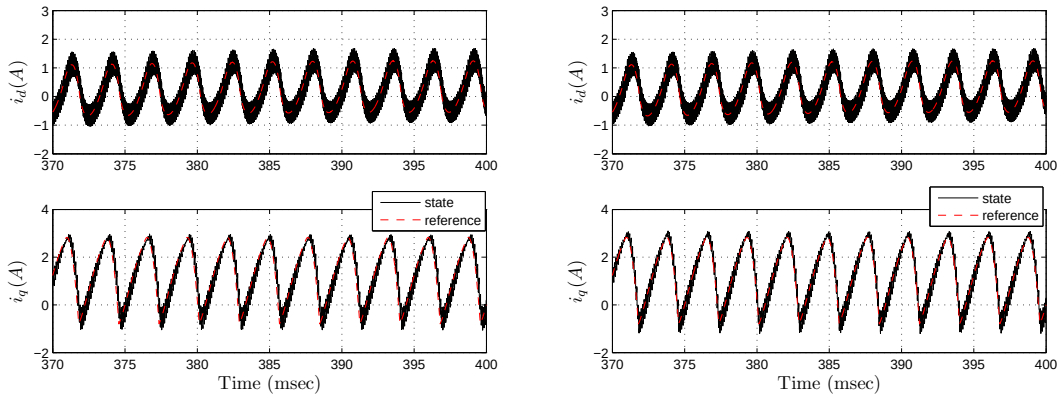

(a) SAPF PI control (b) SAPF adaptive control

Figure 7.4: Simulation results of PI and adaptive control using SAPF nonlinear switched model: zoom in of state trajectories

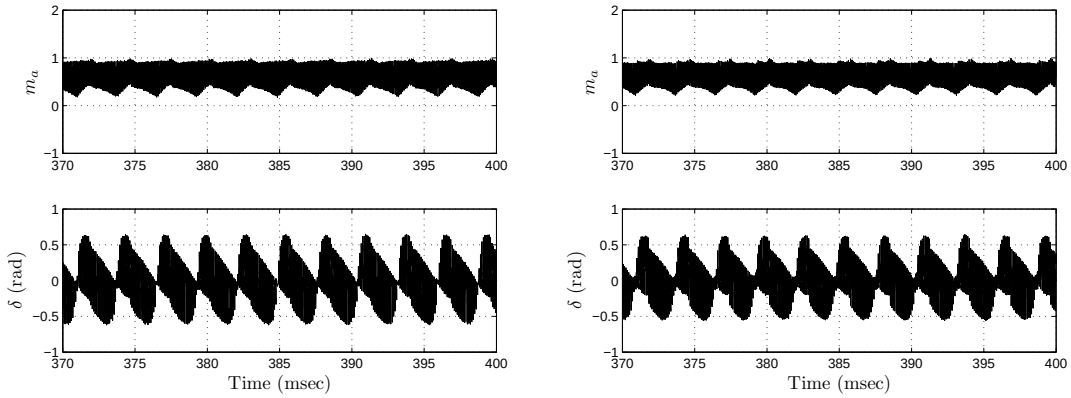

(a) SAPF PI control (b) SAPF adaptive control

Figure 7.5: Simulation results of PI and adaptive control using SAPF nonlinear switched model: zoom in of control inputs m_a and δ

Table 7.1: PI controller gains used for SAPF control

Gains	Value
(k_{p_d}, k_{i_d})	$(71.79$ V/A$, 648000$ V/(A.s)$)$
(k_{p_q}, k_{i_q})	$(71.79$ V/A$, 648000$ V/(A.s)$)$
(k_{p_v}, k_{i_v})	$(0.1$ A/V$, 2.23$ A/(V.s)$)$

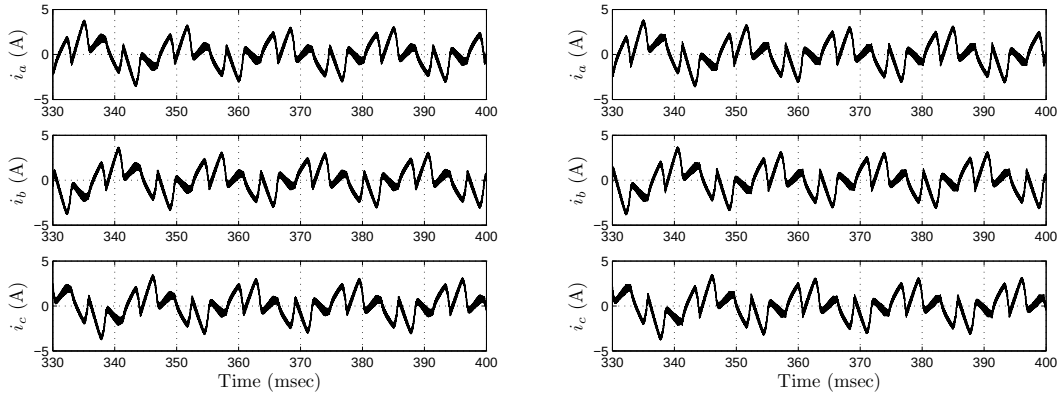

(a) SAPF PI control

(b) SAPF adaptive control

Figure 7.6: Simulation results of PI and adaptive control using SAPF nonlinear switched model: ac output currents

Table 7.2: Adaptive controller gains used for SAPF control

Gains	Value
(k_{p_d}, k_{i_d})	$(71.79\ \text{V/A}, 648000\ \text{V/(A.s)})$
(k_{p_q}, k_{i_q})	$(71.79\ \text{V/A}, 648000\ \text{V/(A.s)})$
(k_{p_v}, k_{i_v})	$(0.1\ \text{A/V}, 2.23\ \text{A/(V.s)})$
(P_{d1}, P_{d2})	$(0.025, 0.01)$
(P_{q1}, P_{q2})	$(0.1, 0.03)$
(Λ_1, Λ_2)	$(0.002, 0.002)$

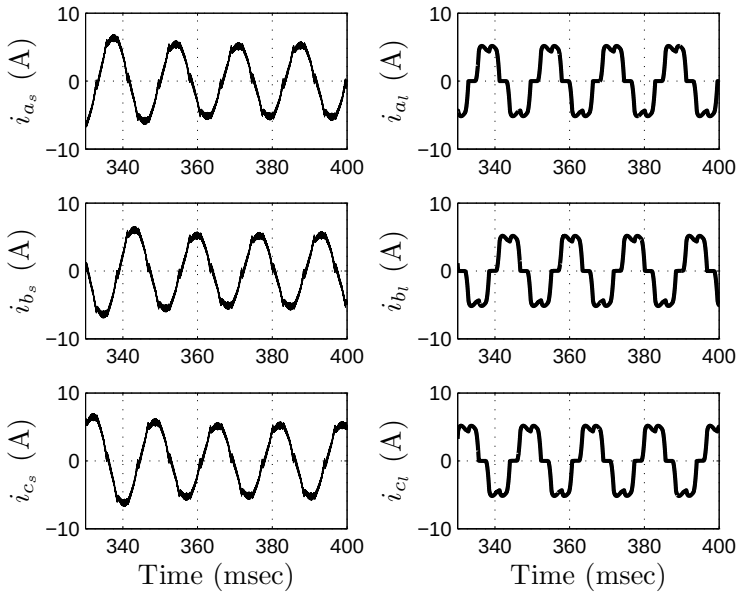

(a) SAPF PI control

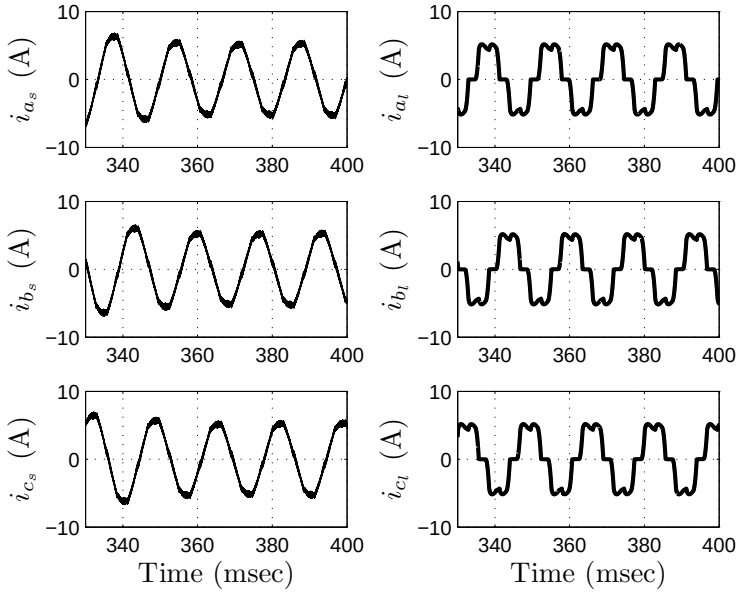

(b) SAPF adaptive control

Figure 7.7: Simulation results of PI and adaptive control using SAPF nonlinear switched model: ac source and nonlinear load phase currents

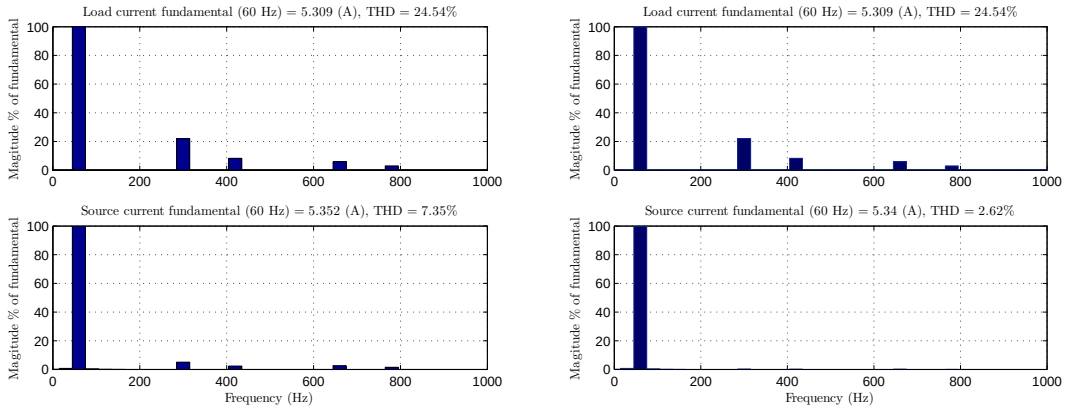

(a) SAPF PI control

(b) SAPF adaptive control

Figure 7.8: Simulation results of PI and adaptive control using SAPF nonlinear switched model: phase-a ac source and nonlinear load current frequency spectrum

7.5 Summary

Harmonic elimination using a three-phase SAPF is investigated in this chapter. It is challenging to design control for APF as the reference trajectories include time-varying high-order harmonics. First, an established PI based control is presented. To improve the control performance in the presence of system uncertainty, the design of an adaptive based control is investigated. The proposed adaptive control method for APF has a PI dc voltage control and adaptive current control loops. The simulation results are carried out for both methods and verify the adaptive approach yields a lower THD for the ac source current.

Chapter 8

Experimental Setup and Experimental Verification

In this chapter experimental results are provided to verify the performance of the VSC vector control, adaptive PI vector control and full adaptive control. The test stand is based on a Semiteach VSC module which is available in the Applied Nonlinear Control Lab (ANCL) at the University of Alberta. The experimental setup overview is provided in section 8.1. The performance of the different control methods is investigated in section 8.2.

8.1 Experimental Setup Components

The Semiteach Power Electronics Teaching System from SEMIKRON is employed in this work for constructing the experimental VSC system setup. This system consists of a three phase diode rectifier, a three phase VSC, a capacitor bank, thermal and electrical protection circuits, cooling fans, a heatsink and gating drivers. A picture of the experimental system is shown in Figure 8.1. The Semiteach system is installed in an insulated cover and the inputs and outputs of the system can be accessed through external banana and BNC connectors.

The VSC is based on the SEMIKRON SKM 50 GB 123 D dual Insulated Gate Bipolar Transistors (IGBT) module, where each module consists of two IGBTs each with an anti-parallel diode [85]. The ON/OFF gate-emitter signal for IGBTs are +15/0 V. These control signals are provided by a driver cir-

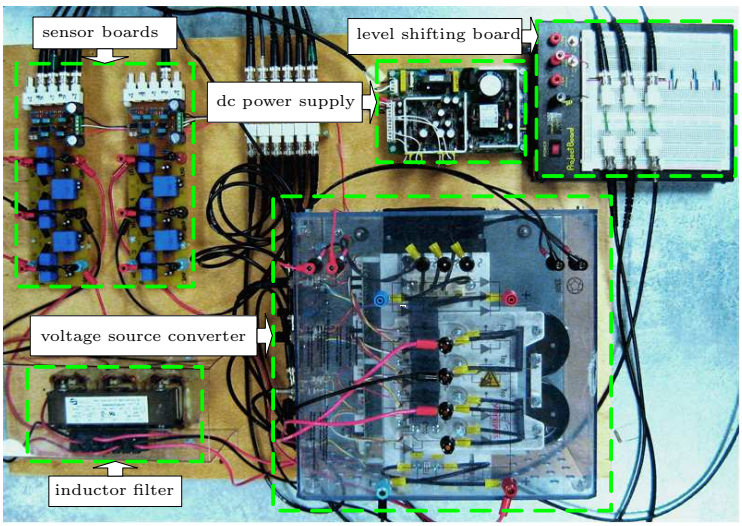

Figure 8.1: VSC test stand showing the Semiteach module, inductor filter, sensor boards, level shifting board and dc supply

cuit which amplifies the logic gating signals and delivers high peak currents to the IGBT gates for switching. The driver also monitors power supply undervoltage and short circuit conditions as well as isolates its input from the output stage to improve safety and reliability. To measure the VSC output voltages and currents, two sensor boards were built. The boards use LA 55-P current transducers and LV 25-P voltage sensors [86]. The control algorithms are implemented on a modular dSpace hardware system. This controller hardware has the advantage of being tightly integrated with the MATLAB/Simulink environment. The dSpace system is equipped with a BNC connector panel which provides access to its analog-to-digital converter (ADC) and digital waveform generator boards. The experiment uses 2 high speed DS2001 ADC boards and the 10 channel DS5101 digital board. The block diagrams of experimental setup and dSpace system are given in Figs. 8.2 and 8.3 respectively. A picture of employed dSpace system is also shown in Fig. 8.4.

8.2 Experimental Results

Experimental results are provided to investigate the performance of the proposed VSC adaptive control techniques i.e., the adaptive vector and full adaptive controls. For purposes of comparison a classical vector control is imple-

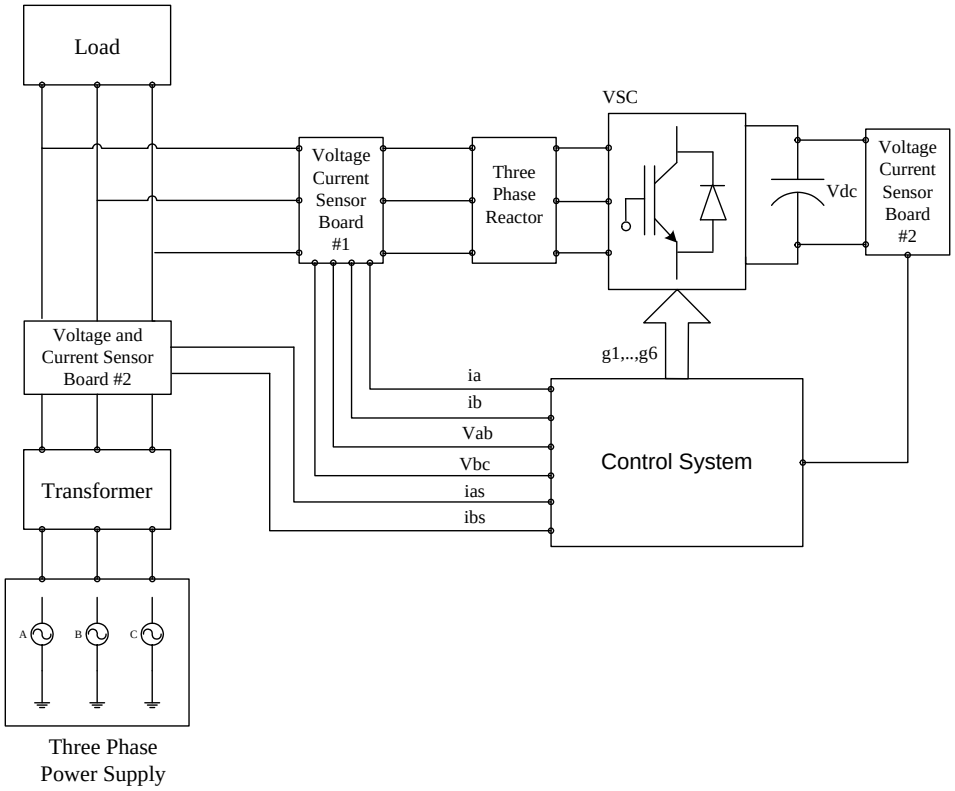

Figure 8.2: Block diagram of experimental setup interconnections

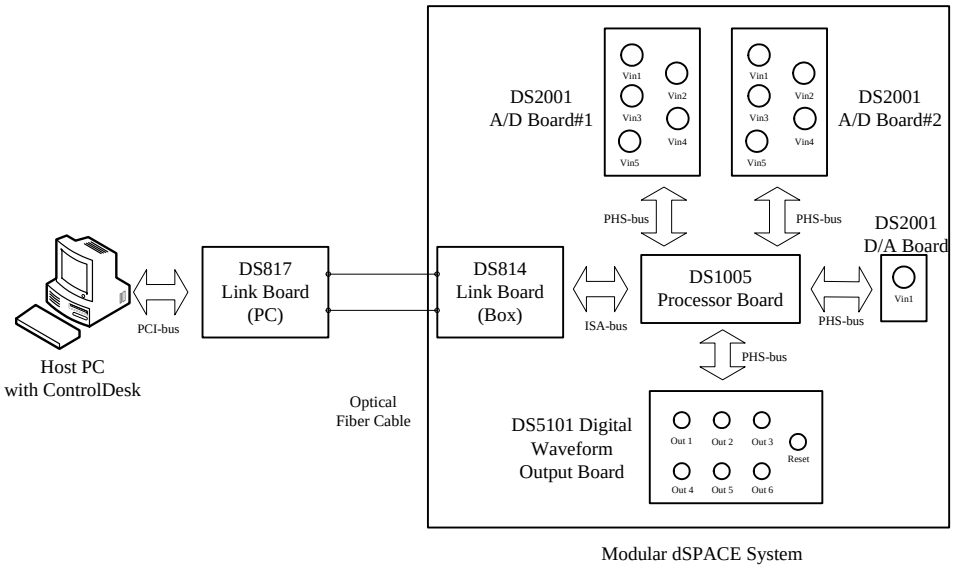

Figure 8.3: Block diagram of dSPACE interconnections

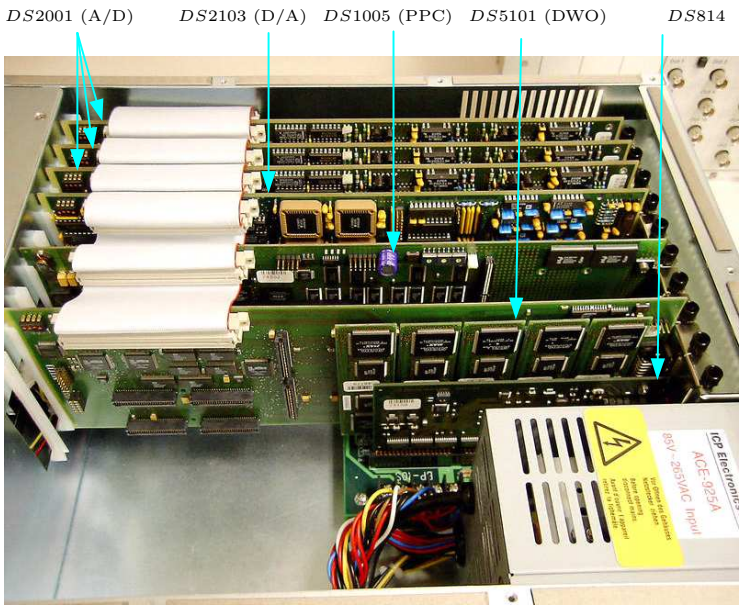

Figure 8.4: The utilized dSPACE system boards

mented for the known and unknown parameter case. In the experiment an ac supply provides a 60 Hz three phase sinusoidal voltage which is approximately balanced. This supply is connected to a variable transformer to gradually ramp the supply voltage for system startup. The transformer is connected to the VSC through a three phase filter inductor. The Semiteach module includes two 2200 μF / 400 V filtering capacitors in series on the dc side. The controller is implemented on the dSPACE system, and dSPACE's Control Desk software is used to develop a graphical interface to control the experiment. The control algorithm itself was programmed graphically in MATLAB/Simulink with code automatically generated using the Simulink's Real-Time Workshop. The PWM carrier frequency is 10^4 Hz. The q-axis current reference changes between -3 A and 3 A, and the dc voltage reference changes between 170 V and 200 V. The VSC parameters corresponding to the experiment are given in Table 8.1.

Parameters	Value
L	2 mH
C	1100 μF
R	0.21 Ω
R_c	1.45 kΩ
ω	120π rad/s
T	100 μs
v_d	60 V
v_q	0 V

Table 8.1: Nominal parameters used in experiment

8.2.1 VSC Vector Control with Known Parameters

In this subsection the experimental tracking performance of the classical vector control is investigated. We assume VSC parameters are known, take a q-axis current reference which varies between ± 3 A, and a constant dc voltage reference of 170 V as shown in Figs. 8.5 and 8.6. The controller provides good tracking performance and control inputs m_a and δ vary within an acceptable range. Fig. 8.6 shows the VSC states and the control inputs on a smaller time scale so that transient response can be inspected. We conclude the time constant of the dc voltage and q-axis current responses is about 1 s.

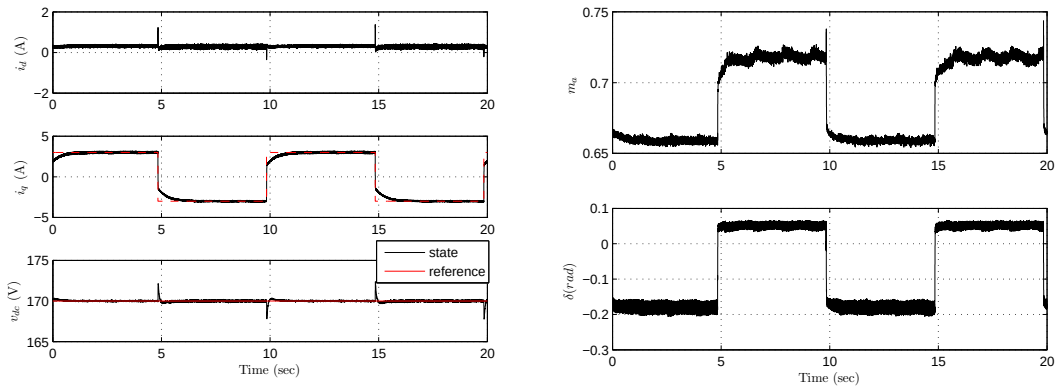

(a) trajectories of state and reference

(b) control inputs m_a and δ

Figure 8.5: Experimental results of the VSC vector control when the nominal VSC parameter values used in the control and the q-axis current reference changes

The performance of the vector control for a dc voltage reference change of

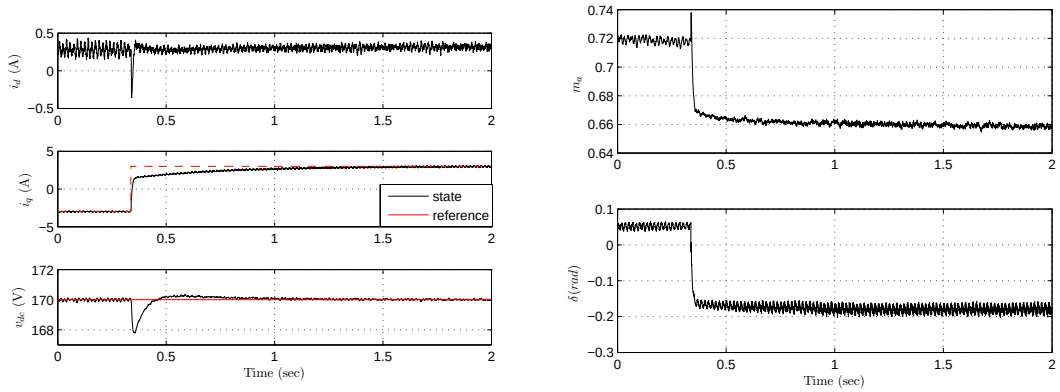

(a) trajectories of state and reference

(b) control inputs m_a and δ

Figure 8.6: Experimental results of the VSC vector control when the nominal VSC parameter values used in the control and the q-axis current reference changes: zoom in view

170 V to 200 V is depicted in Fig. 8.7. The close-up view of the states and the control inputs are shown in Fig. 8.8. The vector control performance demonstrates satisfactory dc voltage tracking and control inputs stay unsaturated.

8.2.2 VSC Vector Control with Unknown Parameters

This subsection provides the experimental results when the vector control is applied with parameter errors. The parameters used in control are $(0.5L, 1.5R, 2/\bar{R}_c)$ where L, R and $\bar{R}_c$ are nominal values. The decoupling of d- and q-axis current dynamics is only possible if L is exactly known, and when L contains errors transient performance is degraded. The results are shown in Figs. 8.9 and 8.10. Although the tracking errors eventually converge to zero, transient performance is worse than the known parameter case.

Controller performance for a dc voltage reference change of 170 V to 200 V is shown in Figs. 8.11 and 8.12. The results show a dc voltage overshoot and increased rise time relative to the case where L is known. The vector control gains used in the experiment are given in Table 8.2.

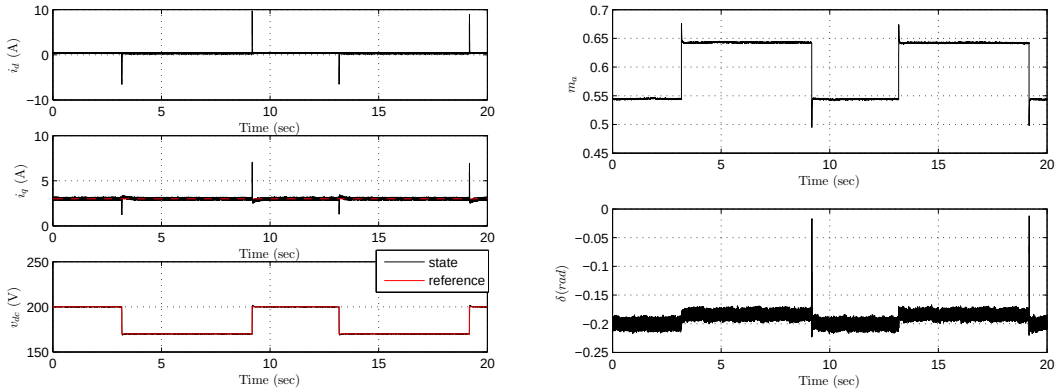

(a) trajectories of state and reference

(b) control inputs m_a and δ

Figure 8.7: Experimental results of the VSC vector control when the nominal VSC parameter values used in the control and the dc voltage reference is changing

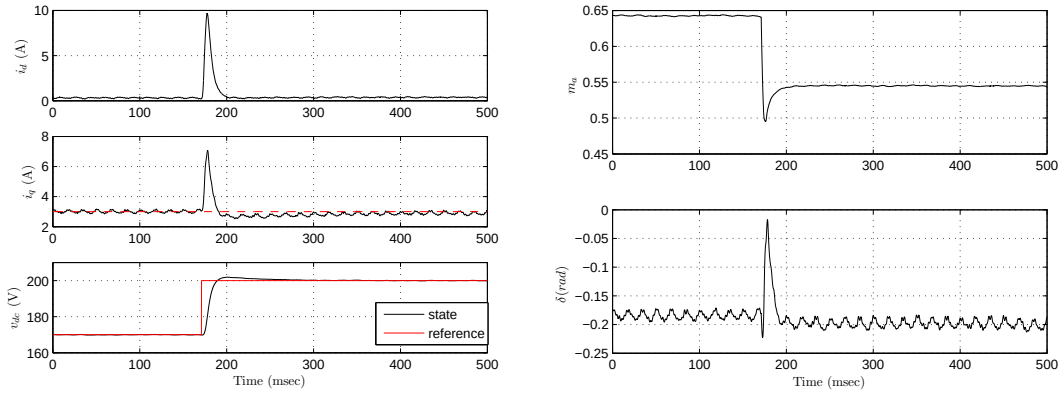

(a) trajectories of state and reference

(b) control inputs m_a and δ

Figure 8.8: Experimental results of the VSC vector control when the nominal VSC parameter values used in the control and the dc voltage reference is changing: zoom in view

Gains	Value
(k_{dp}, k_{di})	$(100\ \text{V/A}, 1000\ \text{V/(A.s)})$
(k_{qp}, k_{qi})	$(2000\ \text{V/A}, 10000\ \text{V/(A.s)})$
(k_{vp}, k_{vi})	$(5\ \text{A/V}, 20\ \text{A/(V.s)})$

Table 8.2: Vector controller gains used in experiment

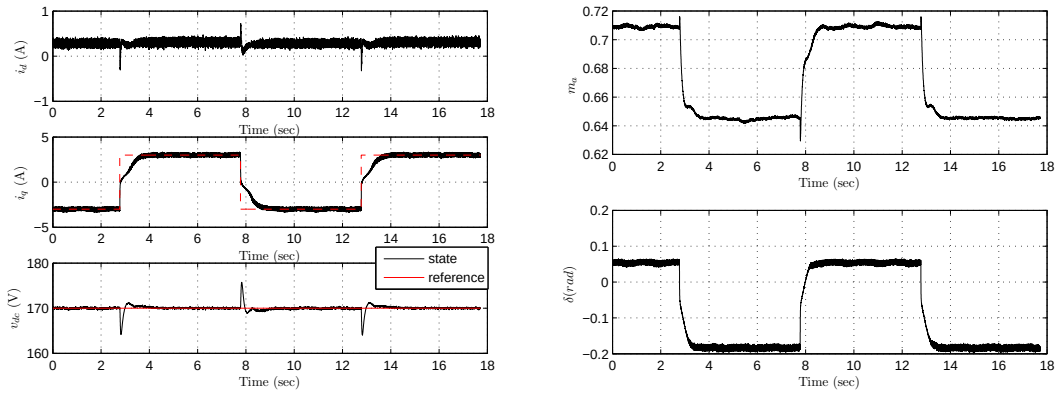

(a) trajectories of state and reference

(b) control inputs m_a and δ

Figure 8.9: Experimental results of the VSC vector control when the system parameters are unknown and the q-axis current reference is changing

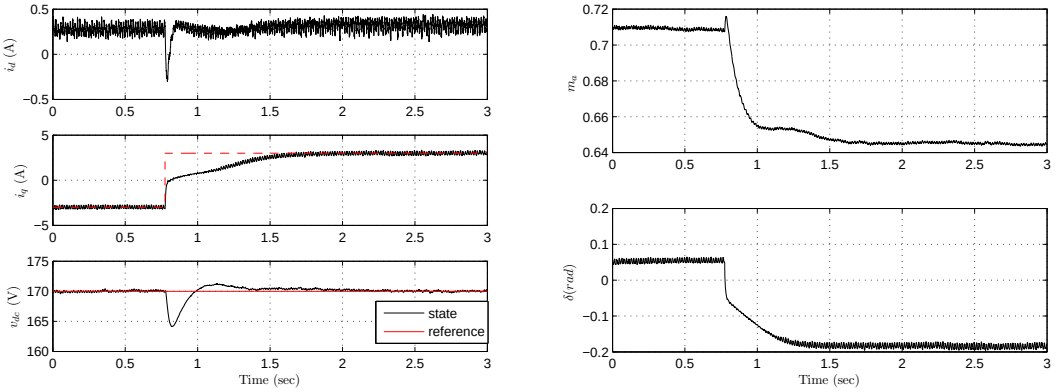

(a) trajectories of state and reference

(b) control inputs m_a and δ

Figure 8.10: Experimental results of the VSC vector control when the system parameters are unknown and the q-axis current reference is changing: zoom in view

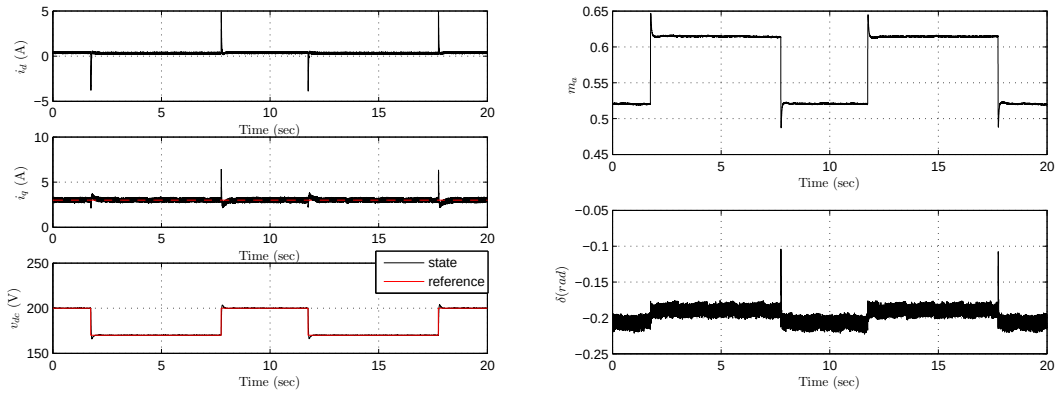

(a) trajectories of state and reference

(b) control inputs m_a and δ

Figure 8.11: Experimental results of the VSC vector control when the VSC parameters are unknown and the dc voltage reference is changing

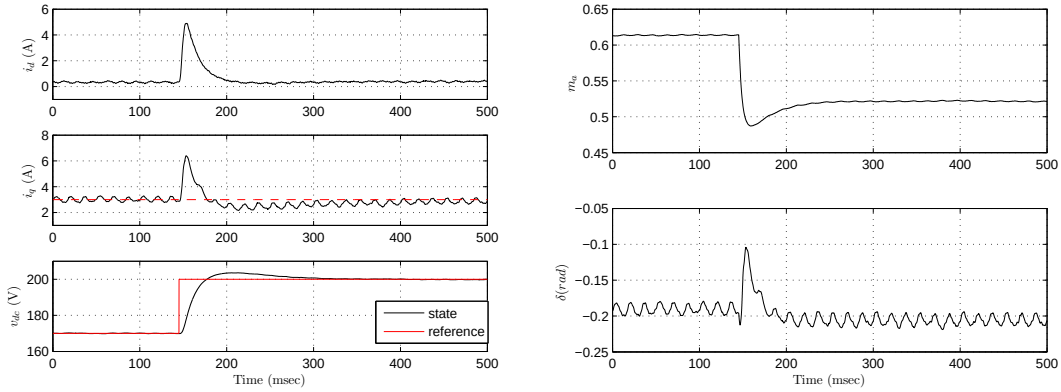

(a) trajectories of state and reference

(b) control inputs m_a and δ

Figure 8.12: Experimental results of the VSC vector control when the VSC parameters are unknown and the dc voltage reference is changing: zoom in view

8.2.3 Adaptive PI Vector Control

In this subsection experimental results are provided to verify the performance of the adaptive PI vector control. The q-axis current reference changes between ±3 A, and the dc voltage reference changes between 170 V and 200 V. Fig. 8.13(a) shows the q-axis current and dc voltage track their references with good transient and steady state performance. The inputs m_a and δ and inductance estimate are shown in Fig. 8.13(b). These plots show acceptable trajectories for the control inputs and an inductance estimate which eventually converges with large variations when the reference input changes. The gains used in the adaptive PI vector control are given in Table 8.3.

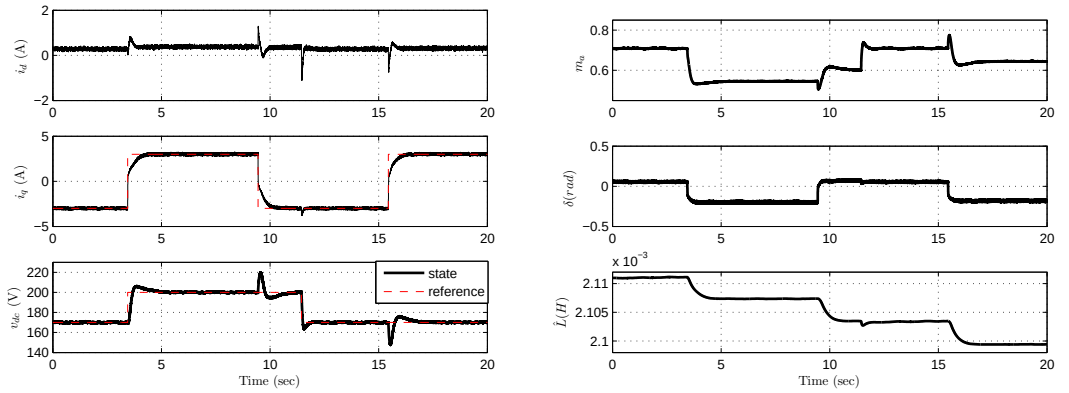

(a) trajectories of state and reference

(b) control inputs and inductance estimate

Figure 8.13: Experimental results of adaptive PI vector control

Gains	Value
(k_{dp}, k_{di})	$(0.04\ \text{V/A}, 0.2\ \text{V/(A.s)})$
(k_{qp}, k_{qi})	$(4\ \text{V/A}, 20\ \text{V/(A.s)})$
(k_{vp}, k_{vi})	$(5\ \text{A/V}, 20\ \text{A/(V.s)})$
Λ	10^{-7}

Table 8.3: Adaptive PI vector controller gains used in experiment

8.2.4 Full Adaptive Control

The experimental implementation of the full adaptive control is investigated in this subsection. First, we vary the q-axis current reference between ±3 A. Fig. 8.14(a) shows that the q-axis current and dc voltage track their references with good transient and steady state performance. The control inputs m_a and δ are shown in Fig. 8.14(b) which vary in their unsaturated ranges. Figs. 8.15(a) and 8.15(b) show the VSC states and control inputs on a smaller time scale so that transient response can be inspected. The q-axis current tracks its reference with a rise time less than 200 msec and without overshoot. A

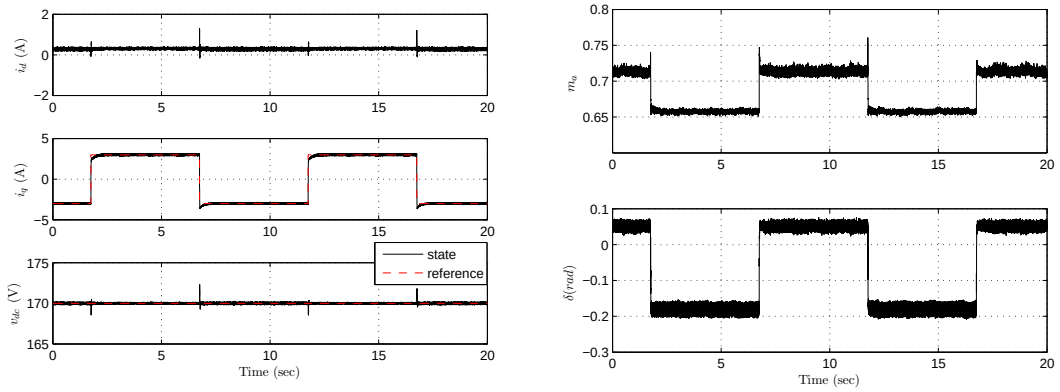

(a) trajectories of state and reference

(b) control inputs m_a and δ

Figure 8.14: Experimental results of VSC adaptive control with q-axis current reference change

VSC can also be used as an ac-dc converter where the objective is to control dc voltage for a dc load. The performance of the controller for a change in dc voltage reference is depicted in Figs. 8.16(a) and 8.16(b). The results show good tracking of the dc voltage and q-axis current references. The adaptive control gains used are provided in Table 8.4.

8.2.5 Full Adaptive Control with RL Load

In order to verify the performance of the adaptive control in a more realistic setting, a three phase RL load is connected in parallel to the VSC.

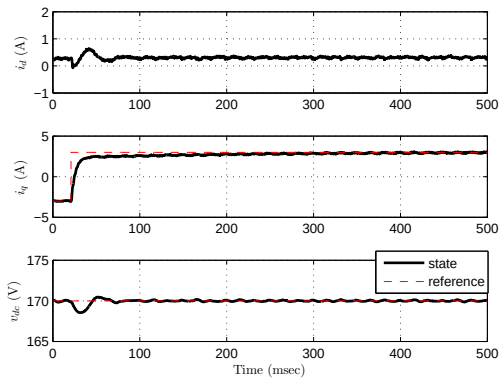

(a) trajectories of state and reference

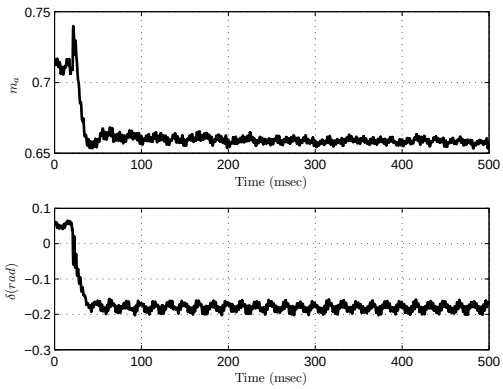

(b) control inputs m_a and δ

Figure 8.15: Experimental results of VSC adaptive control with q-axis current reference change: zoom in view

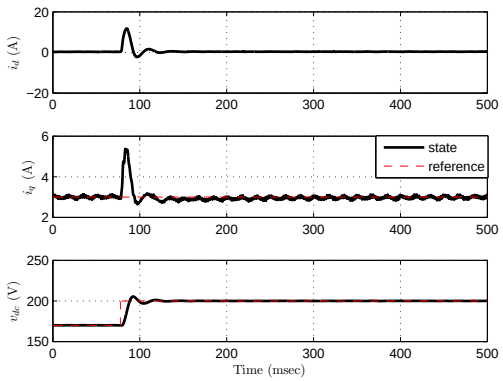

(a) trajectories of state and reference

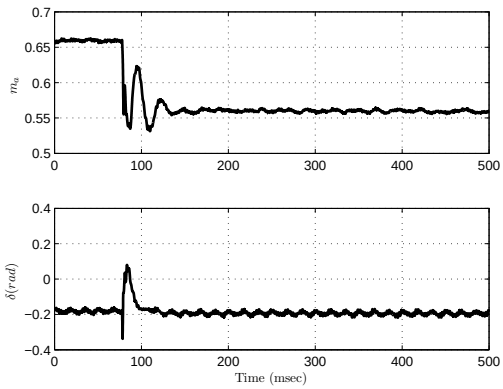

(b) control inputs m_a and δ

Figure 8.16: Experimental results of VSC adaptive control with dc voltage reference change

Gains	Value
(k_1, k_2, k_3)	$(4000, 6000, 150)$ 1/s
(P_1, P_2, P_3)	$(10^{-6}$ V·s^2/A^3, 10^{-5} V/(A^3· s), 1 1/(V^2· s^2))
$(\Lambda_1, \Lambda_2, \Lambda_3)$	$(1, 10^8, 0.01)$

Table 8.4: Adaptive controller gains used in experiment

The Y-connected three phase RL load, depicted in Fig. 8.17, is not perfectly balanced and consists 10 Ω resistors in parallel with inductors which have inductance and internal resistance of $(R_1, L_1) = (3.47\ \Omega, 47.7\ \text{mH})$, $(R_2, L_2) = (3.54\ \Omega, 47.7\ \text{mH})$ and $(R_3, L_3) = (3.43\ \Omega, 47.7\ \text{mH})$. The RL load is connected to the output of the transformer and the control objective is to compensate for the q-axis current of the load so that the source current and voltage are in phase. The reference trajectory $x_{2r} = -i_{qL}$ and the reference trajectory for dc voltage is a constant $v_{dcr} = 170$ V. Since i_{qL} is not constant due to nonidealities and has some small amplitude high frequency harmonic content, the control problem is more challenging.

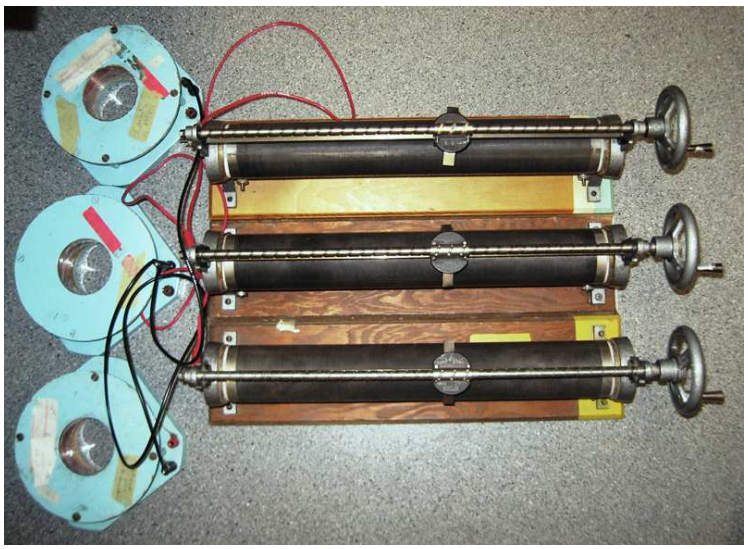

Figure 8.17: RL load used in the experiment

Fig. 8.18 shows the controller performing well and q-axis current tracks its time-varying reference $i_{qr} = -i_{qL}$. The control inputs remain in suitable ranges. Fig. 8.19 shows the voltage and current for phase-a of the ac source for both situations, i.e. when there is no compensation and when there is compensation. As it is clear in Fig. 8.19(a), the current is not in phase with corresponding voltage while in Fig. 8.19(b) the current is in phase with corresponding voltage.

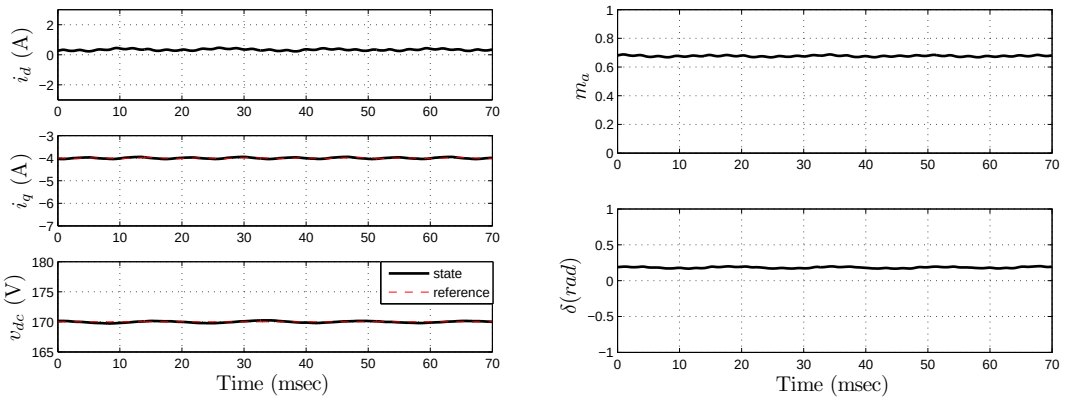

(a) trajectories of state and reference

(b) control inputs m_a and δ

Figure 8.18: Experimental results of VSC adaptive control with RL load

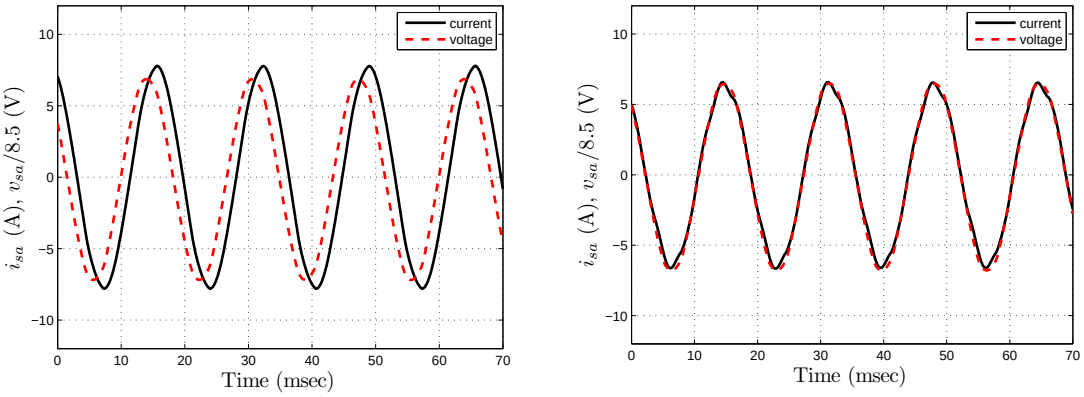

(a) without compensation

(b) with compensation

Figure 8.19: Experimental results of VSC adaptive control with RL load: phase current and scaled voltage signals

8.2.6 PI Control of a SAPF

The experimental results of the PI control for harmonic elimination are provided in this section. The three phase load consists of a diode rectifier which feeds an inductive load which is a 1 mH inductor in series with a 32 Ω resistor. The dc voltage reference is 170 V and results are captured for 70 ms. The SAPF states and control inputs are shown in Fig. 8.20. It is clear that the dc voltage is accurately regulated to 170 V and SAPF currents in $d-q$ frame track their references. The SAPF output currents, load currents and source currents are shown in Fig. 8.21, Fig. 8.22 and Fig. 8.23 respectively. Fig. 8.25 shows the ac source phase-a voltage and current. It is obvious that the current is in phase with the corresponding voltage. Comparison of load and source currents verify the controller's good harmonic elimination performance. The filtered ac source phase-a voltage and current are depicted in Fig. 8.25 which confirm good PFC performance. The PI controller gains used in the experiment are given in Table 8.5.

Gains	Value
(k_{p_d}, k_{i_d})	(5000 V/A, 20000 V/(A.s))
(k_{p_q}, k_{i_q})	(8500V/A, 200000 V/(A.s))
(k_{p_v}, k_{i_v})	(1.1 A/V, 20 A/(V.s))

Table 8.5: PI controller gains used for experimental SAPF control

8.2.7 Adaptive Control of a SAPF

The experimental results of the adaptive control for harmonic elimination are provided in this section. The same load and dc voltage reference is used in the previous section. The SAPF states and control inputs are depicted in Fig. 8.26. It is clear that the dc voltage is regulated to 170 V and the SAPF currents in $d-q$ frame track their references. The SAPF output currents, load currents and source currents are depicted in Fig. 8.27, Fig. 8.28 and Fig. 8.29 respectively. Fig. 8.31 shows the ac source phase-a voltage and current. It is clear that the current is in phase with the voltage. Comparison of load and source currents verify the controller's harmonic elimination performance. The

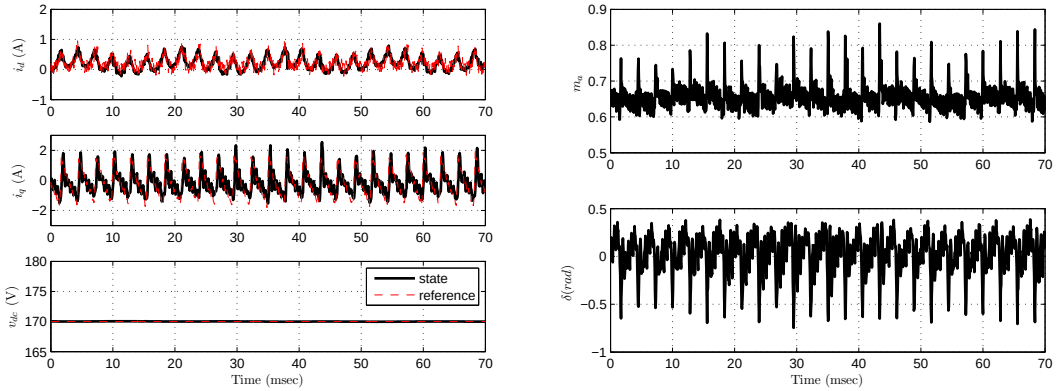

(a) trajectories of state and reference

(b) control inputs m_a and δ

Figure 8.20: Experimental results of the PI Control of a SAPF

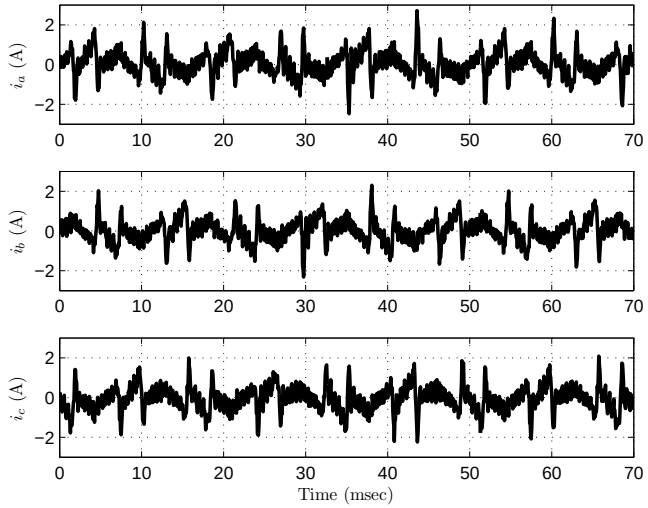

Figure 8.21: Experimental results of PI control of a SAPF: ac output currents

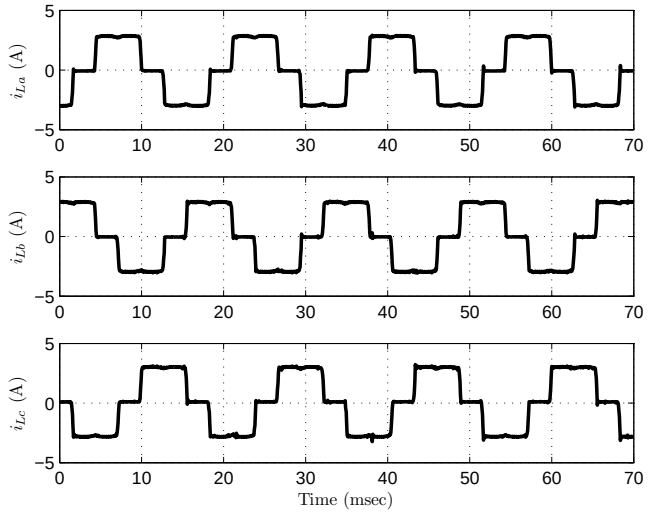

Figure 8.22: Experimental results of PI control of a SAPF: load currents

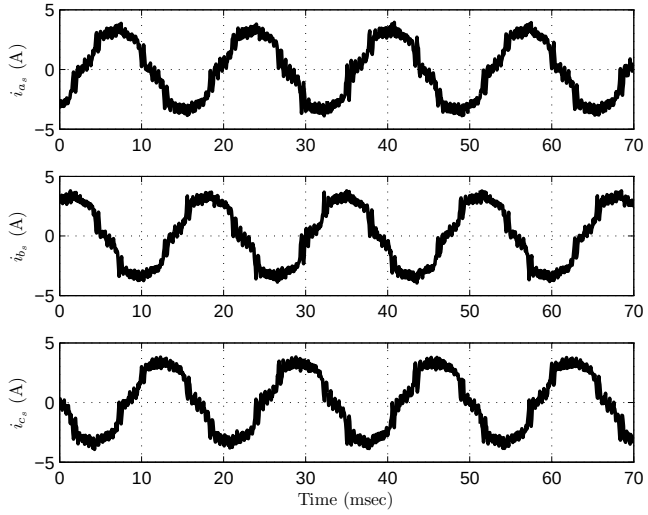

Figure 8.23: Experimental results of PI control of a SAPF: source currents

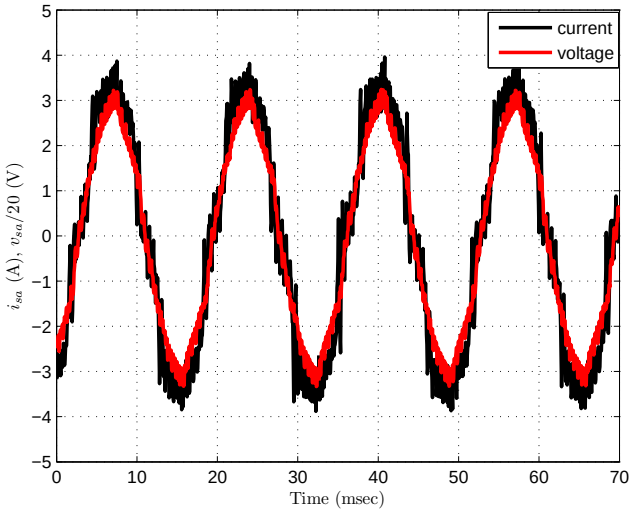

Figure 8.24: Experimental results of PI control of a SAPF: phase a current and voltage

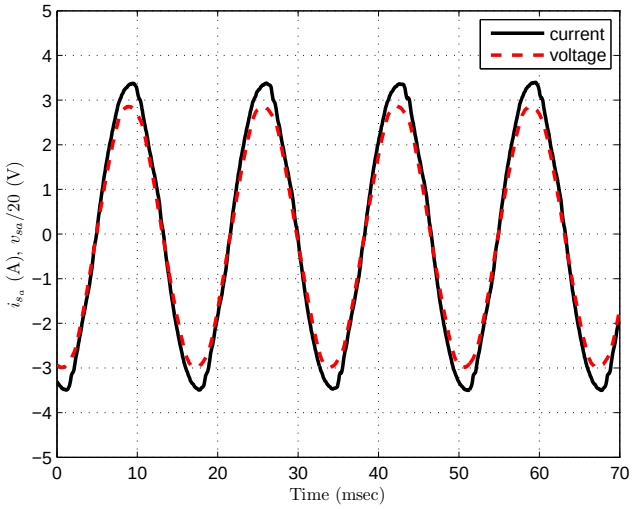

Figure 8.25: Experimental results of PI control of a SAPF: phase a current and voltage

filtered ac source phase-a voltage and current are depicted in Fig. 8.31 which shows PFC is achieved. The adaptive controller gains used in the experiment are given in Table 8.6.

Gains	Value
(k_{p_d}, k_{i_d})	$(780\ \text{V/A}, 7600\ \text{V/(A.s)})$
(k_{p_q}, k_{i_q})	$(710\ \text{V/A}, 123000\ \text{V/(A.s)})$
(k_{p_v}, k_{i_v})	$(5\ \text{A/V}, 20\ \text{A/(V.s)})$
(P_{d1}, P_{d2})	$(0.025, 0.01)$
(P_{q1}, P_{q2})	$(0.1, 0.03)$
(Λ_1, Λ_2)	$(0.002, 0.002)$

Table 8.6: Adaptive controller gains used in experimental SAPF control

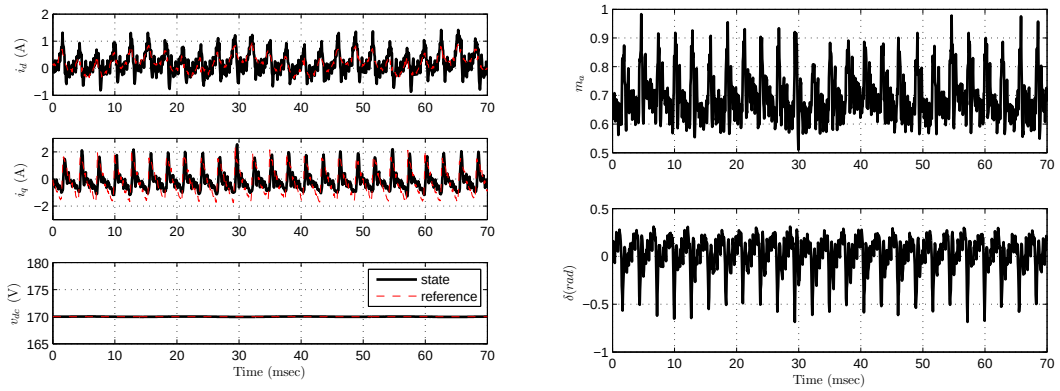

(a) trajectories of state and reference

(b) control inputs m_a and δ

Figure 8.26: Experimental results of the PI control of a SAPF

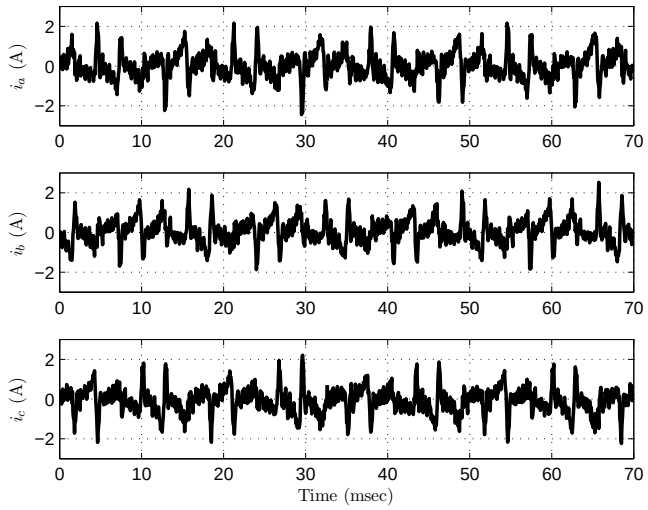

Figure 8.27: Experimental results of adaptive control of a SAPF: ac output currents

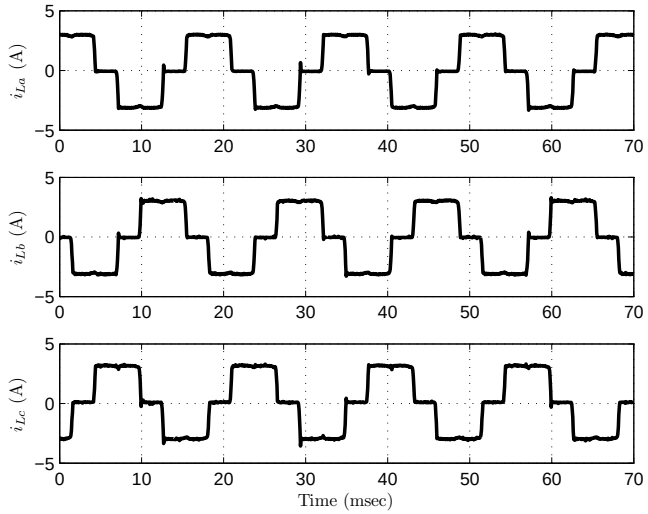

Figure 8.28: Experimental results of adaptive control of a SAPF: load currents

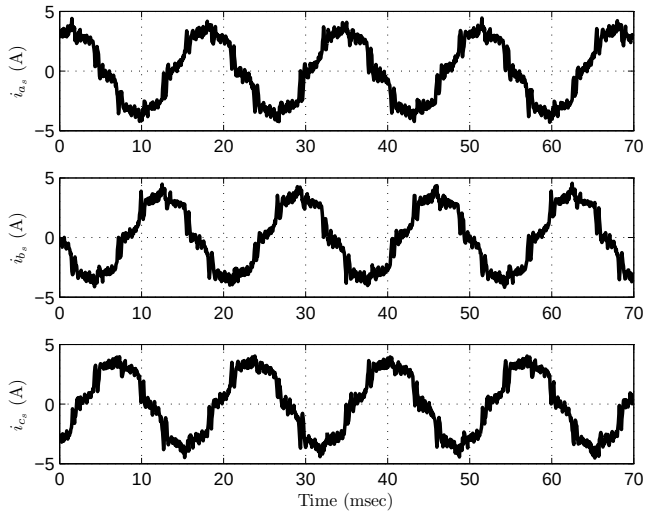

Figure 8.29: Experimental results of adaptive control of a SAPF: source currents

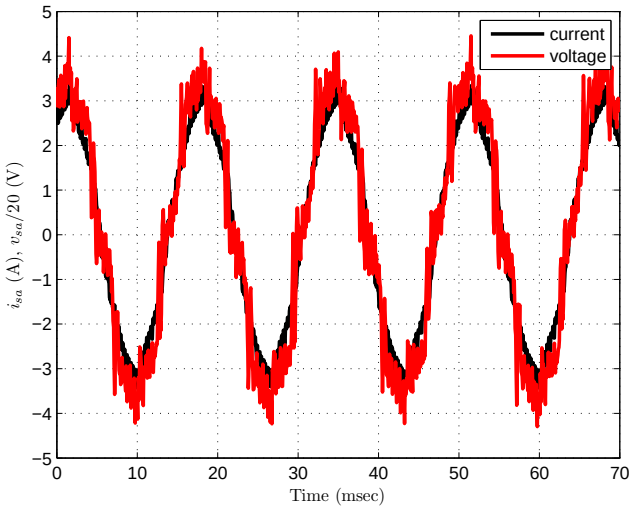

Figure 8.30: Experimental results of adaptive control of a SAPF: filtered phase a current and voltage

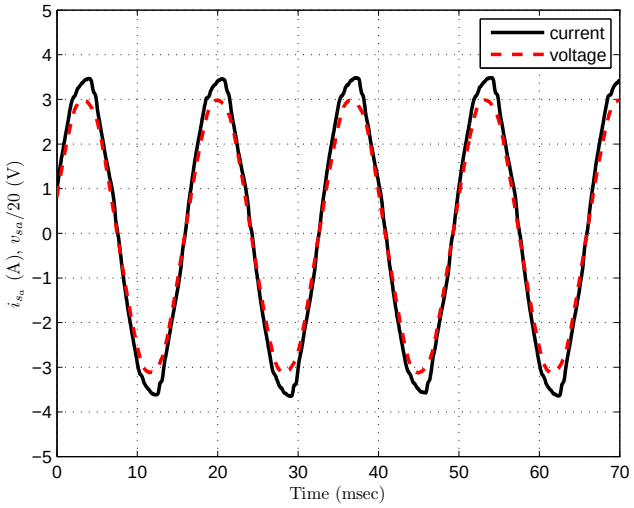

Figure 8.31: Experimental results of adaptive control of a SAPF: filtered phase a current and voltage

8.3 Summary

Experimental validation of the proposed controls for PFC and harmonic elimination applications are given in this chapter. The Semiteach Power Electronics Teaching System from SEMIKRON is used for constructing the experimental VSC system setup. The controller is implemented on the dSPACE system. The dSPACE's Control Desk software and MATLAB/Simulink are employed to develop a graphical interface to control the experiment. The performances of Vector, Adaptive Vector and Full Adaptive control techniques for PFC and established PI based and proposed adaptive based control methods for harmonic elimination are investigated. Also, various loads and reference trajectories are used to demonstrate the controllers' performances. The results verify good performances of the proposed adaptive control techniques.

Chapter 9

Conclusion

9.1 Summary of Research

The main goal of this thesis is to develop novel model-based control techniques for the VSC for harmonic elimination and PFC applications. First the mathematical models of the VSC in different coordinate systems are derived. Both nonlinear and simplified linear models of the VSC system are also developed. These models are used in the rest of the thesis for control design.

While the main focus of this thesis is on adaptive control, the research work starts with the introduce of classic vector control and flatness-based control for PFC applications. The novelty of our work in the flatness-based control lies in the improvement of the steady state dc voltage tracking by using state-state model information. This improvement is especially noticeable for operating points with large d-axis currents e.g. the VSC used in rectifier applications. However, the vector control and flatness-based control require that the VSC parameters to be known exactly. This motivates the investigation of adaptive control in the rest of the thesis.

For controlling VSC with unknown parameters, a review of adaptive control is conducted first. The systematic method for designing an adaptive control for regulation and output tracking of linearly parameterized system is reviewed. The VSC nonlinear model with unknown parameters is a linearly parameterized system. The design is successfully applied on a VSC nonlinear model with two unknown parameters. It is also shown that the systematic method can not be applied to the VSC with uncertainty in three parameters. Therefore, other

adaptive control methods are investigated for the VSC with three unknown parameters.

For the adaptive control design, three novel control methods, i.e. an adaptive PI vector control, an adaptive current control and a full adaptive control of the VSC are proposed in this thesis for PFC applications.

- The adaptive PI vector control method ensures asymptotic tracking of the q-axis current using an inner loop which contains two PI controllers with adaptive decoupling terms. The outer loop PI controller's defines the reference for the d-axis current loop. The asymptotic stability of the inner and outer loop are proven using Barbalet Lemma and Lyapunov's theorem. The proof of the closed-loop dc dynamics stability (outer loop) is valid for both adaptive PI vector control and classic vector control.

- An adaptive control of the inner current loop and a PI control for the outer dc voltage loop are used in the proposed adaptive current control. The compensation of the unknown resistance losses in adaptive current control is directly addressed using the adaptive terms.

- The full adaptive control method rely on the proposed simplified model. Beside, the uncertainty in the parameters R and L which is considered in the adaptive current control, the full adaptive control is also consider the uncertainty in R_c. The adaptive controller is designed which compensates for the ac and dc losses by estimating an effective dc side resistance, and convergence of the trajectory tracking error is proven.

Nonlinear average and switched VSC models are used to investigate the above-mentioned controllers performance in MATLAB/Simulink simulation. Adaptive controller performances are compared with a classical non-adaptive vector control.

Beside PFC, the harmonic compensation in a power system using a three-phase shunt active power filter (SAPF) is also investigated. Two designs are presented: a classic PI control and an adaptive control. The adaptive control is developed based on an adaptive PI current loop. To track the time varying

high order harmonics, adaptive integrator terms are used in the proposed adaptive scheme. Simulation results verify the proposed adaptive control good performance compare to the classic PI control.

Finally, full experimental validation of the proposed designs is performed using a computer controlled lab test stand. The Semiteach Power Electronics Teaching System from SEMIKRON and a modular dSPACE hardware system are employed for constructing the experimental VSC system setup. Also, the dSPACE's Control Desk software and MATLAB/Simulink are used to develop a graphical interface to control the experiment. Various loads and reference trajectories are considered to demonstrate the controllers' performances. Extensive experimental results verify good performances of the proposed adaptive control techniques.

9.2 Future Work

Some natural extensions of the proposed control techniques are

- Design of a nonlinear control for the nonlinear third order model of the VSC for time-varying q-axis current and dc voltage references.
- Different identification techniques such as subspace method can be used to estimate the unknown parameters for linear and nonlinear third order models. Then, control systems can be designed for the estimated VSC models.s
- Since an approximate model of the VSC is used to derive the adaptive control with three unknown parameters, it is logical to derive the theory for an adaptive law using the nonlinear VSC model.
- Stability of the proposed full adaptive control applied on the third order nonlinear model could be investigated.
- Design of a full adaptive control with integrator terms for harmonic elimination can be investigated.
- Other adaptive control methods can be developed and experimentally validated. For example adaptive backstepping could be investigated.
- A more complex motor drive application could be considered.
- The inductor filters could be modified to LC filters.

Bibliography

[1] N. Mohan, T. M. Undeland, and W. Robbins, *Power Electronics Converters, Applications and Design*. Hoboken, New Jersey, USA: John Wiley and Sons, 3rd ed., 2003.

[2] F. Peng, "Application issue of active power filters," *IEEE Industry Applications Magzine*, vol. 4, pp. 21–30, October 1998.

[3] J. Salmon, *Power Electronics Notes*. Edmonton: University of Alberta, 2009.

[4] W. Grady, "Harmonics and how they relate to powe factor," in *Proceeding of the EPRI Power Quality Issue & Opportunities Conference (PQA'93)*, (Sandiego), November 1993.

[5] T. Green and J. Marks, "Control techniques for active power filters," *IEE Proceeding Electronic Power Application*, vol. 152, pp. 369–381, March 2005.

[6] M. H. Rashid, *Power Electronics Circuits, Devices, and Applications*. Upper Saddle River, New Jersey, USA: Prentice Hall, 3rd ed., 2003.

[7] B. Singh, K. Al-Haddad, and A. Chandra, "A review of active filters for power quality improvement," *IEEE Transactions on Industrial Electronics*, vol. 46, pp. 960–971, October 1999.

[8] M. El-Habrouk, M. Darwish, and P. Mehta, "Active power filters: a review," *IEE Proceedings Electric Power Applications*, vol. 147, pp. 403–413, September 2000.

[9] V. K. Sood, *HVDC and FACTS Controllers: Applications of Static Converters in Power Systems*. Kluwer Academic Publishers, April 2004.

[10] G. Reed, T. Croasdaile, J. Paserba, R. Williams, R. Takeda, S. Jochi, N. Morishima, T. Aritsuka, Y. Hamasaki, Y. Yonehata, S. Amakasu, and K. Takamiya, "Applications of voltage source inverter (vsi) based technology for facts and custom power installations," in *Proceedings of International Conference on Power System Technology (PowerCon 2000)*, vol. 1, pp. 381 –386, 2000.

[11] S. Cole and R. Belmans, "Transmission of bulk power," *IEEE Industrial Electronics Magazine*, vol. 3, pp. 19–2 4, September 2009.

[12] C. Schauder and H. Mehta, "Vector analysis and control of advanced static var compensators," *IEE Proceedings - Generation, Transmission and Distribution*, vol. 140, pp. 299–306, July 1993.

[13] S. Rahmani, N. Mendalek, and K. Al-Haddad, "Experimental design of a nonlinear control technique for three-phase shunt active power filter," *IEEE Transactions on Industrial Electronics*, vol. 57, pp. 3364–3375, October 2010.

[14] K. Astrom and T. Hagglund, "The future of pid control," *Control Engineering Practice*, vol. 9, pp. 1163–1175, November 2001.

[15] T. Lee, "Lagrangian modeling and passivity based control of three phase ac/dc converters," *IEEE Transactions on Industrial Electronics*, vol. 51, pp. 892–902, August 2004.

[16] E. Song, "Nonlinear flatness-based control of a pulse width modulated voltage source converter," Master's thesis, University of Alberta, Edmonton, Alberta, Canada, 2006.

[17] R. Milasi, A. Lynch, and Y. Li, "Adaptive control of voltage source converter," in *Proceedings of the 23rd Canadian Conference on Electrical and Computer Engineering*, (Calgary, Canada), pp. 1–4, 2010.

[18] D. Lee, G. Lee, and K. Lee, "Dc-bus voltage control of three-phase ac/dc pwm converters using feedback linearization," *IEEE Transactions on Industrial Applications*, vol. 36, pp. 826–832, May 2000.

[19] T. Lee, "Input-output linearization and zero-dynamics control of three-phase AC/DC voltage-source converters," *IEEE Transactions on Power Electronics*, vol. 18, pp. 11–22, January 2003.

[20] A. Gensior, J. Rudolph, and H. Guldner, "Flatness based control of three-phase boost rectifiers," in *European Conference on Power Electronics and Applications*, (Dresden, Germany), September 2005.

[21] A. Gensior, H. Sira-Ramirez, J. Rudolph, and H. Guldner, "On some nonlinear current controllers for three-phase boost rectifiers," *IEEE Transactions on Industrial Electronics*, vol. 56, pp. 360–370, February 2009.

[22] E. Song, A. Lynch, and V. Dinavahi, "Experimental validation of nonlinear control for a voltage source converter," *IEEE Transactions on Control System Technology*, vol. 17, pp. 1135 –1144, August 2009.

[23] H. Komurcugil and O. Kukrer, "Lyapunov-based control for three-phase ac/dc voltage-source converters," *IEEE Transactions on Power Electronics*, vol. 13, pp. 801–813, September 1998.

[24] H. Komurcugil and O. Kukrer, "A novel current control method for three phase pwm ac/dc voltage source converters," *IEEE Transactions on Industrial Electronics*, vol. 46, pp. 544–553, June 1999.

[25] Y. Shtessel, S. Baev, and H. Biglari, "Unity power factor control in three-phase ac/dc boost converter using sliding modes," *IEEE Transactions on Industrial Electronics*, vol. 55, pp. 3874–3882, November 2008.

[26] S. Richter, S. Mariéthoz, and M. Morari, "High-speed online mpc based on a fast gradient method applied to power converter control," in *American Control Conference*, (Baltimore, MD, USA), pp. 4737 – 4743, June 2010.

[27] A. Hadri-Hamida, A. Allag, M. Hammoudi, S. Mimoune, S. Zeroualib, M. Ayad, M. Becherif, E. Miliani, and A. Miraoui, "A nonlinear adaptive backstepping approach applied to a three phase pwm ac-dc converter feeding induction heating," *Communications in Nonlinear Science and Numerical Simulation*, vol. 14, pp. 1515–1525, April 2009.

[28] A. Allag, M. Hammoudi, S. Mimoune, M. Ayad, M. Becheri, E. Miliani, A. Miraoui, and M. Feliachi, "Adaptive nonlinear control applied to a three phase shunt active power filter," in *IEEE Annual Conference on Industrial Electronics*, (Paris, France), pp. 1615 – 1620, November 2006.

[29] Y. Ruan, G. Li, X. Jiao, Y. Sun, and T. Lie, "Adaptive control design for vsc-hvdc systems based on backstepping method," *Electric Power System Research*, vol. 77, no. 5 - 6, pp. 559–565, 2007.

[30] K. Shyu, M. Yang, Y. Chen, and Y. Lin, "Model reference adaptive control design for a shunt active-power-filter system," *IEEE Transactions on Industrial Electronics*, vol. 55, pp. 97–106, January 2008.

[31] M. Perez, R. Ortega, and J. Espinoza, "Passivity based pi contorl of switched power converters," *IEEE Transactions on Control System Technology*, vol. 12, pp. 882–890, November 2004.

[32] M. Gomez, R. Ortega, F. Lagarrigue, and G. Escobar, "Adaptive pi stabilization of switched power converters," *IEEE Transactions on Control System Technology*, vol. 18, pp. 688–698, May 2010.

[33] B. Bahrani, S. Kenzelmann, and A. Rufer, "Multivariable-pi-based dq current control of voltage source converters with superior axis decoupling capacity," *IEEE Transactions on Indusrial Electronics*, vol. 58, pp. 3016–3025, July 2011.

[34] B. Ooi, J. Salmon, J. W. Dixon, and A. Kulkarni, "A three-phase controlled-current pwm converter with leading power factor," *IEEE Transactions on Industry Applications*, vol. IA-23, pp. 78–84, January 1987.

[35] R. Wu, S. Dewan, and G. Slemon, "A pwm ac to dc converter with fixed switching frequency," in *Conference Record of the 1988 IEEE Industry Applications Society Annual Meeting*, vol. 1, pp. 706 –711, October 1988.

[36] R. Wu, S. Dewan, and G. Slemon, "A pwm ac-to-dc converter with fixed switching frequency," *IEEE Transactions on Industry Applications*, vol. 26, pp. 880–885, September/October 1990.

[37] R. Wu, S. Dewan, and G. Slemon, "Analysis of an ac-to-dc voltage source converter using pwm with phase and amplitude control," *IEEE Transactions on Industry Applications*, vol. 27, pp. 355–364, April 1991.

[38] V. Blasko and V. Kaura, "A new mathematical model and control of a three-phase ac-dc voltage source converter," *IEEE Transactions on Power Electronics*, vol. 12, no. 1, pp. 116–123, 1997.

[39] A. Tabesh and R. Iravani, "Multivariable dynamic model and robust control of a voltage source converter for power system applications," *IEEE Transactions on Power Delivery*, vol. 24, pp. 462–471, January 2009.

[40] W. Chen and Y. Hsu, "Controller design for an induction generator driven by a variable-speed wind turbine," *IEEE Transactions on Energy Conversion*, vol. 21, pp. 625–635, September 2006.

[41] A. Consoli, E. Cerruto, A. Raciti, and A. Testa, "Adaptive vector control of induction motor drives based on a neuro-fuzzy approach," in *25th Annual IEEE Power Electronics Specialists Conference, PESC '94 Record*, vol. 1, pp. 225 – 232, June 1994.

[42] E. Cerruto, A. Consoli, A. Raciti, and A. Testa, "Fuzzy adaptive vector control of induction motor drives," *IEEE Transactions on Power Electronics*, vol. 12, no. 6, pp. 1028 – 1040, 1997.

[43] K. Madani, A. Chebira, J. Depecker, and G. Mercier, "An intelligent adaptive vector control technique using a multi-neural networks based

hybrid structure," in *International Joint Conference on Neural Networks, IJCNN '99.*, vol. 3, pp. 2141 – 2145, 1999.

[44] P. Kokotovic, I. Kanellakopoulos, and A. Morse, "Adaptive feedback linearization of nonlinear system," *Foundations of Adaptive Control, Lecture Notes in Control and Information Sciences, Springer-Verlag*, vol. 160, pp. 309–346, 1991.

[45] I. Kanellakopoulos, P. Kokotovic, and A. Morse, "Systematic design of adaptive controllers for feedback linearizable systems," *IEEE Transactions on Automatic Control*, vol. 36, pp. 1241–1253, November 1991.

[46] N. Mendalek, K. Al-Haddad, F. Fnaiech, and L. Dessaint, "Nonlinear control technique to enhance dynamic performance of a shunt active power filter," *IEE Proceedings Electric Power Applications*, vol. 150, no. 4, pp. 373–379, 2003.

[47] B. K. Bose, *Modern Power Electronics and AC Drives*. Upper Saddle River, New Jersey: Prentice Hall, 2002.

[48] T. Satish, K. Mohapatra, and N. Mohan, "Steady state over-modulation of matrix converter using simplified carrier based control," in *33rd Annual Conference of the IEEE Industrial Electronics Society, IECON 2007*, pp. 1817 –1822, November 2007.

[49] A. Hava, R. Kerkman, and T. Lipo, "Carrier-based pwm-vsi overmodulation strategies: analysis, comparison, and design," *IEEE Transactions on Power Electronics*, vol. 13, pp. 674–689, July 1998.

[50] R. Park, "Two reaction theory of synchronous machines," *Transactions of the American Institute of Electrical Engineers*, vol. 48, pp. 716–727, 1929.

[51] G. Valderrama, P. Mattavelli, and A. Stankovic, "Reactive power and unbalanced compensation using statcom with dissipativity-based control,"

IEEE Transactions on Control System Technology, vol. 9, pp. 718–727, September 2001.

[52] M. Fliess, J. Levine, P. Martin, and P. Rouchon, "Sur les systèmes non linéaires différentiellement plats," *Comptes Rendus de lÁcadémie des Sciences*, vol. 315, pp. 619–624, 1992.

[53] M. Fliess, J. Levine, P. Martin, and P. R. P., "Flatness and defect of nonlinear systems: Introductory theory and examples," *International Journal of Control*, vol. 61, pp. 1327–1361, June 1995.

[54] R. Marino and P. Tomei, *Nonlinear Control Design: Geometric, Adaptive, and Robust*. Hertfordshire, UK: Prentice-Hall, 1995.

[55] A. Isidori, *Nonlinear Control Systems*. Springer, 3rd ed., 1995.

[56] B. Charlet, J. Levine, and R. Marino, "On dynamic feedback linearization," *Systems and Control Letters*, vol. 13, pp. 143–51, 1989.

[57] Z. Dydek, A. Annaswamy, and E. Lavretskyavretsky, "Adaptive control and the nasa x-15 program: A concise history, lessons learned, and a provably correct design," in *American Control Conference*, pp. 2957 – 2962, june 2008.

[58] R. Kalman, "A new approach to linear filtering and prediction problems," *Journal of Basic Engineering*, vol. 82, no. 1, pp. 35–45, 1960.

[59] R. Kalman and L. Bertram, "General synthesis procedure for computer control of single and multiloop linear systems," *Transactions of the American Institute of Electrical Engineers*, vol. 77, pp. 602–609, 1958.

[60] R. Kalman and J. Bertram, "A unified approach to the theory of sampling systems," *Journal of the Franklin Institute*, vol. 267, no. 5, pp. 405–436, 1959.

[61] C. Hutchinson, "The kalman filter applied to aerospace and electronic systems," *IEEE Transactions on Aerospace and Electronic Systems*, vol. AES-20, pp. 500–504, july 1984.

[62] W. Hahn and A. Baartz, *Stability of Motion*. Grundlehren der mathematischen Wissenschaften, Springer, 1967.

[63] B. Egardt, *Stability of Adaptive Controllers*. Lecture notes in control and information sciences, Springer, 1979.

[64] Y. Landau, *Adaptive Control: the Model Reference Approach*. Control and systems theory, Dekker, 1979.

[65] R. Marino and P. Tomei, "Global adaptive output-feedback control of nonlinear systems. i. linear parameterization," *IEEE Transactions on Automatic Control*, vol. 38, no. 1, pp. 17–32, 1993.

[66] R. Marino and P. Tomei, "Global adaptive output-feedback control of nonlinear systems. ii. nonlinear parameterization," *IEEE Transactions on Automatic Control*, vol. 38, pp. 33–48, January 1993.

[67] M. Krstic, I. Kanellakopoulos, and P. Kokotovic, "Nonlinear design of adaptive controllers for linear systems," *IEEE Transactions on Automatic Control*, vol. 39, no. 4, pp. 738–752, 1994.

[68] S. Sastry and A. Isidori, "Adaptive control of linearizable systems," *IEEE Transactions on Automatic Control*, vol. 34, no. 11, pp. 1123–1131, 1989.

[69] G. Tao, *Adaptive Control Design and Analysis*. Hoboken, New Jersey, USA: John Wiley and Sons, 2003.

[70] K. J. Astrom and B. Wittenmark, *Adaptive Control*. Addison-Wesley, Reading, MA, 2nd ed., 1995.

[71] H. Khalil, *Nonlinear Systems*. Upper Saddle River, New Jersey, USA: Prentice-Hall, 2002.

[72] G. Campion and G. Bastin, "Indirect adaptive state feedback control of linearly parametrized nonlinear systems," *International Journal of Adaptive Control and Signal Processing*, vol. 4, pp. 345–358, 1990.

[73] K. Narendra and A. Annaswamy, *Stable Adaptive Systems*. Prentice-Hall Inc., 1989.

[74] M. Zhuang and D. Atherton, "Automatic tuning of optimum pid controllers," *IEE Proceedings on Control Theory and Applications*, vol. 140, pp. 216–224, may 1993.

[75] C. Kallstrom, K. Astrom, N. Thorell, J. Eriksson, and L. Sten, "Adaptive autopilots for tankers," *Automatica*, vol. 15, no. 3, pp. 241–254, 1979.

[76] G. Stein, G. Hartmann, and R. Hendrick, "Adaptive control law for f-8 flight test," *IEEE Transactions on Automatic Control*, vol. AC-22, no. 5, pp. 758–767, 1977.

[77] K. J. Astrom and B. Wittenmark, *Adaptive Control*. Addison-Wesley, Reading, MA, 1st ed., 1989.

[78] W. Rugh, "Analytical framework for gain scheduling," *IEEE Control Systems Magazine*, vol. 11, no. 1, pp. 79–84, 1991.

[79] J. Shamma and M. Athans, "Analysis of gain scheduled control for nonlinear plants," *IEEE Transactions on Automatic Control*, vol. 35, no. 8, pp. 898–907, 1990.

[80] W. Rugh and J. Shamma, "Research on gain scheduling," *Automatica*, vol. 36, October 2000.

[81] I. Kanellakopoulos, P. Kokotovic, and R. Marino, "Robust adaptive nonlinear control under extended matching conditions," tech. rep., DTIC Document, 1990.

[82] I. Kanellakopoulos, P. Kokotovic, and R. Marino, "An extended direct scheme for robust adaptive nonlinear control," *Automatica*, vol. 27, pp. 247–255, 1991.

[83] R. Marino, I. Kanellakopoulos, and P. Kokotovic, "Adaptive tracking for feedback linearizable siso systems," in *Proceedings of the 28th IEEE Conference on Decision and Control*, pp. 1002–1007, 1989.

[84] V. Mastrosov, "On the stability of motion," *Journal of Applied Mathematics and Mechanics*, vol. 26, no. 5, pp. 1337–1353, 1962.

[85] F. Sargos, "Application note of igbt power electronics teaching system principle for sizing power converters," *Semikron*, September 2008.

[86] N. Xu, "Nonlinear control of a voltage source converter," Master's thesis, University of Alberta, 2010.